STUDY OF DUST DEVILS AS RELATED TO THE MARTIAN YELLOW CLOUDS

Volume II-Basic Data
(Appendix to Final Report)

PREPARED BY
J.A. RYAN
SPACE SCIENCES DEPARTMENT

APPROVED BY

A. D. Goedeke (signature)

A.D. GOEDEKE
CHIEF SCIENTIST
SPACE SCIENCES DEPARTMENT
RESEARCH AND DEVELOPMENT

STUDY OF DUST DEVILS AS RELATED TO THE MARTIAN YELLOW CLOUDS

Volume II-Basic Data
(Appendix to Final Report)

PREFACE

This report summarizes work performed by the Space Sciences Department,
McDonnell Douglas Astronautics Company - Western Division for the National
Aeronautics and Space Administration under Contract NASw-1620. The work
consisted of field experimental studies of dust devils, the establishment of
a quantitative dust devil model, and the transformation of this model to Martian
conditions to determine whether dust devils could occur on Mars and be
responsible for the Martian yellow clouds. Volume I comprises the technical
discussion and presents the program findings. The basic field experimental
data are given in Volume II.

Page intentionally left blank

TABLE OF CONTENTS

1.0 INTRODUCTION AND SUMMARY

This report presents a summary of work performed during the period June 1, 1967 through December 5, 1968 on a study of dust devils as related to the Martian yellow clouds. The objective of this study was to determine whether dust devils could occur on Mars, and be responsible for the observed yellow clouds. Particular emphasis was given to field studies of dust devils since relatively few good data were available concerning their structure and the conditions under which they form.

Field data were obtained in the Mojave Desert of Southern California. Quantities measured were temperature as a function of height (surface to 1500 meters above the surface) and time, background wind velocity and direction, atmospheric vorticity, wind velocities inside dust devils, and dust devil diameter, sense of rotation, height, location, and time of occurrence. Sufficient data were obtained to allow a quantitative dust devil model to be formulated. It was found that dust devil generation occurs adjacent to the surface and that dust devil frequency and diameter is determined by the near surface (< 10 meters) temperature lapse rate. It was also found that the vertical velocities in dust devils are dependent only upon the thickness of the total superadiabatic layer (typically several hundred meters in height) and the mean lapse rate in this layer; and that the tangential (rotational) velocities are dependent only upon the vertical velocity, dust devil diameter, and the effective height of the inflow layer.

A computer program was formulated, which predicts the possible temperature profiles in the lowermost Martian atmosphere. Utilizing these profiles and the physical dust devil model, it is found that dust devils should occur on Mars and could be responsible for the yellow clouds.

2.0 PREVIOUS RELATED WORK

2.1 Martian Yellow Clouds

The Martian yellow clouds are generally believed to consist of granular material which has been swept from the surface by the atmospheric winds. The primary evidence for this is the various polarization and photometric observations of these clouds and the surface, made by a number of investigators, which indicate that both the clouds and the surface are composed of generally similar, and particulate, material. Additional indications have been provided by (1) the general belief that water is essentially absent at the surface so that surface granular material should be in a "loose" form susceptible to wind action, (2) the relatively high wind velocities, up to $\approx$100 km/hr, observed to be associated with cloud generation (implying that winds are required for formation), and (3) the observation that yellow clouds appear to occur preferentially at times of maximum surface heating, and in the areas of maximum heating, i.e., when a maximum amount of atmospheric internal and potential energy may be available for conversion to kinetic energy.

Alternative explanations for the yellow clouds have been proposed in the past. These are (1) that the clouds are formed by volcanic activity, (2) that they are formed by asteroidal impact, or (3) that they are formed by a phase change of surface NO_2 caused by surface warming; in this case the clouds would consist of NO_2 rather than dust. The principal arguments against a volcanic origin are (1) the clouds are formed predominantly in relatively narrow belts in the vicinity of the equator (it would be quite fortuitous if zones of volcanic activity showed such a decided equatorial proximity), and (2) a volcanic origin would require an implausibly high rate of volcanic activity on Mars. The principal arguments against asteroidal impact production are also the noted

2

equatorial proximity and the impact rate required. The arguments against nitrogen oxide phase changes are (1) the geologic difficulties in accounting for the large amount of NO_2 required, (2) the low present upper bound for nitrogen oxides in the Martian atmosphere (Sagan et al., 1965), and (3) the point noted by Sinton (1961) that NO_2 is highly absorbing and hence if the clouds were composed of NO_2 they would appear dark, contrary to observation.

Ryan (1964a, b) considered the wind velocities required to remove granular material from the surface. He finds that for a reasonable surface model the required velocities are about 80 km hr^{-1} (for a surface pressure = 80 mb), and 200 km hr^{-1} (if 25 mb). For 10 mb the velocity becomes 330 km hr^{-1}, and for 5 mb it is $\approx$450-500 km hr^{-1}. Mariner IV and recent spectroscopic studies indicate that the pressure is most likely in the approximate range 4-10 mb. It is seen then that the velocities apparently required for initiation of grain motion far exceed any ever observed on the planet. It was concluded by Ryan that the most plausible ways in which compatibility could be achieved are either if (1) the initiating winds are of such short duration that they have escaped detection, or (2) the initiating winds are part of a tight cyclonic system (or systems) and hence not observable from Earth, the observations of cloud drift pertaining then to the general atmospheric circulation. The former possibility implies that gusts associated with frontal systems could be primarily responsible for cloud generation. This appears now to be less likely on the basis of the Mariner IV result for the surface pressure. The very low pressure indicated requires much higher initiating gust wind velocities than would be expected to be superimposed on the relatively low velocity winds (<30 km hr^{-1}) of the general circulation (as determined from long-duration cloud movement observations).

As for the latter possibility, it was noted by Ryan (1964 b) that with the "dry" conditions pertaining on Mars, dust devils would be a possible source mechanism for the yellow clouds. This possibility has been considered further by Neubauer (1966).

The question of the nature of the yellow clouds has received added importance as the result of Mariner IV, particularly due to the discovery of craters on the Martian surface. Leighton et al. (1965), by analogy with the moon, noted that the craters should be quite old, possibly 2-5 x 10^9 years. This, coupled with the evidence that the craters do not appear to be eroded to a degree significantly greater than the ancient lunar craters, would imply that erosional processes on Mars were never very effective. Leighton (1965) subsequently did state, however, that there was some indication that for a given crater size, the Martian craters were shallower than the lunar craters.

He noted that this difference may be due to eolian erosion. More recently, three articles, by Anders and Arnold (1965), Witting et al. (1965), and Baldwin (1965), have appeared in which the age proposed by Leighton et al. for the Martian craters has been challenged. In particular, the respective writers conclude, on the basis of the expected asteroidal influx rate on Mars, that the craters are no older than 800 million years and possibly as young as 300 million years (Anders and Arnold), that they are about 300 million years old (Witting et al.) and about 700 million years old (Baldwin). Anders and Arnold note that such a low age implies a significant amount of surface erosion, possibly accounted for entirely by dust storms. Baldwin notes that a substantial amount of erosion on Mars is indicated.

Opik (1966) criticized all of the above estimates on the grounds that they wholly or in part used the Moon as the calibration standard for collision frequencies. Opik concluded that erosion on Mars is about 30 times slower than in terrestrial deserts and about 70 times faster than on the Moon.

The processes involved in the generation of the yellow clouds are probably one of the primary erosional mechanisms which may act at the Martian surface. Wind action alone cannot contribute significantly because even if high wind velocities are present, the dynamic pressures exerted are quite low (due to the low atmospheric surface pressure). Rather, the primary erosive agents would be the granular material accelerated to high velocities by these winds. Hence, it appears that studies of the yellow clouds can provide information as to the effectiveness of eolian erosional processes on Mars (alternatively, whether significant wind erosion is likely at all), and thus aid in the understanding of the age(s) of the craters.

2.2 Dust Devils

2.2.1 General

Dust devils are the only terrestrial tight cyclonic systems which do not derive any of their energy from, or depend upon, water phase changes. On Earth they occur in areas where "loose" granular material is present (this is a necessary condition for granular materials to be carried aloft and for the devil to be visible, but not for these cyclonic systems to be present); in the presence of a superadiabatic temperature lapse rate; and when atmospheric vorticity is present. The Martian yellow clouds tend to occur under the same conditions, that is around the areas and times of maximum surface heating (Gifford, 1964; Wells, 1966) implying superadiabatic lapse rates, and when the atmospheric circulation is most vigorous (Kuiper, 1961) implying a maximum amount of atmospheric vorticity. Also, the essential lack of water on Mars

implies that the surface material may be in a loose (dry) state susceptible to wind action.

The only presently observed difference between the yellow clouds and terrestrial dust devils is one of scale, the yellow clouds at times covering a thousand or so square kilometers of area whereas an individual dust devil on Earth rarely has a diameter in excess of about 100 meters. However, this scale difference question can be resolved on a qualitative basis by the arguments that (1) it is likely that a much more plentiful supply of granular material susceptible to being carried aloft is present on Mars than on Earth due to the lack of dust sinks, e.g., oceans, vegetated and moist areas, etc., on Mars, (2) the Martian atmosphere, even if the surface pressure is only 5 mb, can maintain granular material aloft in the grain size range of primary interest (10-200 μ) at least as easily as the Earth's atmosphere, and (3), when conditions are proper for dust devil formation on Earth, dust devils can become quite numerous: if the surface of Mars is, as generally believed, much more uniform than the Earth's then considerable dust devil activity could occur over a large area and this activity might be responsible for the yellow clouds.

2.2.2 Field Studies

Field studies of dust devils have been made sporadically for a number of years. Few individuals have been involved in these, however, and as a result of this general lack of interest by the scientific community few data have been obtained. Also, most of the available data consist of visual observations with some approximate and very few precise measurements included. The bulk of the work has been done by Flowers (1936), Ives (1947), Williams (1948), and Sinclair (1964, 1965a,b, 1966). Flowers found, from 409 observations in the Near East,

that (1) most dust devils occurred during the hottest time of the year, also at the hottest time of the day, (2) they varied in diameter from about a few meters to about 100 meters (all diameters being visual estimates), (3) they varied in height (to top of dust column) from about 25 meters to greater than 300 meters (again a visual estimate), the height increasing as diameter increases, (4) their forward velocity averaged between about 10-40 km hr^{-1}, (5) they were generated only when a superadiabatic temperature lapse rate was present, (6) individual devils persisted for as long as twenty minutes and (7) horizontal wind velocities as great as 50 km hr^{-1} were present in the devils, with associated vertical velocities as great or greater than 10 km hr^{-1} (velocity estimates obtained from visual observation of debris contained within the devils). Ives (1947), from studies in the Western United States, notes cases of dust devils lasting more than four hours, reaching a height (height to top of dust column) of almost a kilometer (visual estimate), and traveling distances of about 60 kilometers. He also notes that (1) dust devils are most frequent in broad, arid basins, where there is little or no surface vegetation and much loose surface dust; alternatively, where local relief is considerable, devils are seldom reported, (2) dust devils most frequently occur in clear weather when there is little or no surface wind, and occur only in the presence of a super-adiabatic lapse rate, and (3) the largest devils occur only in the most arid areas. Ives obtained a few rough measures of the temperature lapse rates present during times of dust devil activity finding lapse rates up to a few hundred meters above the surface of as much as 4-5 times dry adiabatic. He also obtained crude measurements of the horizontal wind velocities in the devils, finding that they often exceeded $\approx$120 km hr^{-1}, but probably did not exceed $\approx$180 km hr^{-1}. Williams (1948) performed his observations in Central California concluding that local atmospheric shear might be important in dust devil formation.

Sinclair (1964, 1965a, b, 1966) was the first investigator to attempt to make precise measurements of dust devil internal dynamics, and his work is considerably more comprehensive than that of the previous investigators. He measured atmospheric pressure, temperature, wind velocity and wind direction changes in dust devils at 2 and 10 meter heights above the surface, and performed a number of sailplane flights above dust devils, measuring temperature and vertical wind velocity. He confirmed that a pressure drop (typically a few millibars) occurred inside dust devils and that a temperature rise of several °C was associated with the dust devil. Tangential wind velocities as great as 40 km hr^{-1} were recorded with lesser vertical (upward) and radial wind velocities. A small magnitude downdraft was observed in the vicinity of the dust devil center. The sailplane flights indicated that updrafts associated with dust devils were present several kilometers above the surface.

2.2.3 Kinematic Description

It has been known for some time that the visible dust devil consists of a core in essentially solid rotation, insofar as the tangential velocity is concerned, surrounded by a region in which the tangential velocity decreases outward monotonically with distance from the core boundary. However, it has not been until recently, primarily from the work of Sinclair (1966), that experimental data required to advance our knowledge of dust devil kinematics were obtained. Sinclair has shown that, geometrically, the mature dust devil can be divided into three vertical regions. Region I comprises the lower boundary layer characterized by turbulent inflow and visible as a diffusing, shallow, dust cloud near the ground. It is in this region, the friction layer, that air (and dust) is entrained into the dust devil core. That is, above this region there is a balance between pressure gradient and centrifugal forces (stable vortex) whereas in the friction layer the rotational velocity, and hence

centrifugal force, is considerably reduced (Scorer, 1958, pp. 52-54). Above this, Region II is characterized by a thin, sharply defined cylindrical or slighly conical rotating dust column having a very large height to diameter ratio. Surrounding this sharply defined region is a surrounding volume of rotating airflow. Little or no mixing occurs between the core and surrounding air. Region III begins where the top of the dust column becomes turbulent, with the dust (if still visible) diffusing radially with height in a manner analogous to an extraining jet or plume. The rotary motion appears to decay rapidly with height above Region II. Reported sizes of dust devils are almost invariably the visual estimates of dust dimensions in Region II. Reported heights vary from a few meters to several hundred meters with diameters from tenths of a meter to several tens of meters. The extent of Region III is less well defined because it is not visible (e.g. dust density is low). Sinclair's sailplane flights over dust devils, however, indicate that it is still well developed at altitudes of several kilometers with diameters of 1 to 2 km. No upper limit to the structure has as yet been determined.

The major features of the velocity field (after Sinclair) are as follows. In Region II the maximum tangential (rotational) velocity (v_{max}) is typically larger than, but of the same order of magnitude as, the vertical component (w_{max}), and both occur at the core boundary. The radial variation of v in a mature dust devil corresponds closely to that of a "combined Rankine vortex". The magnitude of the radial component (u) is about half the tangential at the lower levels and a smaller fraction above. However, due to (Sinclair's) measuring techniques less confidence should be given to the measured values reported for u, than those for v. Secondary evidence exists for the existence of radial inflow throughout Region II, except into the core itself, in the fact

that the dust is not centrifuged out of the vortex. For instance, if the boundary of the dust is at r = 2 meters and has a tangential velocity of v = 5 msec^{-1} then the centrifugal acceleration, $\frac{v^2}{2}$ = 12.5 msec^{-2} = 1.2 g. Sample dust sizes (Sinclair) range from 5μ to 200μ with a median of about 40μ. For a 40μ particle to have sufficient inward drag to balance this 1.2g acceleration, u = 0.25 msec^{-1} is required; for a 200μ particle, u = 2 msec^{-1} is required (though v_{max} for well developed dust devils is usually in the range 10 to 20 msec^{-1}, there is no apriori reason for expecting that the dust boundary corresponds exactly to the core boundary). While the values of u are smaller than the other two components, the total radial convergence in the layer comprising Region II can be large.

Along the core axis there is a relatively low velocity downdraft with radial outflow, at least near the ground, and in this sense the dust devil can be considered to be a two-cell vortex. Sinclair suggests that this downdraft is due to the lack of hydrostatic equilibrium associated with the strong vertical accelerations occurring near the ground.

2.2.4 Generation Dynamics

It became clear to the early investigators that necessary conditions for the formation of dust devils were the presence of a superadiabatic temperature lapse rate near the ground with the associated convectively unstable layer extending to some height, say h, and light surface winds, $\overline{U} < 5$ msec^{-2}. The superadiabatic lapse rate was necessary to furnish an energy source for the generation of kinetic energy. Low background winds were necessary to prevent the destruction of the incipient vortex by mechanical turbulence.

The first attempt to formulate the generation dynamics on a quantitative basis

was made by Flowers (1936). Flowers considered a devil to be formed by local overturning of the superadiabatic column with the resulting decrease in internal energy of the column appearing initially as rotational kinetic energy. He also devised a physical model for a dust devil, consisting of a core in "solid rotation" surrounded by a rotating air mass whose velocity at any point is inversely proportional to the distance from the center of the devil. The resultant equation is:

$$E = \pi \omega^2 h_d \rho_a r_o^4 \ [0.25 + \ln n] \qquad (1)$$

where E = kinetic energy, ω = angular velocity of solid core, h_d = height of devil, ρ_a = air density, r_o = radius of solid core, and n = ratio of devil diameter to core diameter.

Flower's work was extended by Battan (1958) to include atmospheric potential energy. Battan considered two models for dust devil generation. For the first model, he assumed that the overturning of the unstable air column was complete, i.e., that a unit mass at the base of the column was raised adiabatically to the top, and vice versa for the air mass initially at the top. This model is unrealistic, as noted by Battan, since it leads to a temperature inversion. For the second model, Battan required that the overturning be isentropic and that the final lapse rate be dry adiabatic. This model is also unrealistic since it results in a significant temperature discontinuity at the top of the column. An additional difficulty with Battan's treatment is that the numerical results obtained are critically dependent upon the numerical values used (solution requires subtraction between two quantities which are very nearly the same). This difficulty can be overcome by expansion into series form, which apparently Battan did not do, from which numerical values are obtained that are orders of magnitude smaller than those presented by Battan,

11

and which are in considerable disagreement with the available field data.

Ryan and Fish (1965) extended Battan's approach, utilizing what appeared to be a more realistic model. The temperature at the top of the column was maintained constant. The overturning of the column, initially having a superadiabatic lapse rate (assumed linear), then continued until the lapse rate became dry adiabatic. The equation for the change in internal and potential energy of the column, which energy is assumed to be converted initially into kinetic energy, was then determined to be:

$$E_a \simeq h^2 g P_o \; [(\nu_i C_p/g) - 1] \; (2RT_{o_i})^{-1} = \frac{h^2}{2} g \rho_a \; [(\nu_i C_p/g) - 1] \qquad (2)$$

where E_a = kinetic energy per unit surface area, h = height to which the superadiabatic lapse rate extends, g = gravitational acceleration, ρ_a = surface atmospheric density, P_o = atmospheric pressure at surface, ν_i = initial lapse rate, C_p = specific heat of atmosphere at constant pressure, R = universal gas constant divided by molecular weight, and T_{o_i} = initial temperature at surface. This equation says that the available kinetic energy per unit area column increases as the initial lapse rate becomes more and more super-adiabatic, as the height to which the superadiabatic lapse rate extends increases, and as the atmospheric surface density (or P_o/T_{o_i}) increases. Note also the dependence upon g, and C_p; and that E_a is most sensitive to h, varying with the square of this quantity. This equation was then equated to Flower's dust devil model, Equation (1), assuming that the energy input comes solely from the devil core to give:

$$v^2_{max} = h^2 g \; [(\nu_i/\nu_a) - 1] \; / \; h_d \; (0.5 + 2 \ln n) \qquad (3)$$

where v_{max} = maximum tangential (rotational) wind velocity developed in the dust devil.

There are several difficulties with the "overturning" approach to dust devil generation, which must be noted carefully. First it assumes that all kinetic energy appears initially as rotation (assuming otherwise creates considerable mathematical difficulty). This represents only some sort of upper bound to the degree of rotation produced, since it is known (Sinclair, 1966) that radial and vertical wind velocity components are present also. Second, the approach represents only a possible initial process in dust devil formation. That is, following initiation the dust devil will enter a "steady state" condition where it is extracting energy from the surrounding air at some rate and dissipating it upward at the same rate. The wind velocities produced will depend in some manner upon what the rate is. Third, the approach assumes kinetic energy is distributed uniformly over a height h_d. Fourth, this h_d is difficult to assess, since the only available measurements are for the height of the dust column and there need be no direct relation between dust height and height of rotary motion. Fifth, the equations tell the energy that is available for conversion to kinetic energy if overturning proceeds in a specified manner and to a specified degree. However, there is at present no knowledge regarding what this "manner" and "degree" may be. Finally, the approach disregards any other source of dust devil rotation energy. Of particular note is atmospheric vorticity whose possible role has been discussed by several investigators. Some of the early authors (Ives, 1947; Williams, 1948) recognized the role of small disturbances, such as local shear, in initiating dust devils. However, it has been only recently that a number of theoretical treatments on atmospheric convective vortices, such as by Dergarabedian and

Fendell (1967), Gutman (1957), and Kuo (1966, 1967), have appeared, which emphasized the possible importance of the general atmospheric vorticity – – that radial inflow associated with the upflow might concentrate atmospheric angular momentum, producing the large tangential velocities in the devil.

Theoretical and experimental studies of convection in a horizontal, thin layer of an initially irrotational fluid, with and without a mean horizontal flow, show that the predominant component of vorticity generated is oriented normal to the local gravity vector, i.e., overturning, with no organized vertical component. The studies which produce vertically oriented vortices are those which start with the fluid in solid rotation about a vertical axis. It is well known that in such a system, vertical motions are suppressed in the body of the fluid, and occur only at the axis of rotation and the radial boundaries (Taylor, 1917, 1921).

These studies imply, as Sinclair also suggests, that background vorticity is a necessary condition for convection to occur in the dust devil mode rather than the plume-bubble (thermal) mode. However, they shed little light on the origins of this vorticity. To help clarify the problem, it is of interest to consider the equation for the local change in the vertical component of vorticity in cylindrical coordinates, for axisymmetric flow. That is:

$$\frac{\partial \zeta}{\partial t} = \frac{\partial \tau\theta}{\partial r} + \frac{\tau\theta}{r} - u\frac{\partial \zeta}{\partial r} - w\frac{\partial \zeta}{\partial z} - \zeta\left(\frac{u}{r} + \frac{\partial u}{\partial r}\right) - \frac{\partial w}{\partial r}\frac{\partial v}{\partial z} \qquad (4)$$

where $\zeta \equiv \frac{1}{r}\frac{\partial}{\partial r}(vr)$ = vertical component of vorticity, u, v, w are velocity component in the r, Θ, z direction, τ_θ = tangential component of shearing stress, and for incompressible flow, which is assumed here after Sinclair,

14

$-(\frac{u}{r} + \frac{\partial u}{\partial r}) = \frac{\partial w}{\partial z}$. From this equation it can be seen that if the background flow is irrotational, then $\zeta \equiv 0$ everywhere, $\tau_\theta \cong 0$, and if no vortex is present initially, $\frac{\partial w}{\partial r} \frac{\partial v}{\partial z} = 0$. Under these conditions no vortex can subsequently form. However, if $\zeta \neq 0$ and over some area has the same sense, then an incipient updraft must be associated with convergence and advection of vorticity, and the spin up process will occur concurrent with the development of the updraft. This increased rotation will tend to suppress vertical motions locally except at the incipient core. As the vortex intensifies, the contribution of the twisting term will increase along with the other terms. Unless there is a significant change in the sense of ζ in the environment, the vortex will grow until the frictional dissipation balances the other terms.

In summary, current thought is that three conditions are necessary and sufficient for dust devil formation: 1) a superadiabatic temperature lapse rate extending from the surface to some height, 2) an appreciable amount of atmospheric vorticity, and 3) sufficiently light winds so as not to mechanically disrupt the vortex. However, the field experimental data have been insufficient in quality, quantity, and type to allow the pertinence of each to be evaluated and a quantitative model constructed.

3.0   EXPERIMENTAL APPROACH

3.1   Field Site

3.1.1   Choice of Site

Prior to the initiation of the program, a survey was made throughout Southern
and Central California to select a site which had the following characteristics:
a) numerous dust devils, b) easy availability, c) suitable for high speed
locomotion, and d) little or no surface relief, and a uniform surface type.
The reasons for desiring a) and b) are obvious; c) is needed for dust devil
penetration; and d) helps toward insuring uniformity in atmospheric conditions.
The site chosen was El Mirage Dry Lake in the Mojave Desert. This playa is
located between Palmdale and Victorville, California about 100 miles from
Santa Monica. It lies at an elevation of 944 meters and in a broad basin of
about 10 x 20 kms in size. The playa itself is exceedingly flat and devoid of
vegetation. The surrounding area is also quite flat and is sparsely populated
with sagebrush. The specific site chosen was just south of the south shore of
the playa. This choice was based on the considerations that very little dust
was present on the playa itself, and the playa surface was sufficiently hard and
compact to make the production of loose material a very difficult task.

El Mirage, in addition to possessing the above-noted desired characteristics,
has other advantages for dust devil studies. These are:

a)   A small airfield is located adjacent to the playa. The field is
     used for sailplane launching and hence aircraft are available for
     making temperature measurements to great height. In addition,
     the sailplane pilots can provide descriptive information from
     their flights over dust devils.

b) The general meteorology of the area is well known - - meteorological observations have been made for a number of years in association with glider launchings. In addition, Mr. John Aldridge, U. S. Weather Bureau, Los Angeles, has made detailed studies in the area.

c) Meteorological conditions in the area are quite variable - - the playa is located sufficiently close to the Transverse Range to be influenced by coastal weather patterns to a greater degree than the playas further inland. This means that dust devil generation can be studied under a variety of conditions, and hence information can be gained as to the conditions under which dust devils would not occur.

3.1.2 Site Preparation

The first step, after selection of the location of the measurement station, was to clear the surrounding area of all sage brush. The basic purpose of this was to obtain optimum locomotion capabilities. The cleared area was approximately 500 x 300 m^2 with the measurement station close to the center. The long dimension of the area was aligned perpendicular to the prevailing wind direction, and only dust devils in the cleared area were studied. The area was scraped, and then rescraped prior to each day's operation. This served to create a quantity of loose dust which acted as a tracer. The granular material produced consisted principally of fines, a few to a few tens of microns in diameter. However, significant amounts of larger grains, up to several hundred microns were also present. Surveyed stakes were placed at various locations in the area to aid in obtaining reasonably accurate estimates of dust devil distance (this allowed measurements of dust devil height, etc. to be obtained by angulation).

17

3.2 Measurement Rationale

It became evident, from study of the results obtained by previous workers, that certain important parameters relating to dust devils had not received sufficient attention, and that many data were needed. It was concluded that the most important quantities to measure were (a) atmospheric temperature, (b) atmospheric wind velocity and direction, (c) atmospheric vorticity, (d) wind velocities inside dust devils, (e) dust devil characteristics such as time of occurrence, location, duration, frequency, diameter, dust and billow heights, and direction of rotation, and (f) general meteorological conditions.

It was decided that atmospheric temperature should be measured from the surface to a height exceeding that at which the lapse rate ceased to be superadiabatic, and that the changes of the profile with time should be monitored. Preliminary studies indicated that measurements to 1500 meters above the surface should suffice. The measurements, at altitude, were made by means of a light aircraft. Continuous profiles were made (about 2 Km each horizontal pass), at heights of 1540, 920, 300, 150, and 77 meters. Temperatures below these levels were monitored by pole mounted sensors at 0.3, 1, 2, 4, 8 and 14 meters above the surface. Three to five minute averages of the pole temperatures were made every fifteen minutes. Each complete aircraft profile took about 20-30 minutes.

Continuous recordings of wind velocity and direction were made in the vicinity of the pole. Continuous recordings were also made of a specially designed "vorticity" meter which indicated atmospheric vorticity.

Recordings of dust devil wind velocities were made utilizing a portable two-axis hot wire anemometer. This device measured the vertical and tangential velocities, it being decided to rely upon Sinclair's (1966) work for estimates

18

of the much smaller radial velocity. The measurement procedure was as follows. Once a dust devil was spotted in the measurement area it would be pursued by car until the car was positioned down wind of the devil. The hot wire crew would then disembark, and align themselves in the devil's path. Immediately before penetration, the man holding the anemometer would align the anemometer, turn on the recorders, and drop to the ground allowing the devil to pass over him. The second man would help direct him to a proper penetration, obtain dust devil diameter and direction of rotation, and note any unusual characteristics of the devil.

Distance from the base station, time of occurrence, duration and diameter were recorded for all dust devils in the measurement area. The time of occurrence was entered directly onto the wind velocity-direction-vorticity record. Dust and billow heights were measured by theodolite (billow height is defined as the height at which the dust devil loses its well defined columnar structure, this being indicative of vortex breakdown). Direction of rotation, as well as being recorded by the hot wire crew, was recorded by four to five personnel spaced over the measurement area. The general meteorological conditions in the region were obtained from Weather Bureau charts.

3.3 Instrumentation

3.3.1 Temperature

Ground temperature was measured utilizing a full-immersion thermometer. This was placed, horizontally, immediately below the surface of the ground in the vicinity of the pole, and covered with a thin dirt cover (<1 mm). The dirt covering was formed to approximate the undisturbed surface as closely as possible. Checks of the thermometer readings against those of a radiometer indicated the thermometer read about 5°C lower than the actual surface temperature.

All pole sensors were Yellow Springs, Model 405, thermistors. These were capped with chrome plated copper cups to increase their time constant. With this arrangement, a time constant of 2 minutes in an 8 km hr^{-1} wind was attained. All thermistors were calibrated in a water bath using the 0.3 meter sensor as the standard. The same leads, and lead lengths, used in the field were utilized during the calibration. The calibration was good to about $\pm$ 0.1°C (relative to the reference sensor). All the pole sensors were radiation shielded from the sun and ground by four aluminum sheets arranged in pagoda fashion with the sensor being in the center. The plates were held in position, and separated, by lucite rods. A battery driven fan was mounted adjacent to each sensor for aspiration purposes. Utilizing these fans it was possible to maintain a 15-20 km hr^{-1} wind flow over the sensors. The sensor outputs were monitored with a Yellow Springs Multi-Channel, Multi-Probe Tele-Thermometer.

The aircraft sensor was also a Model 405 thermistor. It was attached to a wooden dowel which was itself mounted to the end of the pitot tube at the wing tip (the sensor protruded beyond the forward end of the pitot tube and the sensor element was directly exposed to the air flow). No radiation shielding was utilized. The sensor was monitored by a modified Yellow Springs Single Channel Tele-Thermometer and the output recorded with a D.C. operated Rustrak recorder (the Tele-Thermometer modification consisted of making its output compatible with the recorder). The aircraft sensor system was calibrated in the same manner as were the pole sensors, utilizing the 0.3 meter sensor as reference. The recorder itself could be read to about $\pm$ 0.3°C.

3.3.2 Background Wind Velocity and Direction

Background wind velocity was measured utilizing a modified Danforth/White Remote Reading Cup Anemometer. The modification consisted of increasing sensitivity at low wind velocities. Wind direction was measured utilizing a specially built vane mounted on a low-torque, continuous, linear potentiometer. Both measurements were made at a height of 2 meters above the surface and the outputs were recorded with an 8-channel Sanborn recorder.

3.3.3 Vorticity

Measurements of ζ_e (atmospheric vorticity) directly is a difficult task using standard instrumentation. In view of this a new type of sensor was designed. This instrument consisted of four 8 cm diameter styrofoam spheres mounted on the ends of two mutually perpendicular one meter rods. The intersection of these rods was mounted perpendicular to the shaft of a one turn, low-torque, continuous potentiometer wired as a voltage divider. The output voltage was continuously recorded with the 8-channel Sanborn recorder. Each arm was balanced and the device mounted two meters above the ground with the plane of the arms level. Wind tunnel tests showed that the device was insensitive to changes in wind direction and speed (below 65 km hr^{-1}) and responded only to horizontal gradients in horizontal velocity, or rotary motion (i.e. ζ_e). The starting threshold of the device is not known but appeared to be very low. With this "vorticity" meter, good indications of the sense and magnitude of the background rotation in the vicinity of the meter were obtained.

3.3.4 Wind Velocities in Dust Devils

A two axis hot wire anemometer was constructed to measure tangential and vertical wind velocities in dust devils. The basic sensor consisted of two

one mil platinum wires, 0.5 cm long mounted on Flowtronic Corporation tips.

Each wire was mounted perpendicular to the axis of a teflon tube about 3 cm

long and 1 cm in diameter. A perforated sphere was mounted surrounding each

tube, the purpose of the sphere being to produce an approximation to a cosine

law angular dependence. The purpose of the perforations was to decrease the

noise in the velocity measurements caused by shed eddies around the sphere.

The tubes were mounted at the ends of two colinear rods which were attached

to a two meter pole. With the pole in the vertical position the rods were

horizontal with one tube being aligned in the vertical direction and the other

horizontal, perpendicular to the rod axis. The alignment-for-measurement

procedure consisted thus of placing the pole in a vertical position and pointing

the rods at the dust devil center. The associated electronics, ambient temp-

erature compensation circuits, and recorders were mounted on the pole. The

entire system was calibrated by spinning it on a turntable at various, and

controlled, speeds. This calibration was good to about $\pm$ 0.2 Km hr^{-1}, within

the accuracy limitations of the field measurements themselves.

4.0   EXPERIMENTAL DATA AND INTERPRETATION

4.1   Basic Data

The basic temperature data are given in Volume II.   The data are for 11 days,
presented sequentially, which were the most suitable as regards uniform
meteorological conditions (essentially no cloud cover, winds not too strong,
very low humidity).   Data analysis, with one exception noted later, is limited
to these days.   The first graph for each day shows the aircraft temperature
profiles.   Following this, the complete temperature profiles versus height are
shown in time sequence.

The basic wind velocity, direction, and vorticity data are not presented since
they appear as continuous recordings, but peak wind velocities per two minute
interval, and smoothed wind direction plots are given following each set of
temperature profiles.   Derived vorticity data are presented in Sections 4.2.3
and 4.2.5.

Data concerning dust devil characteristics such as time, location of occurrence,
and diameter, are also shown in Volume II following each temperature set.
Additional data on duration, dust height, billow height, direction of rotation,
and form are not presented, but are discussed in the following sections where
applicable.

Dust devil penetration data are presented in Tables 1 and 2 (following immediately).
Table 1 represents those devils penetrated during the eleven days covered by
Volume II.   Table 2 gives data for devils penetrated on other days, the data
being utilized solely in the search for correlation between maximum tangential
wind velocity and devil diameter (Section 4.2.5).   In these tables v_{max} is the

Table 1

VALID DUST DEVIL PENETRATIONS, 1968

Date	Time PDT	Diameter (meters)	(1) v_{max} (km hr^{-1})	(2) w_{max} (km hr^{-1})	(3) Comments
3-28-68					
	1224	10	17	-	
	1235	6-8	11	-	
	1348	<1	-	2.5	
	1426	10	25	-	
5-3-68					
	1325	1	4.5	-	
	1336	8-10	32	-	
6-13-68					
	1308	2-3	≈4.6	≈2.6	Calibration base line uncertain
6-26-68					
	1100	<1	5.4	1.9	
	1110	1	11	3.5	
	1128	1	8.8	2.3	
	1137	<1	6.7	2.8	
	1144	<1	5.4	1.6	
	1156	2	9.4	1.6	
	1213	1	9.2	4.4	
	1225	<1	4.4	0.9	
	1229	3	13.0	6.5	
	1256	<1	10.5	5.9	

(1) maximum tangential velocity
(2) maximum vertical velocity
(3) The use of the word "ring" in the comments column indicates that a series of dust devils were traveling about a circle. The diameter given in this case is that of the circle.

Table 1 (Cont'd)

Date	Time PDT	Diameter (meters)	v_{max} (km hr^{-1})	w_{max} (km hr^{-1})	Comments
6-26-68 (cont'd)	1315	1	11.7	3.2	
	1327	3	14.4	3.2	
	1349	2	6.7	0.9	
6-27-68					
	1100	3-4	11.7	2.8	Confused structure
	1113	6-9	-	1.8	Confused structure
	1216	2	10	2.3	
	1223	6-8	12.5	0.7	
	1224	3	7.2	0.7	
	1231	2-3	9.4	1.2	
	1239	1	10.4	1.2	
	1241	4	7.5	1.2	
	1248	9	12.5	2.7	
	1306	5	8.0	1.9	
	1323	6-9	-	2.0	
	1352	9	-	1.5	Confused structure
	1358	13-17	20	2.3	Two join
	1424	10	20	1.2	
7-25-68					
	1205	2-3	19.4	1.7	
	1222	1-2	19.1	1.2	
	1225	1-2	15.1	1.9	
	1302	1-2	16.2	1.4	
	1305	1-2	17.6	0.7	

Table 1 (Cont'd)

Date	Time PDT	Diameter (meters)	v_{max} (km hr^{-1})	w_{max} (km hr^{-1})	Comments
7-25-68 (Cont'd)	1314	1-2	21.6	1.1	
	1317	1-2	14.4	3.0	
	1322	1	12.2	-	
	1330	<1	10.5	1.6	
	1347	2-3	11.7	2.3	Possibly more than one
	1355	3-4	-	0.9	Confused structure
	1356	1	11.7	0.9	
	1430	1	10.4	1.2	
	1430	1	16.9	2.3	
8-22-68					
	1222	1	10.4	2.7	
	1225	<1	9.9	1.5	
	1226	1-2	17.7	4.3	
	1234	2-3	17.7	1.9	
	1309	<1	14.9	4.3	
	1326	4	17.7	3.2	Ring
	1330	2-3	21.6	3.2	
	1352	1	7.2	3.7	
	1355	<1	11.5	6.5	
	1435	1-2	14.2	3.0	
	1528	1	4.0	1.6	
	1605	<1	3.4	2.3	
	1609	1	11	2.3	

Table 1   (Cont'd)

Date	Time PDT	Diameter (meters)	v_{max} (km hr^{-1})	w_{max} (km hr^{-1})	Comments
8-23-68					
	1050	2-3	22.1	1.2	
	1114	~7	21.6	6.8	Confused structure Uncertain diameter measurement
	1115	2-3	-	1.4	
	1125	4-6	10.8	1.4	Confused structure
	1129	2	10.4	0.7	
	1137	2-3	19.5	0.9	
	1147	2-3	-	1.6	Confused structure
	1332	1	14.3	3.2	
	1432	3	19.5	6.8	
	1433	<1	8.3	1.5	
	1456	5-6	21.6	5.4	Ring
	1458	4	13	2.7	Confused structure
	1508	<1	6.8	1.5	
	1524	<<1	5.9	1.8	
8-28-68					
	1129	1	9.4	<0.7	Vertical doubtful
	1132	<1	13.6	3.8	
	1134	1-2	26.1	1.6	
	1208	<1	16.4	2.0	

Table 1 (Cont'd)

Date	Time PDT	Diameter (meters)	v_{max} (km hr^{-1})	w_{max} (km hr^{-1})	Comments
8-28-68 (Cont'd)	1210	2	20.4	2.2	Ring
	1239	5	31.5	3.2	Ring
	1251	<1	12.2	2.5	
	1307	4-5	34.2	7.0	
	1311	4	31.7	7.2	
	1326	2	21.6	3.8	
	1358	<1	16.7	2.7	
	1404	1	13.7	2.7	
	1405	1	17.7	5.7	
	1500	<1	17.6	6.8	
9-5-68	1200	4	14.4	2.3	Ring
	1217	3	23.8	3.7	
	1234	5	14.4	1.8	Breaking up
	1306	5	14.4	3.2	Breaking up
	1342	5	18.5	7.2	
	1358	2-3	14.6	4.4	
	1413	3	8.3	1.3	
	1420	1	3.7	1.0	
	1451	<<1	7.2	< 0.7	
	1538	7	18	7.7	
	1606	2	15.8	2.9	
9-12-68	1128	1	14.4	4.3	

Table 1   (Cont'd)

Date	Time PDT	Diameter (meters)	v_{max} (km hr^{-1})	w_{max} (km hr^{-1})	Comments
9-12-68 Cont'd	1155	1-2	16.1	5.1	
	1207	<<1	9.5	4.6	
	1213	<1	9.0	2.5	
	1230	1-2	9.9	2.2	
	1233	1	6.7	2.2	
	1341	<1	9.2	7.8	Probe movement
	1349	2-3	9.9	0.9	Ring: No. of 0.5-1m DD
	1357	<1	9.5	0.7	
	1358	<1	10.8	2.3	
	1441	15	17.7	3.2	Ring: No. of 2-4m DD
	1457	2	14.4	1.2	
	1528	1	10.5	2.3	

Table 2

ADDITIONAL DUST DEVIL PENETRATIONS

(Utilized solely to search for correlation between maximum

tangential velocity, v_{max}, and dust devil diameter,

as a complete data set was not taken)

Date	Time PDT	Diameter (meters)	v_{max} (km hr^{-1})
7-27-67			
	1112	2	12
	1218	3-4	20
	1345	1-2	15
	1402	20	43
8-10-67			
	1115	2-3	23
	1149	2-3	15
	1152	3	18
8-24-67			
	1400	2	23
	1405	1	8
	1418	3	17
	1425	2	22
	1429	1-2	15
	1438	2-3	15
	1441	1-2	9
	1445	1-2	9

maximum tangential, and w_{max} the maximum vertical, wind velocity in the devil measured at a height of two meters.

Volume II contains plots of ΔT_s, $\Delta T_s/h_s$, ΔT, h, and dT/dZ for each day. These quantities, which serve to specify the temperature profiles in a quantitative fashion, are defined as follows. It was found that the temperature versus height profiles could be well approximated by a three layer model, the temperature lapse rate in each layer being taken as constant. The first layer, extending from the base thermistor (0.3 meters) to heights varying between about 5-10 meters above the surface, was always highly superadiabatic. The quantity ΔT_s represents the temperature difference between the top and base of this layer, h_s represents the layer thickness, and $\Delta T_s/h_s$ is thus the lapse rate (linear approximation). Choosing the base of this layer at 0.3 meters is, of course, artificial. However, the average temperature differences between 0.3 meters and the surface change quite slowly, with the layer variability occurring principally above 0.3 meters. Thus, this upper portion of the base layer can be used in the search for correlations between the variables (as will be seen such correlations are indeed present).

Overlying this base layer is a second layer which is also superadiabatic, but much less so. This layer typically has thicknesses ranging from one hundred to several hundred meters, the top being defined as the point where the lapse rate ceases to be superadiabatic. The temperature difference between the top of this layer and the 0.3 meter sensor is defined as ΔT, and the corresponding height as h. The second layer thickness (h_2) is thus ($h - h_s$), the temperature difference (ΔT_2) is ($\Delta T - \Delta T_s$), and the lapse rate (dT/dZ) is $\Delta T_2/h_2$.

4.2 Discussion of Data

4.2.1 Frequency of Dust Devil Occurrence

It was concluded, from the observations of previous investigators, that dust devil frequency was probably associated in some manner with the degree of atmospheric instability, and possibly associated with wind velocity, its variability, and vorticity. Accordingly, a search was made for such correlations.

The Figures on pp. 18-21, 32-35, 48-51, 68-71, 89-92, 108-111, 130-133, 160-163, 186-189, 210-213, and 238-241 of **Volume II** show dust devil counts, ΔT, h, ΔT_s, $\Delta T_s/h_s$ and dT/dZ as a function of time for the eleven days of measurement. Studies of these indicate that dust devil frequency increases as ΔT_s, or more particularly, as $\Delta T_s/h_s$ increases. No such correlation is evident for the other temperature parameters[*]. This was verified by computing dust devil frequency versus the various quantities, utilizing the above-referenced figures. The results for dust devil frequency versus $\Delta T_s/h_s$, the only direct correlation found, are presented in Table 3. This shows that frequency increases monotonically as $\Delta T_s/h_s$ increases, and thus that insofar as the temperature profile is concerned it is the highly superadiabatic, shallow (<10 meter) layer adjacent to the ground in which triggering occurs. Qualitatively one would expect this to be the case since the atmosphere is most highly unstable in this layer.

---

[*] Indications of a slight possible inverse correlation with dT/dZ can be noted. This is not a physically meaningful correlation, rather it can be explained as due solely to interaction between the $\Delta T_s/h_s$ and dT/dZ layers. As the surface is heated, $\Delta T_s/h_s$ increases. Eventually convection begins, transferring heat initially into the base region of the overlying layer, thus increasing dT/dZ and decreasing $\Delta T_s/h_s$. Subsequently, dT/dZ will tend to decrease as heat is transferred upward in the layer, while $\Delta T_s/h_s$ is increasing again.

Table 3

DUST DEVIL FREQUENCY VERSUS $\Delta T_s/h_s$, THE TEMPERATURE LAPSE RATE

IN THE SHALLOW (<10 METER) LAYER ADJACENT TO THE GROUND

$\Delta T_s/h_s$ ($^\circ C m^{-1}$)	0.10 to 0.15	0.15 to 0.20	0.20 to 0.25	0.25 to 0.30	0.30 to 0.35	0.35 to 0.40	0.40 to 0.45	0.45 to 0.50
D.D. rate (no. min^{-1}	.151	.388	.412	.457	.471	.507	.512	.584
% of time particular $\Delta T_s/h_s$ range was present	1.3	8.5	28.6	26.7	13.5	13.0	5.0	2.4

Total No. of Dust Devils in Sample = 1119

Total Counting Time = 2494 minutes (approx. 41.5 hrs.)

Next, attempts were made to determine whether atmospheric vorticity, wind, and wind variation correlated with dust devil frequency. This was done by holding $\Delta T_s/h_s$ constant and plotting dust devil frequency versus ten minute averages of the quantities $\Sigma|\zeta_e|$, ΣV, and their product. Here $\Sigma|\zeta_e|$ is the sum of the magnitudes of the vorticity meter movement in the ten minute interval, divided by time, which gives a measure of the amount of vorticity present; ΣV is the sum of the peak background wind velocities per two minute interval, divided by the number of intervals, which gives a measure of the mean background wind. No correlation was found. It would then appear that vorticity plays a minor role in determining dust devil frequency compared to that of $\Delta T_s/h_s$. However, much more detailed analysis of the records will be necessary to confirm this.

4.2.2 Dust Devil Diameter

The pages in **Volume II** referenced at the beginning of the previous section (4.2.1) show, among other things, dust devil diameter. Comparison of these diameters with the quantities ΔT, h, dT/dZ, ΔT_s and $\Delta T_s/h_s$ for each day indicate a possible correlation between ΔT_s, or more particularly $\Delta T_s/h_s$, and the diameter of dust devil that occurs. This correlation is shown in Figure 1. This figure shows all dust devils observed for which a good measure of diameter was obtained, except that only representative samplings are plotted in those areas of the graph where data point density is high. It is seen that the average dust devil diameter increases as $\Delta T_s/h_s$ increases. In particular, it is seen that for a given $\Delta T_s/h_s$ there is a maximum dust devil diameter that can occur with all smaller diameters possible, and that this maximum possible diameter increases as $\Delta T_s/h_s$ increases. There is also an indication of a low $\Delta T_s/h_s$ dust devil cutoff, no devils occurring for $\Delta T_s/h_s < 0.14°C \, m^{-1}$. Exactly

RM 30-692-9 (8-68)
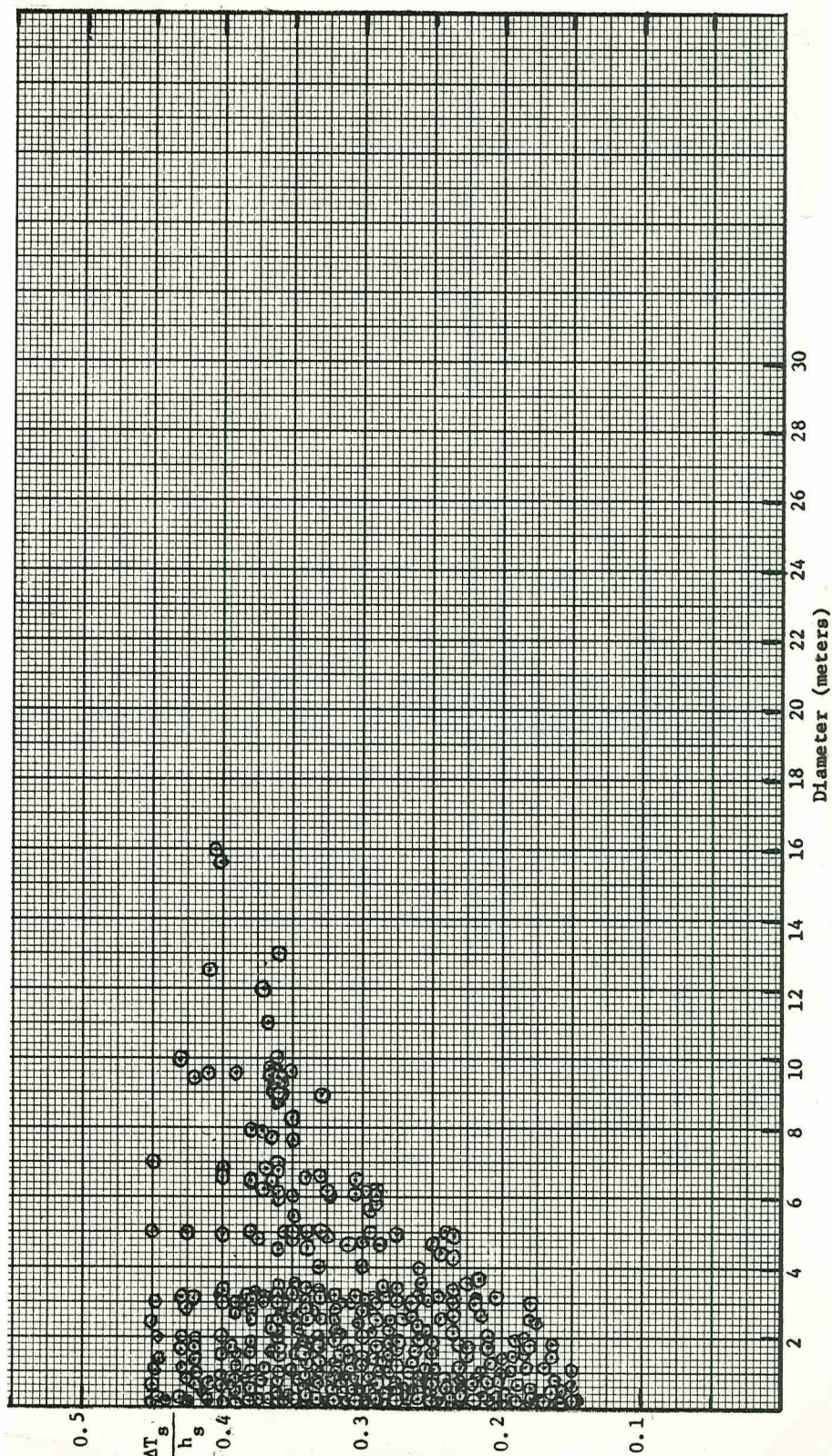
Figure 1: Dust Devil Diameter versus $\Delta T_s / h_s$ the Lapse Rate in Highly Superadiabatic Layer Adjacent to Surface

where the cutoff point is, however, is uncertain since the lowest $\Delta T_s / h_s$ observed was 0.13 and values less than 0.14 occurred for a total of only a few tens of minutes. Nevertheless, it seems reasonable to conclude from the figure that the cutoff point is not less than $\Delta T_s / h_s = 0.10°C \ m^{-1}$. This appears to demonstrate the requirement of a superadiabatic lapse rate for dust devil generation (note that $\Delta T_s / h_s = 0.10$ is still highly superadiabatic).

In summary, these findings show that the shallow, highly superadiabatic layer adjacent to the surface plays a dominant role in determining the maximum dust devil diameter that can be produced (it also, as seen from the previous section, determines dust devil frequency). It is hence concluded that dust devil generation occurs in this base layer. The relationship between $\Delta T_s / h_s$ and dust devil diameter can be explained qualitatively in the sense that as the temperature lapse rate in the base layer increases, an air parcel accelerated upward (by bouyancy forces) can more easily trigger adjacent parcels to move upward; also, the disturbance can be effective in triggering to a greater distance from the source parcel, the exact distance being influenced by other factors such as wind and vorticity (further data analysis is required to evaluate the precise role of these other factors).

4.2.3 Direction of Dust Devil Rotation

Table 4 shows the data pertaining to direction of dust devil rotation, background wind velocity, and the correlation coefficients between dust devil rotation direction and vorticity sense, for the days in which sufficient data were obtained. In this Table, Column 1 is the total number of dust devils observed in the counting area, Columns 2 and 3 give the direction of rotation for those measured (direction of rotation was obtained by observers immediately

Table 4

DIRECTION OF DUST DEVIL ROTATION, BACKGROUND WIND VELOCITY
AND CORRELATION COEFFICIENTS BETWEEN
DUST DEVIL ROTATION AND VORTICITY

Date	1. Total D.D.	2. CW	3. CCW	4. $\overline{V}_{peak}$ (km hr^{-1})	5. $\overline{\Delta V}_{peak}$ (km hr^{-1})	6. Correlation Coefficient			
						Total Sig.	All	Near Sig.	All
6-13-68	23	3	8	24.2	5.5	+.33	+.30	+1.0	+0.8
6-26-68	88	31	19	9.3	4.9	.14	.11	.18	.21
6-27-68	118	32	31	25.4	4.6	.44	.33	.48	.43
7-25-68	222	59	64	18.3	6.3	.55	.45	.80	.70
8-22-68	157	44	29	12.2	3.6	.35	.25	.55	.40
8-23-68	119	33	45	18.2	4.2	.40	.30	.40	.33
9-5-68	126	23	43	16.9	4.1	.24	.20	.33	.29
9-12-68	158	38	52	10.6	3.3	.33	.24	.30	.20

adjacent to, or in, the dust devil), Column 4 gives the peak background wind velocity in a two minute period averaged over the whole observational period, Column 5 gives the averaged net change in peak background wind between the same two minute periods, and Column 6 gives the correlation coefficients between direction of vorticity meter and dust devil rotation. The sub-headings under Column 6 are defined as follows: total = all measured dust devils in the counting field (500 x 300 m^2); near = those within 100 m of the station; sig. = correlations computed using only those dust devils that occurred during periods of measurable vorticity meter rotation; and all = all dust devils regardless of whether vorticity meter rotation could be measured.

It is seen that there is a definite correlation between direction of dust devil and vorticity meter rotation, the correlation improving with decreasing dust devil distance from the station and with increasing background wind velocity. This indicates that atmospheric vorticity determines the direction of dust devil rotation.

4.2.4 Dust Devil Vertical Wind Velocity (w)

The data for the maximum vertical velocities (w_{max}) in dust devils are given in Table 1. The purpose of this section is to determine the functional relationship, if any, between w_{max} and the other parameters measured (though the profile of w through the dust devil was recorded it was decided to utilize w_{max} since is the most easily definable quantity). The approach used is to first find correlations between w_{max} and the other variables, second, determine the exact functional dependence involved, and third, complete the solution through dimensional analysis based on the results of others relating to convective processes in the atmosphere. The solution obtained pertains directly only to w_{max} at a height of 2 meters (measurement height). However, it is applicable to w_{max} in

the entire dust devil column since Sinclair (1966) has shown that there is little change in w_{max} between 2 and 10 meters, and even at a few kilometers above the surface w is down by only a factor of about two to three.

The variables upon which the vertical wind velocities in dust devils may depend are: the temperature lapse rates, the heights to which the lapse rates are superadiabatic, the ΔT's or temperature excesses involved, dust devil diameter, gravitational acceleration (g), atmospheric density (ρ), and viscosity-friction effects (g and ρ are obviously constants for the data, and viscosity-friction effects are included implicitly in the data). Attempts were first made to determine whether w_{max} correlated in any physically acceptable manner with ΔT_2, $\Delta T_s/h_s$ (h_s varied so little that it was not considered independently), h_2 and dT/dZ, holding dust devil diameter constant. Diameter ranges of <1m, 1-2m, 2-4m, and greater than 4m were chosen. The results are shown in Table 5. In each diameter group for which sufficient samples are available, the Table shows an average w_{max} for a range of values of the independent variable. The numbers in brackets following each w_{max} value are the number of samples involved in the averages: three samples per average was considered marginally acceptable. Averages were utilized since the data show a fair amount of scatter. This scatter was expected because (1) temperature profiles were taken only at ~15 minutes intervals (for practical reasons) which means that the temperature profile at the exact moment of dust devil occurrence can only be approximated, and (2) the profiles were obtained at one point in the working area, and there is no assurance that conditions were exactly the same in other portions.

It is seen, Table 5, that there is no correlation between w_{max} and ΔT_2; there appears to be a slight inverse correlation between w_{max} and $\Delta T_s/h_s$ particularly

(Numbers in brackets represent
number of samples)

d (meters)	w_{max} (km hr⁻¹) Ave.	ΔT_2 (°C)	w_{max} (km hr⁻¹) Ave.	$\frac{\Delta T_s}{h_s}$ (°C m⁻¹)	w_{max} (km hr⁻¹) Ave.	h_2 (m)	w_{max} (km hr⁻¹) Ave.	$\frac{dT}{dZ}$ (°C m⁻¹)
< 1	3.3(7)	1.6-2.5	2.8(6)	.16-.20	3.1(10)	101-200	1.8(8)	.0106-.0115
	2.5(4)	2.6-3.5	2.4(8)	.21-.25	-	201-300	3.6(6)	.0116-.0125
	2.8(7)	3.6-5.5	2.9(9)	.26-.30	-	301-400	3.8(3)	.0126-.0135
	2.5(6)	5.6-7.5			2.9(10)	401-500		
1-2	2.2(4)	1.6-2.5	2.8(7)	.16-.20	2.8(9)	101-200	2.0(20)	.0106-.0115
	3.0(8)	2.6-3.5	2.8(8)	.21-.25	-	201-300	2.4(4)	.0116-.0125
	2.9(5)	3.6-4.5	2.3(12)	.26-.30	2.5(5)	301-400	2.2(3)	.0126-.0135
	2.3(13)	4.6-5.5	2.1(5)	.31-.35	2.4(11)	401-500	3.6(4)	.0136-.0145
	1.4(5)	5.6-6.5	1.3(5)	.36-.40	1.6(7)	501-600	-	.0146-.0155
	2.3(3)	6.6-7.5					3.4(3)	.0156-.0165
							3.9(3)	.0166-.0175
2-4	3.1(4)	2.1-3.0	3.7(10)	.21-.25	2.9(4)	101-200	1.8(15)	.0106-.0115
	3.7(7)	3.1-4.5	2.0(12)	.26-.30	4.2(6)	201-300	2.3(9)	.0116-.0125
	2.3(9)	4.6-5.5	3.0(6)	.31-.35	1.7(3)	301-400	3.2(4)	.0126-.0135
	1.3(6)	5.6-6.5	1.5(4)	.36-.40	2.2(10)	401-500	4.0(3)	.0136-.0145
	3.0(6)	6.6-7.5			2.3(9)	501-600		
> 4			2.7(3)	.21-.25	-	101-200	1.6(7)	.0106-.0115
			4.2(4)	.26-.30	3.4(4)	201-300	4.2(10)	.0116-.0125
			-	.31-.35		301-400		
			3.1(4)	.36-.40	2.4(5)	401-500		
			2.1(3)	.41-.45	3.4(5)	501-600		

for dust devils with $d \geq 1$ meter; w_{max} tends to decrease as h_2 increases; and finally a rather clear cut direct correlation between w_{max} and dT/dZ can be seen. The possible inverse correlation with $\Delta T_s/h_s$ can be excluded from consideration since it is opposite to the behavior expected of a causal mechanism and because, as noted previously, the $\Delta T_s/h_s$ and dT/dZ layers appear to interact roughly in an inverse manner. Inspection of Table 5 also reveals that, no matter which parameter is held constant, there is no correlation between w_{max} and d. It therefore appears that w_{max} is primarily dependent upon dT/dZ with a possible additional dependence upon h_2 (note that h_2 actually appears implicitly in dT/dZ).

Accordingly, a search was made for possible correlations between w_{max} and the product $h^n (dT/dZ)^m$ where n and m are constants to be determined. Values of n and $m > 2$ were quickly found unacceptable; also, it is evident from Table 5 that $m > 0$. The combinations then tried were the applicable combinations of $n, m = \pm 2, \pm 1.5, \pm 1, \pm 0.5, 0$. It was found that a definite correlation was present only for $h_2^{\frac{1}{2}} dT/dZ$, w_{max} increasing as this product increased. All the data points for this function (for $d \geq 1$ meter) are shown in Figure 2a. Figure 2b shows the average values for w_{max}, averaged over $h_2^{\frac{1}{2}} \frac{dT}{dZ}$ intervals of 0.02 ($^\circ C\ m^{-1/2}$). The plot is quite linear and intersects the origin, qualifications necessary for the correlation to be correct. Figures 3a, 3b, and Figures 4a, 4b, show the products $h_2\ dT/dZ$ (which is simply ΔT_2) and $h_2\ (dT/dZ)^{1/2}$ versus w_{max}. These show how rapidly the correlation disappears as n and m depart from the values $n = \frac{1}{2}$ and $m = 1$.

As a final check that $h_2^{\frac{1}{2}} dT/dZ$ completely expressed the w_{max} dependence on the variables considered, the quantities d and $\Delta T_s/h_s$ were plotted as a function of w_{max}, holding $h_2^{\frac{1}{2}} dT/dZ$ constant. Table 6 shows w_{max} versus d and it is seen

41
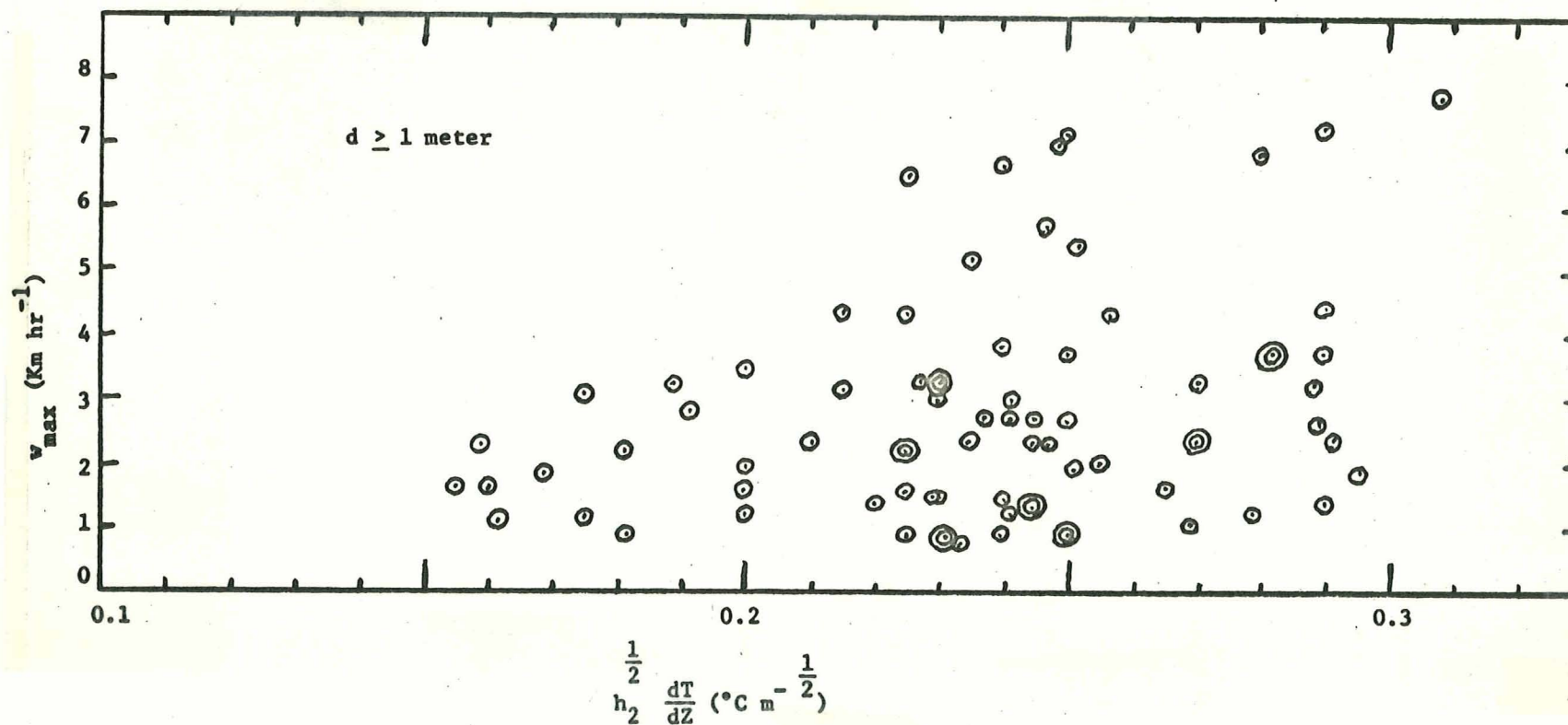
Figure 2a: w_{max} versus $h_2^{1/2} \frac{dT}{dZ}$. w_{max} = maximum vertical wind velocity in dust devil, h_2 = thickness of superadiabatic layer overlying highly superadiabatic surface layer, and dT/dZ = lapse rate in h_2 layer. Minimum measurable w_{max} = 0.7 km hr^{-1}.
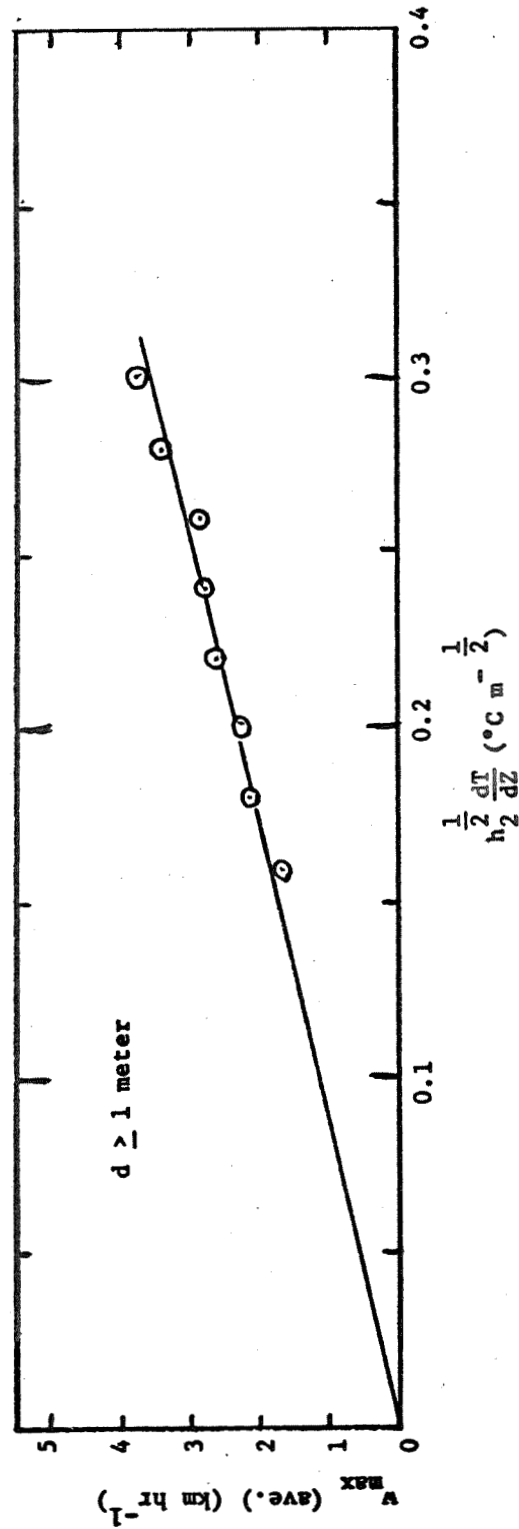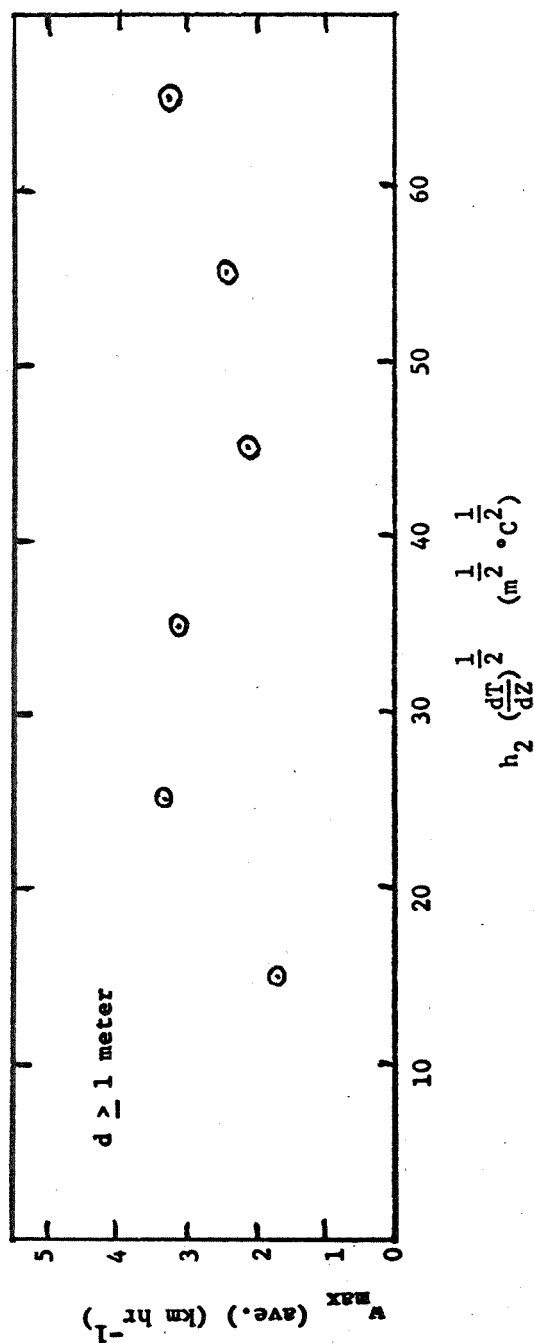
Figure 2b: Average values of w_{max} for 0.02 °C m$^{-1/2}$ intervals of $h_2^{1/2} \frac{dT}{dZ}$. Note linear relationship and that the curve passes through the origin of coordinates, indicating a real correlation.
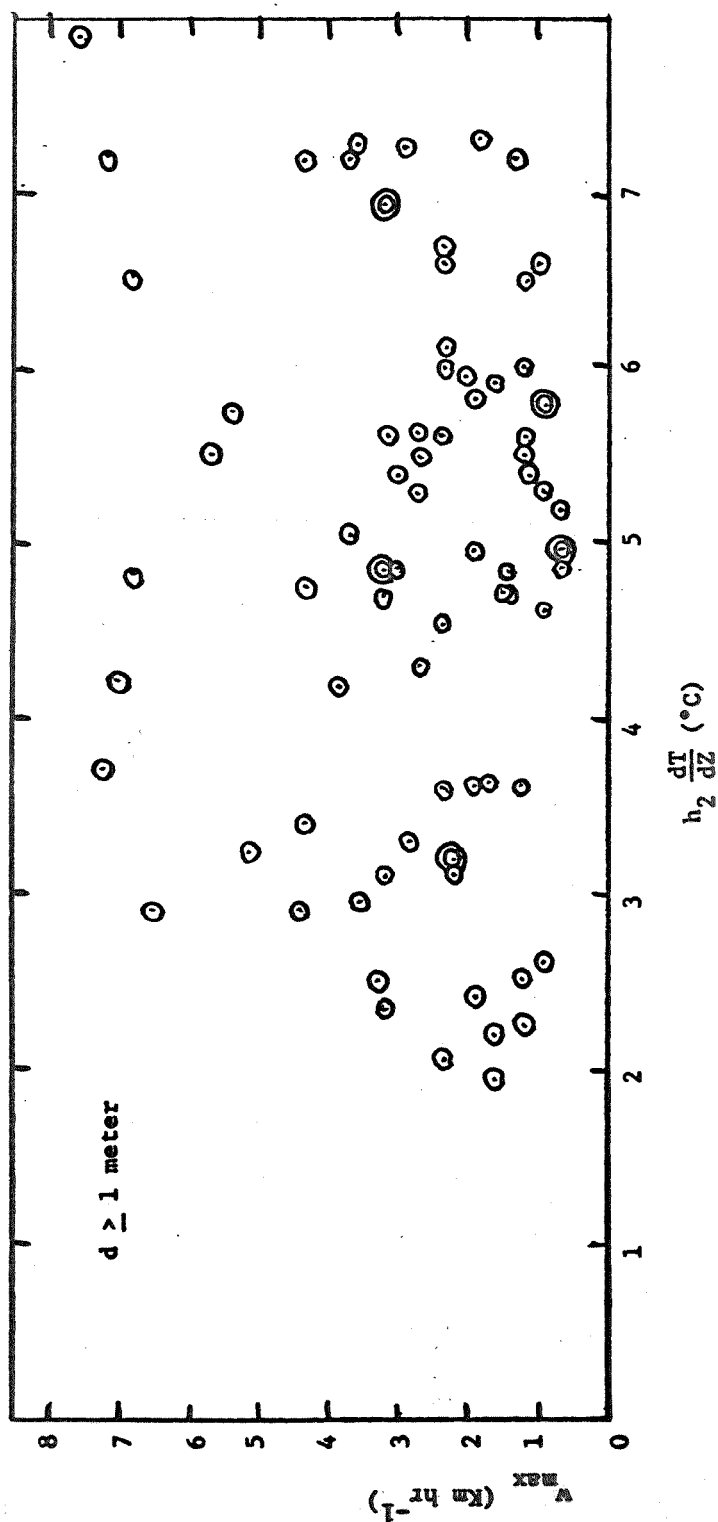
Figure 3a: w_{max} versus $h_2 \frac{dT}{dZ}$. w_{max} = maximum vertical wind velocity in dust devil, h_2 = thickness of superadiabatic layer overlying highly superadiabatic surface layer, and dT/dZ = lapse rate in h_2 layer. Minimum measurable w_{max} = 0.7 km hr^{-1}.
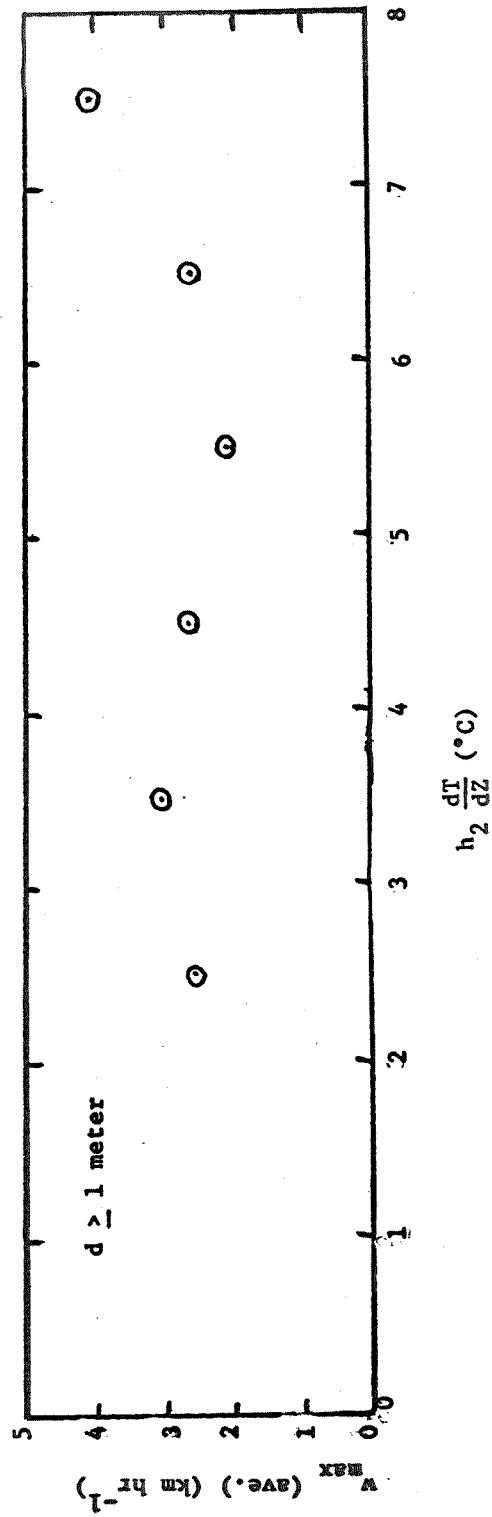
Figure 3b: Average values of w_{max} for 1°C intervals of $h_2 \frac{dT}{dZ}$. No correlation is evident.
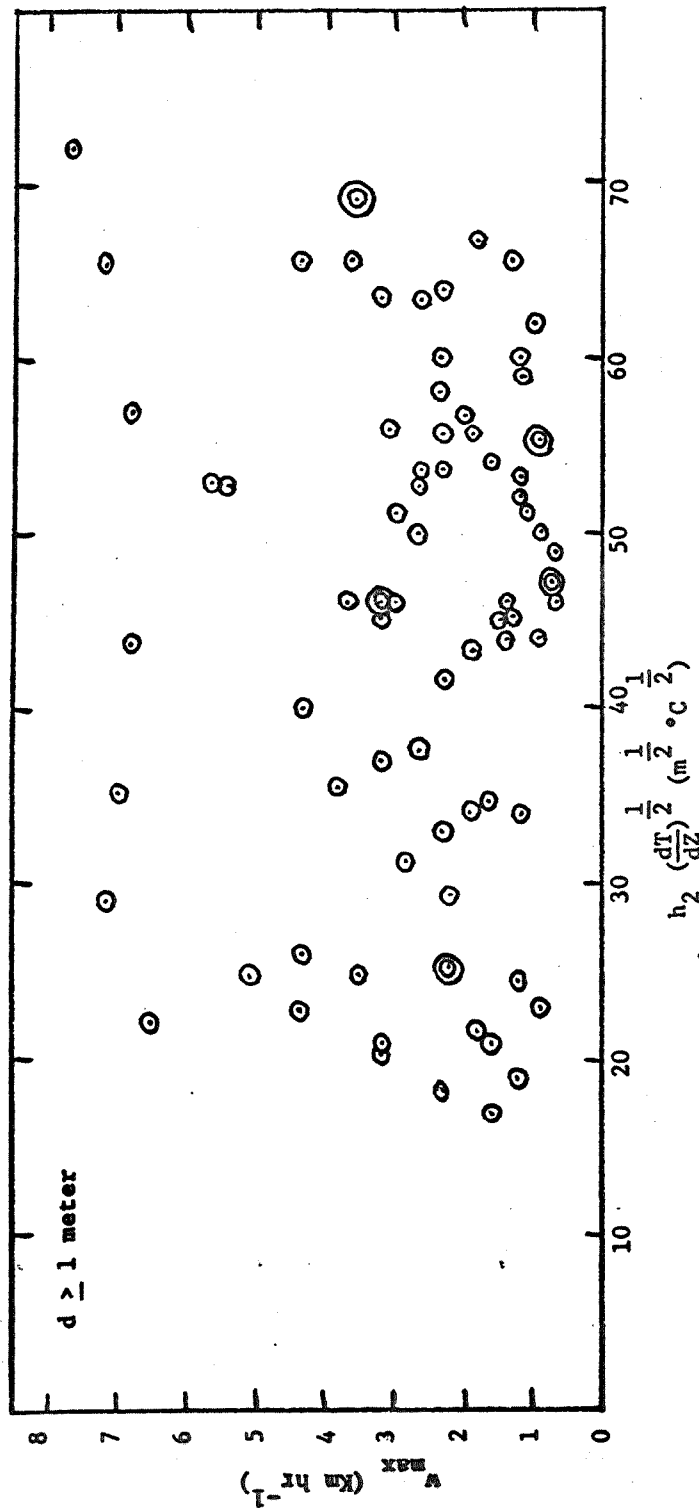
Figure 4a: w_{max} versus $h_2 \left(\frac{dT}{dZ}\right)^{1/2}$. w_{max} = maximum vertical wind velocity in dust devil, h_2 = thickness of superadiabatic layer overlying highly superadiabatic surface layer, and $\frac{dT}{dZ}$ = lapse rate in h_2 layer. Minimum measurable w_{max} = 0.7 km hr^{-1}.

Figure 4b: Average values of w_{max} for 10 $m^{1/2}$ $°C^{1/2}$ intervals of $h_2 (\frac{dT}{dZ})^{1/2}$. No correlation is evident.

Table 6

$$w_{max} \text{ VS. d FOR CONSTANT } h_2^{\frac{1}{2}} \frac{dT}{dZ}$$

(Numbers in brackets represent

number of samples)

$h_2^{\frac{1}{2}} \frac{dT}{dZ}$ (°C m$^{-\frac{1}{2}}$)	d (meters)	1-2	2-4	> 4
.16-.20		2.1(6)	1.9(7)	1.5(3)
.21-.25		2.5(24)	2.7(15)	2.7(6)
.26-.30		2.6(7)	3.0(12)	3.0(7)

that there is no correlation. The quantity $\Delta T_s/h_s$ still, however, shows a slight possible inverse correlation (not shown) with w_{max}. This is not considered to be a direct functional dependence for reasons given earlier. These results demonstrate that, whereas the highly superadiabatic layer adjacent to the surface controls dust devil generation, the resultant vertical velocity is controlled by the overlying, thick, moderately superadiabatic layer.

In order to obtain the complete expression for w_{max} it is necessary to utilize dimensional analysis, considering the additional variables (g, ρ, etc.) noted earlier. This gives, in the simplest and most realistic form

$$w_{max} = (const.) \; g^{\frac{1}{2}} \; h_2^{\frac{1}{2}} \; \frac{dT}{dZ} \; / \; \gamma_a \tag{5}$$

where γ_a = dry adiabatic lapse rate.

Other forms require additional length factors, but no correlations with length other than $h_2^{\frac{1}{2}}$ have been found. It is therefore concluded that the above equation correctly represents the maximum vertical wind velocity in dust devils.

This equation is quite similar to that given by Sutton (1953, p. 150) for bouyant air parcels breaking through more stable air layers and subject to bouyancy and drag forces, with h_2 representing a mixing length. The principal difference is that dT/dZ appears to the first rather than the one half power. Why this difference in power should exist is not clear, but it may result, in some manner, from the highly organized structure of dust devils. As far as h_2 is concerned, field observations have shown that dust devils maintain their columnar structure to heights equal to or somewhat greater than h_2, the structure becoming confused and the motion turbulent above this. Physically, this is to be expected since it is at the top of the superadiabatic layer that bouyancy forces begin to decrease. For these reasons, it appears that h_2 should be a good measure of dust devil mixing length.

4.2.5 Dust Devil Tangential Wind Velocity (v)

The data for the maximum tangential velocities (v_{max}) in dust devils are given
in Tables 1 and 2. The purpose of this section is to determine the functional
relationship, if any, between v_{max} and the other parameters measured. The
variables upon which v_{max} may depend are: the temperature lapse rates, the
heights to which the lapse rates are superadiabatic, the vertical wind velocity
in the dust devils, dust devil diameter, atmospheric vorticity (ζ_{ℓ}), thickness
of the inflow layer, g, ρ, and viscosity-surface friction effects.

Attempts were first made to see whether v_{max} correlated with w_{max}, correlation
being expected from continuity considerations. This was done considering all
diameters (w_{max} had been found to be independent of diameter) and for all back-
ground vorticities (it being assumed that differences in background vorticity,
if involved in the magnitude of v, would cause only random scatter in the plot).
The results are shown in Figures 5a and 5b. It is seen that v_{max} increases
as w_{max} increases, possibly in a linear fashion. Next, v_{max} was plotted
versus d, Figures 6a and 6b, correlation also being expected from continuity
considerations. A definite correlation is seen, v_{max} increasing as d increases.
No correlation was evident, however, for $\Delta T_s/h_s$.

Attempts were then made to determine the manner in which the product $w_{max}^n d^m$
correlated with v_{max}. The values of n and m chosen for test, on the basis
of the indications shown by Figures 5a, b and 6a, b, were combinations of 1/2,
1, 3/2 and 2. Two dust devils in Table 1 were excluded from consideration:
6-13-68, 1308 PDT for which the v_{max} calibration base line is uncertain; and
9-12-68, 1441 PDT which was a grouping of moderately sized (2-3 m) dust devils
in a 15 meter ring (though several dust devil rings were observed during the
program this is one of the few where the secondary whirl diameter was an
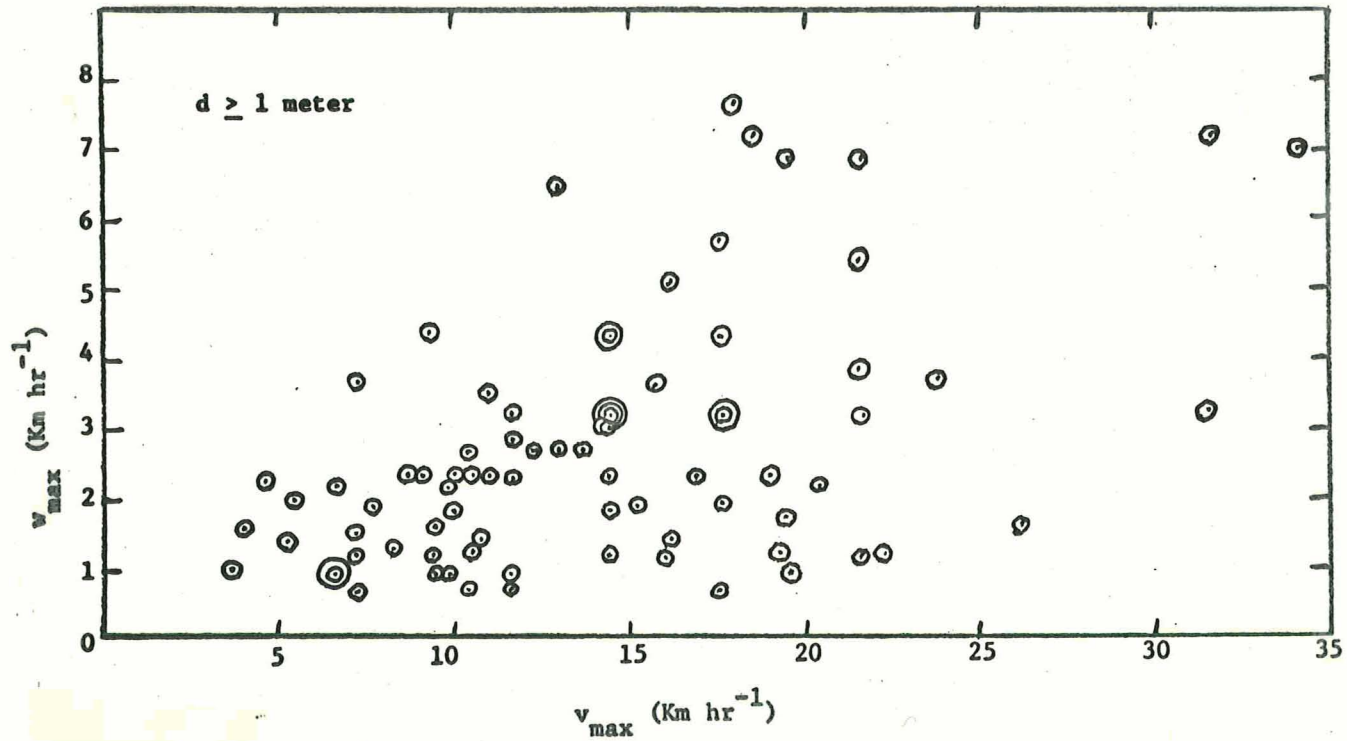
Figure 5a: w_{max} versus v_{max}. w_{max} = maximum vertical wind velocity in dust devil, and v_{max} = maximum tangential (rotational) wind velocity in dust devil.
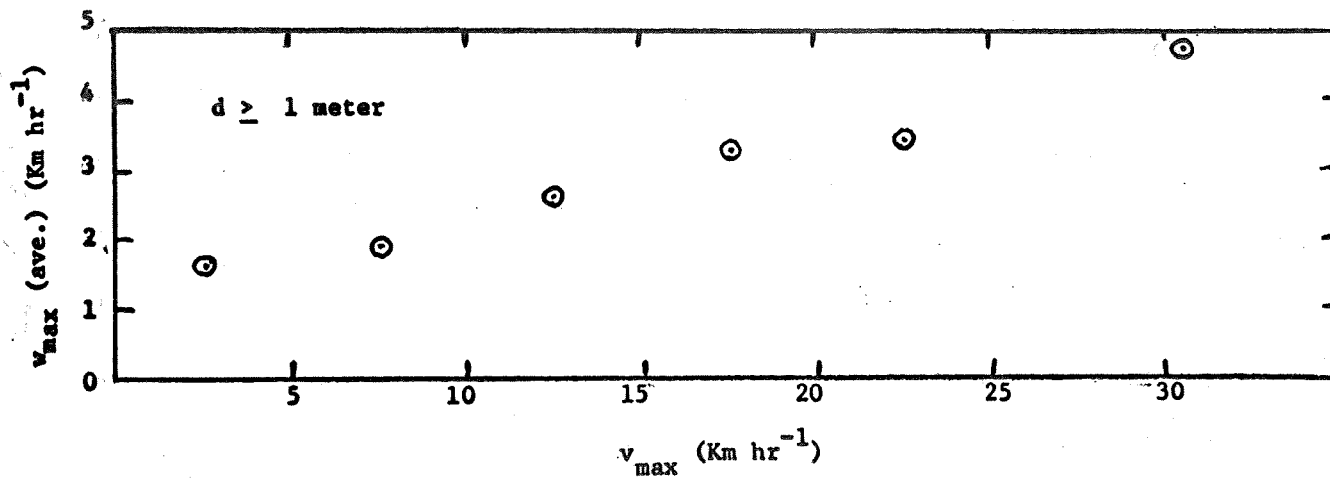
Figure 5b: Average values of w_{max} for 5 km hr^{-1} intervals of v_{max} (except that $25 \le v_{max} \le 35$ has been taken as one interval). Note correlation.
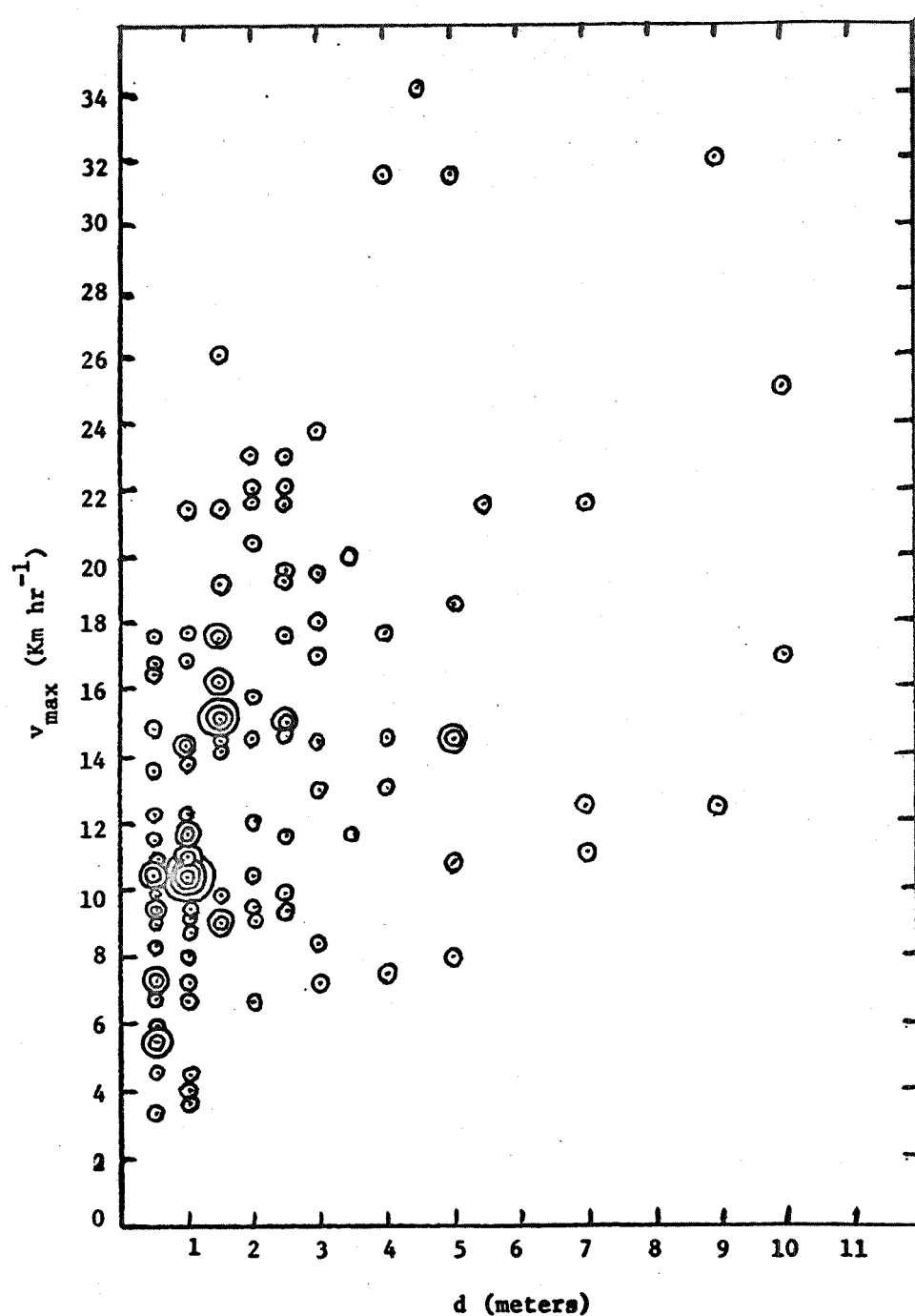
Figure 6a: v_{max} versus d. v_{max} = maximum tangential (rotational) wind velocity in dust devil, and d = dust devil diameter.
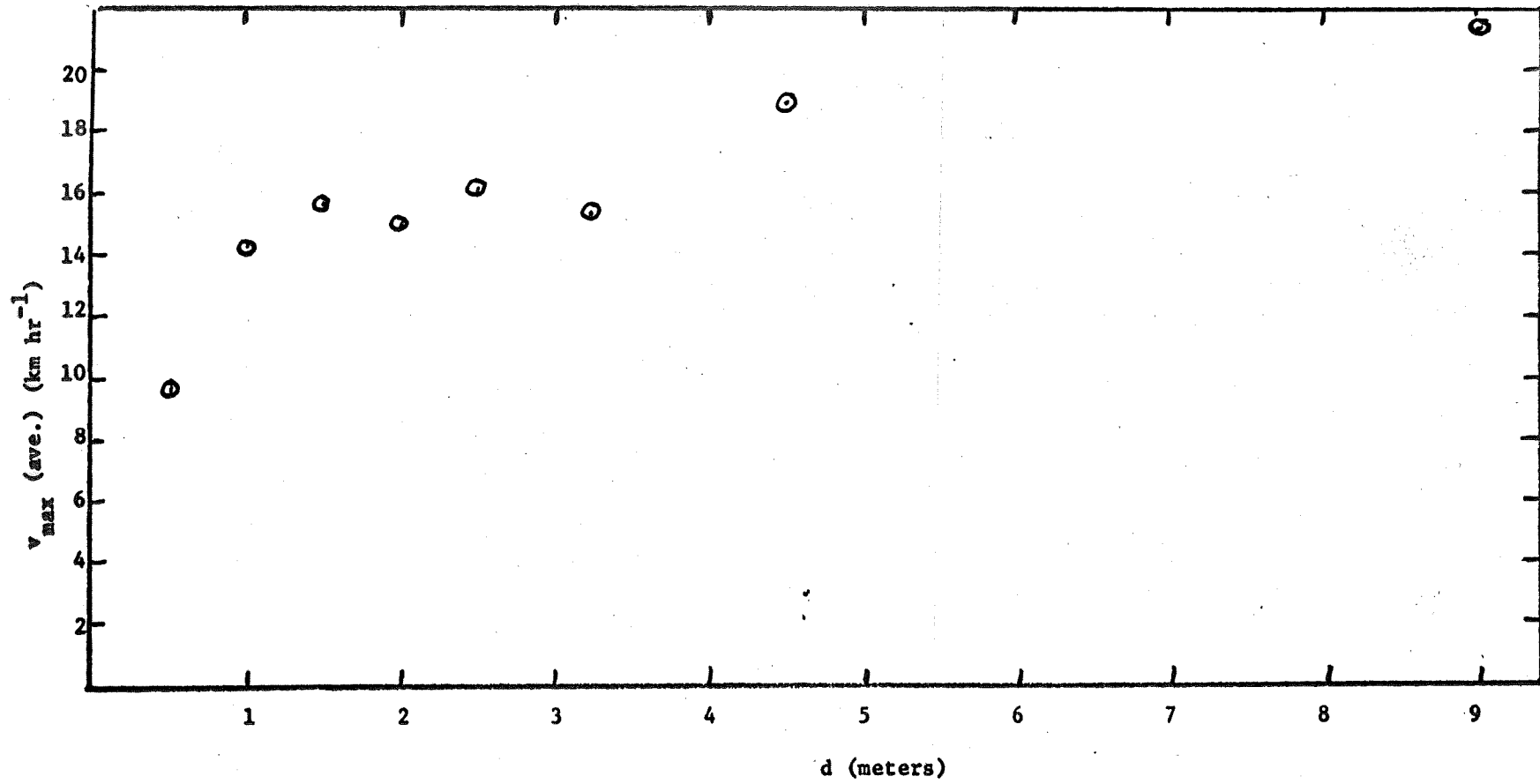
Figure 6b: Average values of v_{max} versus dust devil diameter. The averages were obtained in the intervals (or regions): $d < 1$, 1, 1.5, 2.0, 2.5, 3-4, 4-5, and 5 meters. Correlation is evident.

appreciable fraction of the primary diameter, indicating that a significant amount of the total rotational energy was in the secondary whirls). A distinct direct correlation between v_{max} and $w_{max} d^{1/2}$ was found (Figures 7a and 7b). Figure 7b shows that the functional dependence is linear; also that the plot passes through the origin of coordinates. None of the other values of n, m showed any signs of correlation except $w_{max} d$. This is shown in Figure 8. It is evident, however, that increasing d from the half to first power produces a notable increase in scatter. Accordingly, it is concluded that $w_{max} d^{1/2}$ is the correct correlation.

Once the correlation was found, attempts were again made to find correlations between v_{max} and $\Delta T_s/h_s$, also with h_2 and dT/dZ (in case the entire functional dependence upon these later quantities was not contained in w_{max}), holding $w_{max} d^{1/2}$ constant. Sample results are shown in Figures 9 and 10. No correlations were found.

Finally, attempts were made to determine whether any correlations existed between v_{max} and vorticity or wind velocity. For this, four measures of vorticity were used, each being determined for a four minute period centered on the time of dust devil penetration. The first measure was the maximum rate of vorticity meter rotation in the direction of dust devil rotation (ζ_1), the second was the maximum rate of vorticity meter rotation regardless of sign (ζ_2), the third was the sum of the magnitudes of all vorticity meter rotations during the period (ζ_3) (this being a measure of the variability in the interval, or the higher frequency rotational energy flowing through the area), and the fourth was the net rotation (algebraic sum) of the vorticity meter rotations (ζ_4) (giving a measure of the very low frequency rotational energy flowing through the area). Two measures of wind velocity, peak (ΣV) and mean (V_{ave}), were used.
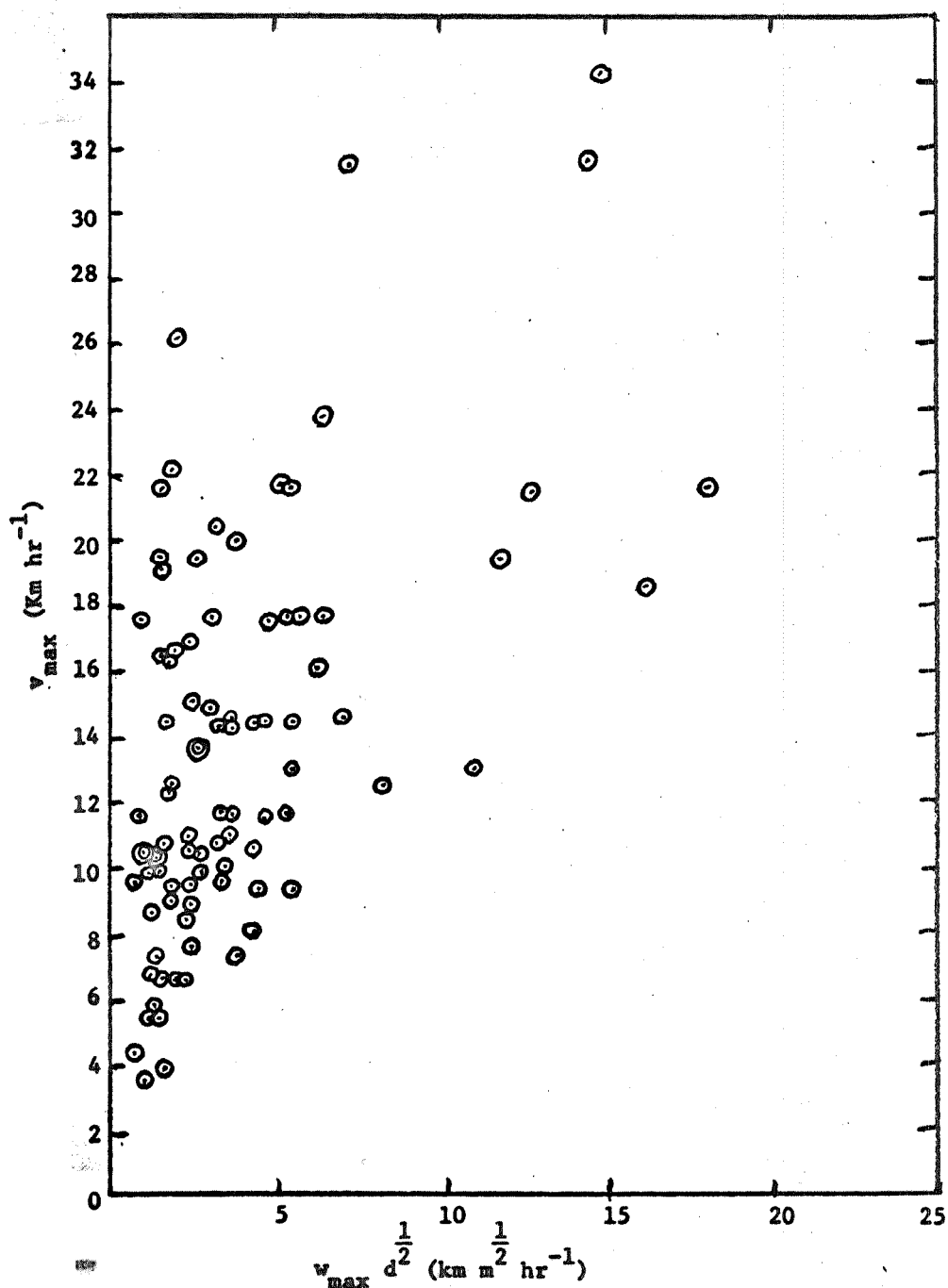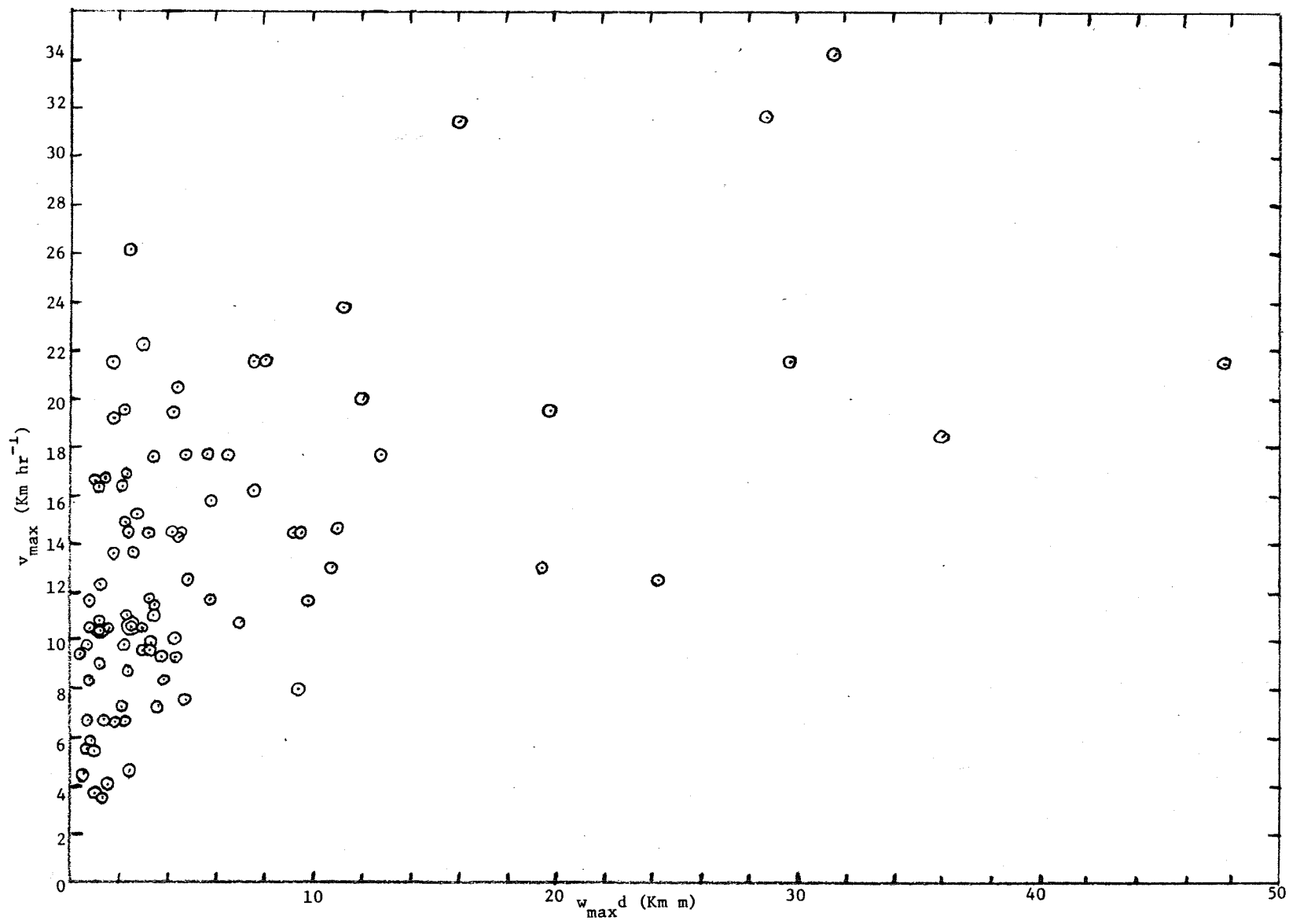
RM 30-692-6 (8-68)

Figure 7a: v_{max} versus $w_{max} \, d^{1/2}$. v_{max} = maximum tangential (rotational) wind velocity in dust devil, w_{max} = maximum vertical wind velocity in dust devil, d = dust devil diameter.
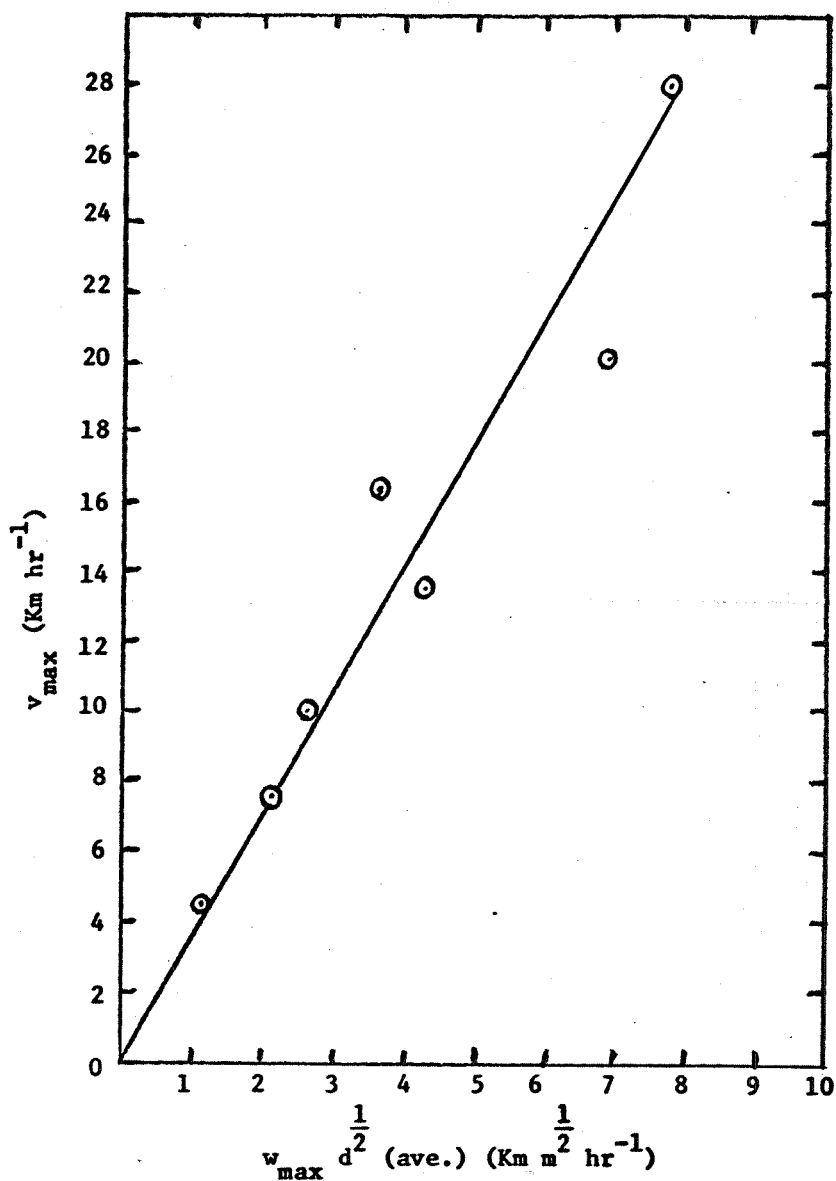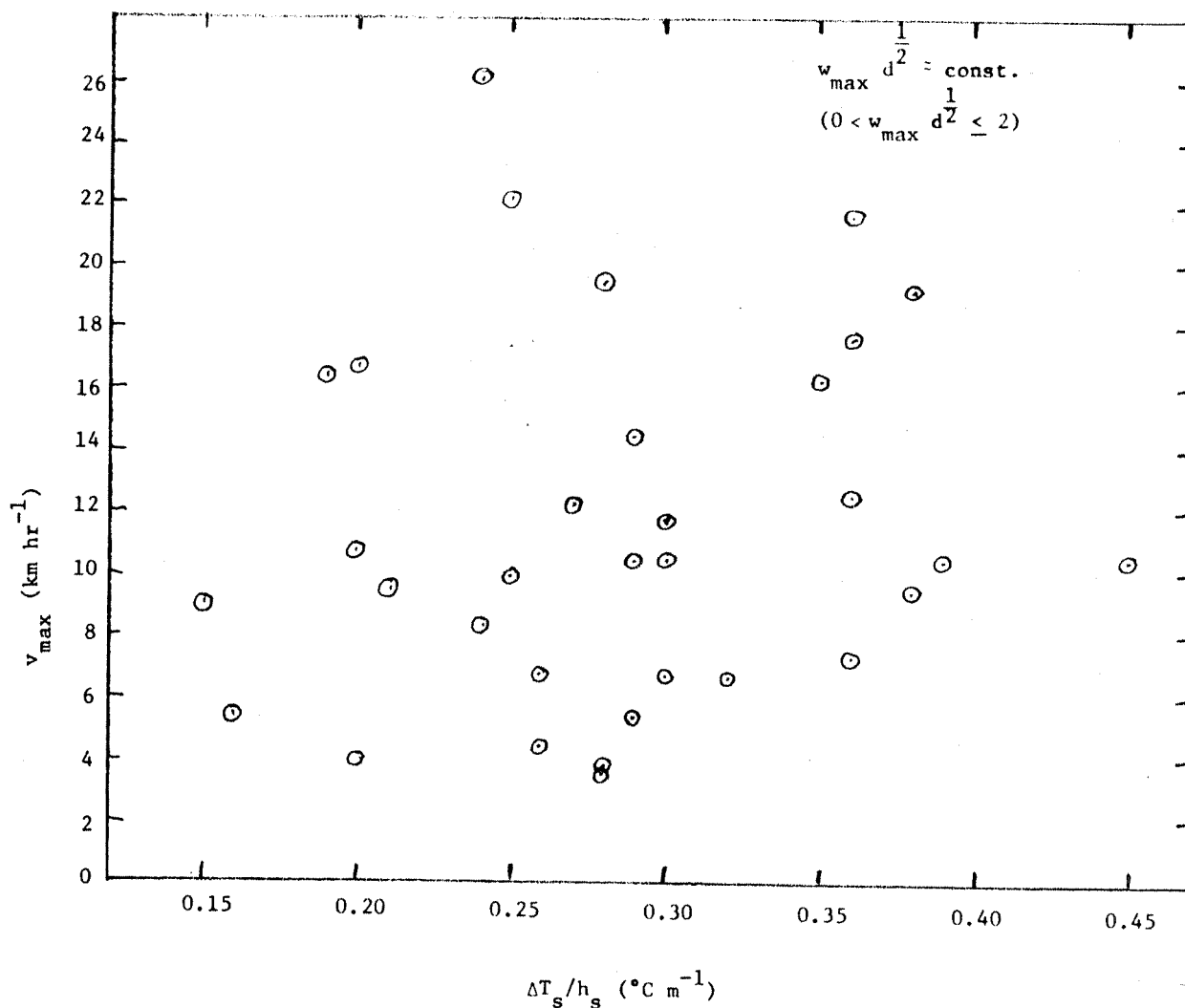
Figure 7b: Average values of $w_{max} \, d^{1/2}$ for 3 Km hr^{-1} intervals of v_{max} (except that for $v_{max} > 18$ km hr^{-1} the intervals utilized are 18-22 km hr^{-1} and > 22 km hr^{-1}). Correlation is evident.

Figure 8: v_{max} versus w_{max} d. v_{max} = maximum tangential (rotational) wind velocity in dust devil, w_{max} = maximum vertical wind velocity in dust devil, and d = dust devil diameter.

Figure 9:

v_{max} versus $\Delta T_s/h_s$. v_{max} = maximum tangential (rotational)
wind velocity in dust devil, and $\Delta T_s/h_s$ = temperature lapse rate in shallow
($\approx$10 m) highly superadiabatic layer adjacent to the surface. The quantity w_{max}
$d^{1/2}$ has been held constant to determine whether any residual functional
dependence remains. None is evident.
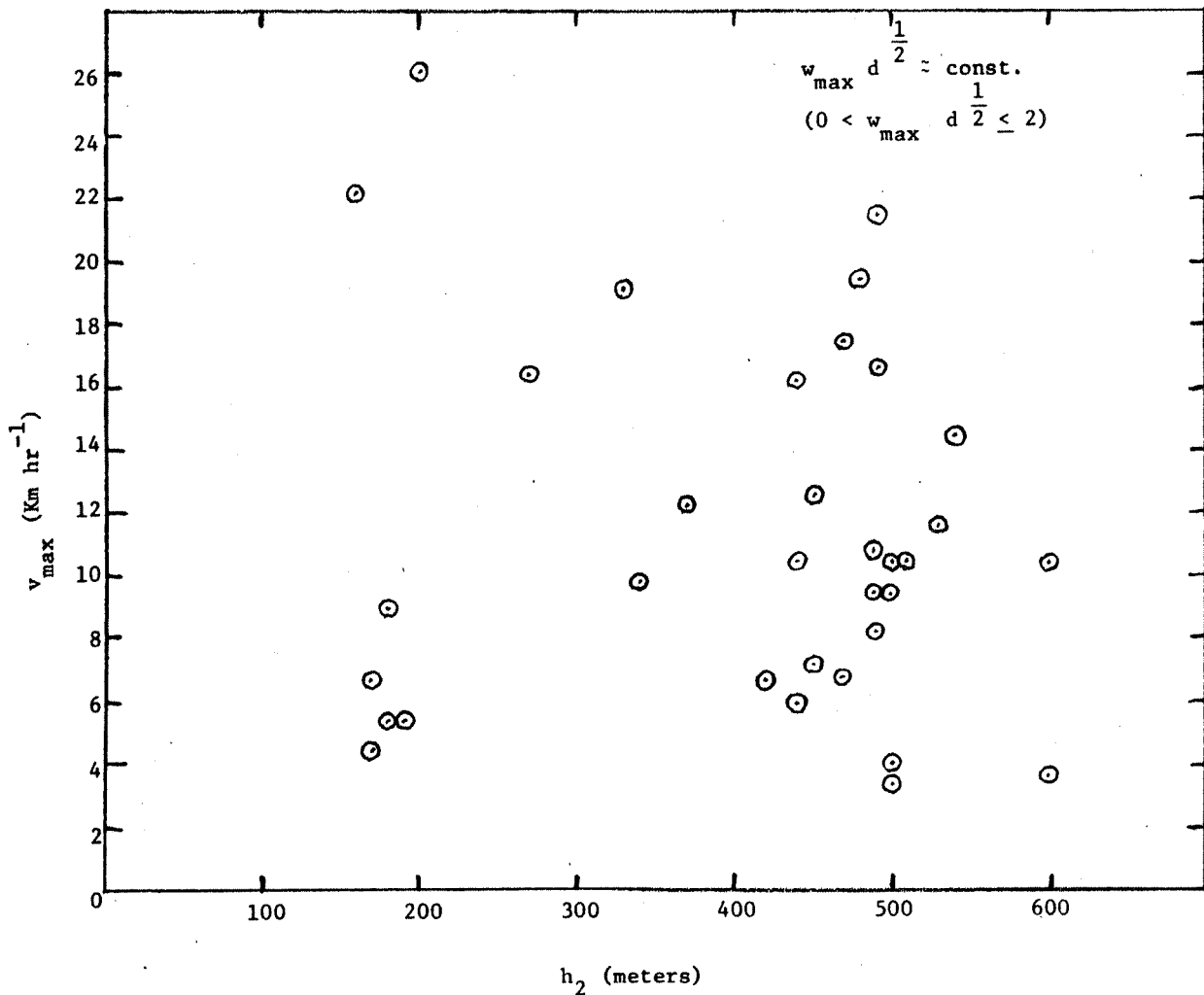
Figure 10:

v_{max} versus h_2. v_{max} = maximum tangential (rotational)
wind velocity in dust devil, and h_2 = thickness of superadiabatic layer
overlying shallow, highly superadiabatic base layer. The quantity $w_{max} \, d^{1/2}$
has been held constant to determine whether any residual functional dependence
remains. None is evident.

The quantity v_{max} was plotted against each of these quantaties, and against all combinations of vorticity-wind velocity, for fixed $w_{max} d^{1/2}$. No correlations were found (see sample plots in Figures 11-15) except with $|\zeta_2|$, for $w_{max} d^{1/2}$ <2.0 km hr^{-1} m$^{1/2}$. It would appear then that though the initial dust devil rotation is established by the background vorticity, the contribution of this to the mature (steady) dust devil state is negigible, unless $w_{max} d^{1/2}$ is sufficiently small. As an example for w_{max} = 2.7 km hr (the average for all dust devils penetrated), only dust devils less than 0.5 meters in diameter would be affected. The question as to where the steady state rotational energy may come from, if not from background atmospheric vorticity, is discussed shortly.

It appears then, that except for the very smallest dust devils,

$$v_{max} \propto w_{max} d^{1/2} \qquad (6)$$

In order to complete this expression it is necessary to use dimensional analysis. It is evident that the simplest form is

$$v_{max} = (const) \, w_{max} \, (d/h_L)^{1/2} \qquad (7)$$

where h_L = some linear dimension. What h_L may be, physically, can be seen from the following arguments. When a dust devil is formed, the upward moving bouyant air must be replaced by air moving in from below. It is only near the surface, in the friction layer, that air can flow into the core (Scorer, 1958, 52-54). If the vertical velocity in the core were a constant, independent of position, then the inflow velocity, disregarding ground friction effects, would simply be proportional to $w(d/h_d)$ where h_d = height of inflow layer. This expression is quite similar to the derived expression for v_{max} except for the power of the d/h_2 ratio. This power difference may well result from the
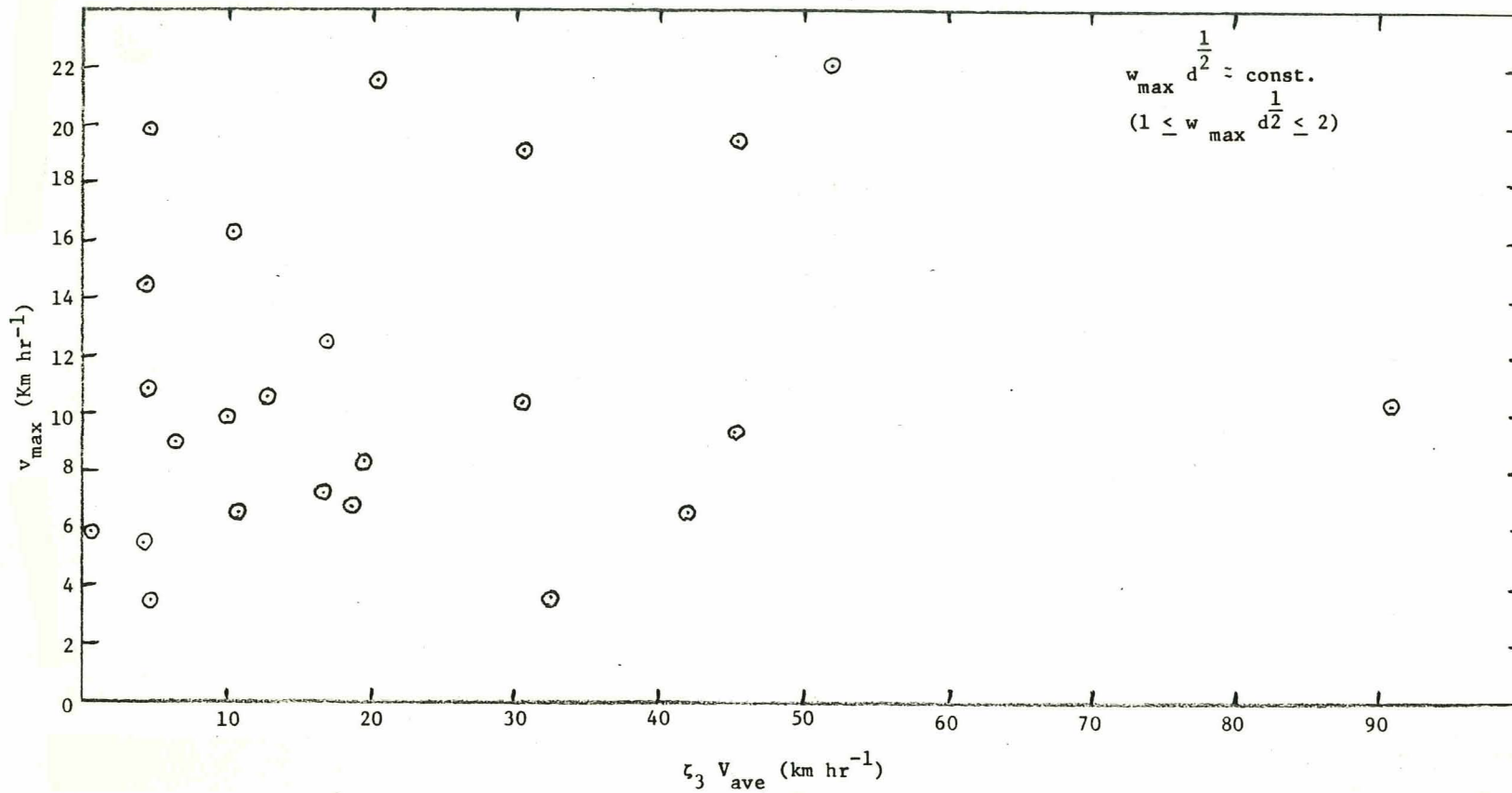
61

Figure 11: v_{max} versus $\zeta_3 V_{ave}$. v_{max} = maximum tangential (rotational) wind velocity in dust devil, ζ_3 = sum of magnitudes of slopes of vorticity meter trace in four minute interval about time of dust devil occurrence, and V_{ave} = average background wind velocity in same four minute interval. The quantity $w_{max} d^{1/2}$ has been held constant to determine whether any residual functional dependence remains. None is evident.
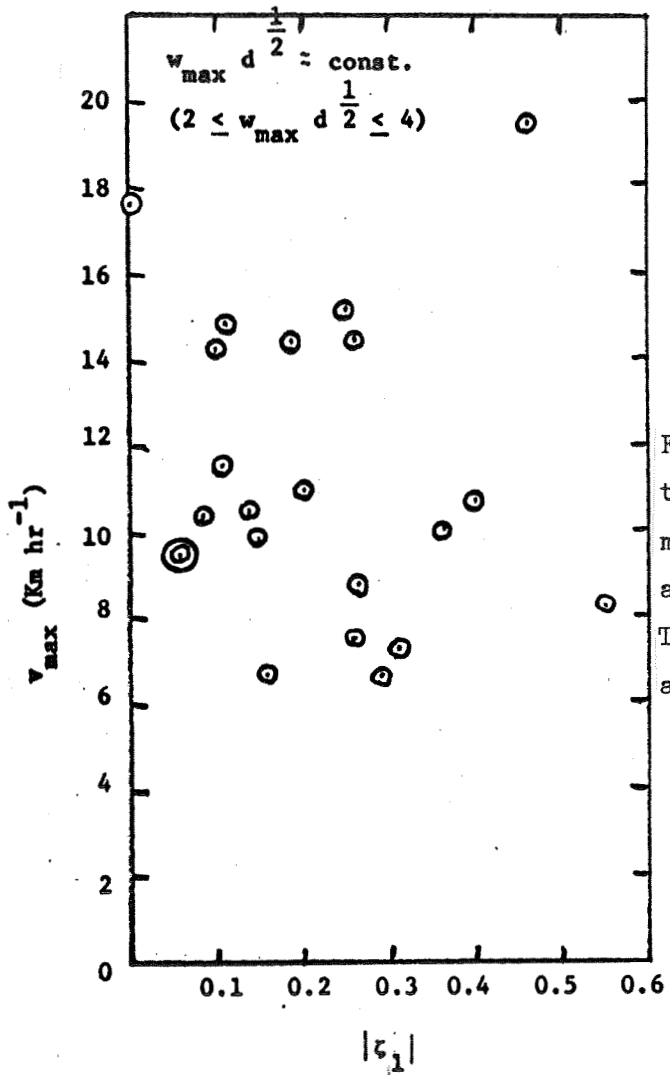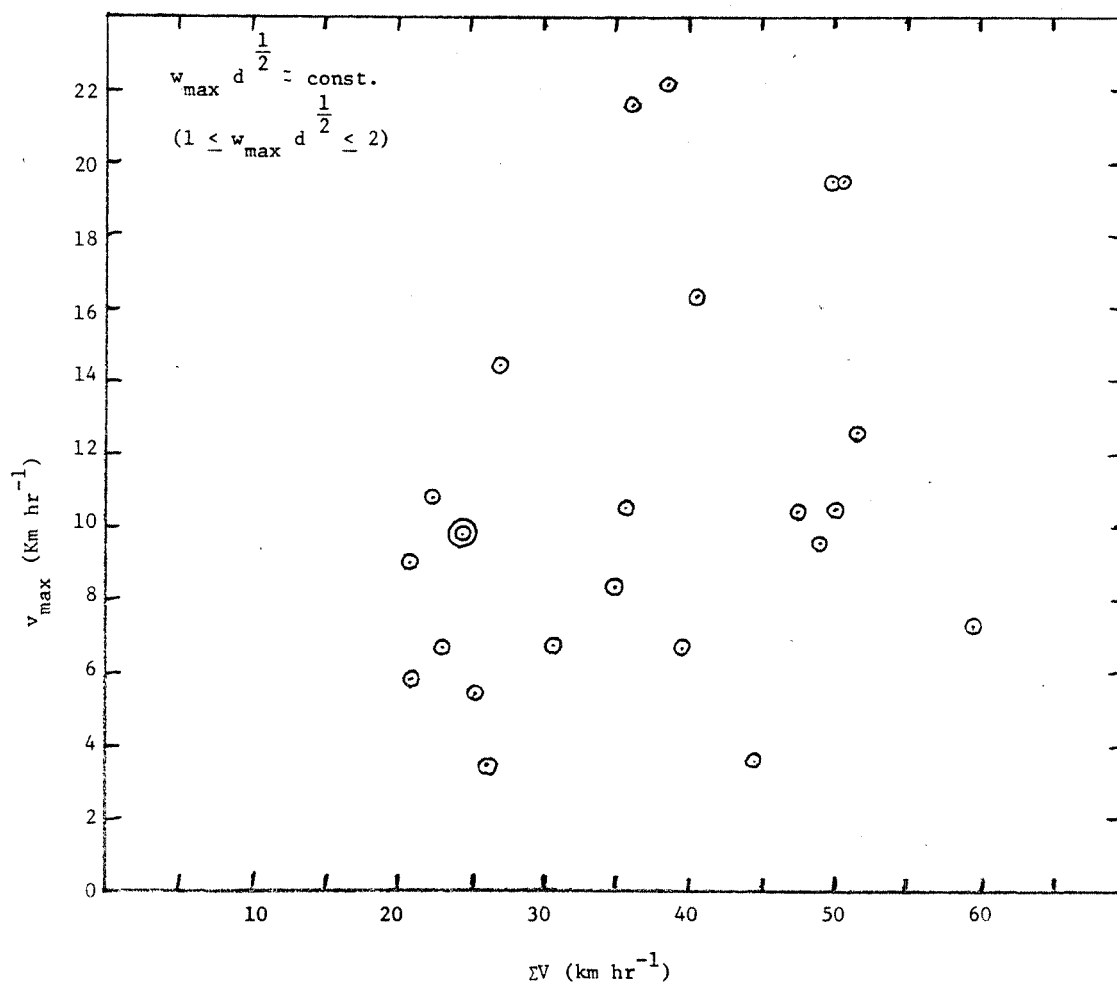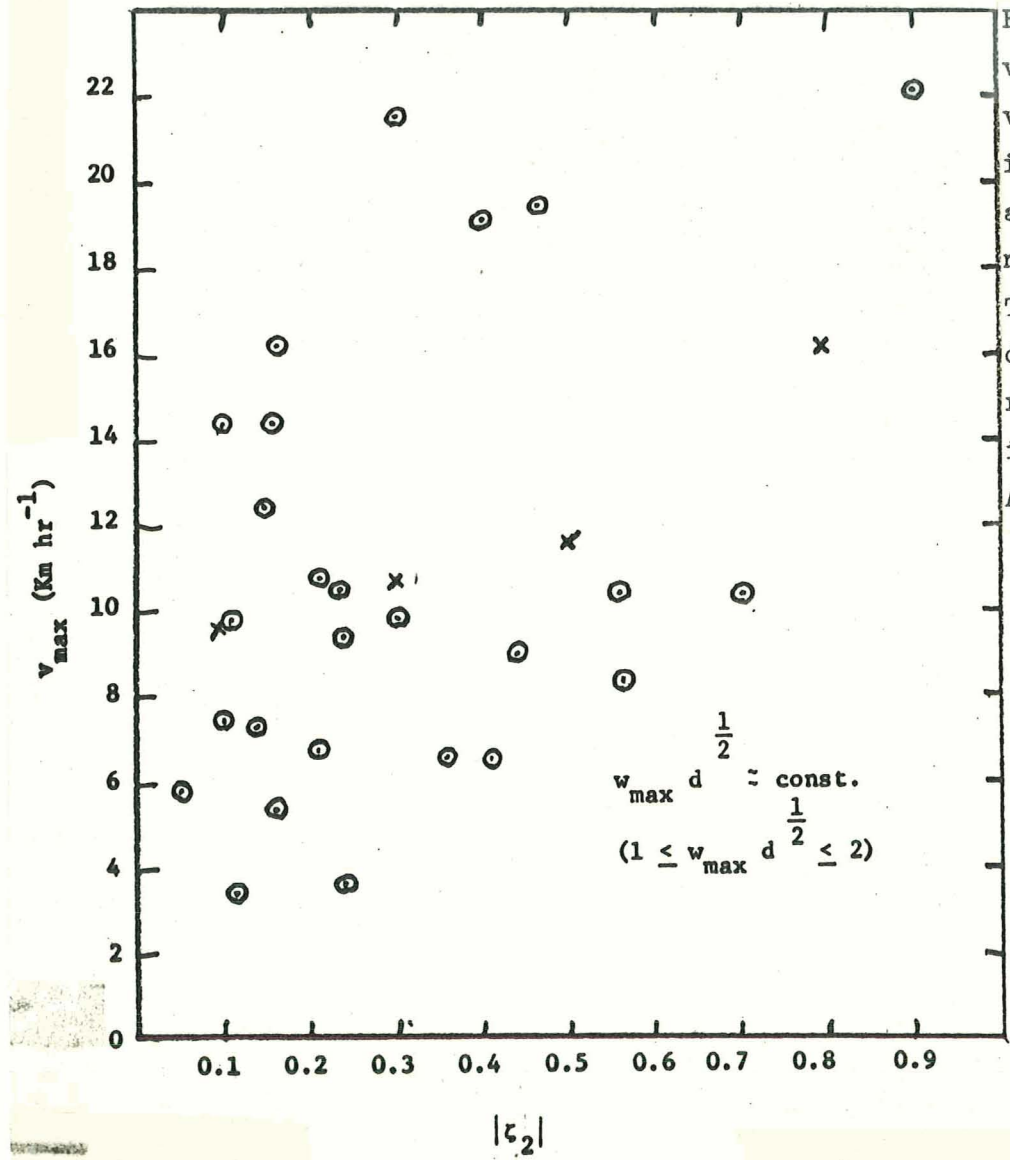
$w_{max} d^{\frac{1}{2}} \approx const.$

$(2 \leq w_{max} d^{\frac{1}{2}} \leq 4)$

Figure 12: v_{max} versus the magnitude of ζ_1. v_{max} = maximum tangential (rotational) wind velocity in dust devil, and ζ_1 = maximum slope of vorticity meter trace in four minute interval about dust devil time, in direction of dust devil rotation. The quantity $w_{max} d^{1/2}$ has been held constant to determine whether any functional dependence remains. None is evident.

Figure 13:

v_{max} versus $\sum V$. v_{max} = maximum tangential (rotational) wind velocity in dust devil, and $\sum V$ = sum of peak background wind velocities in two minute intervals, one on each side of dust devil time. The quantity $w_{max}\, d^{1/2}$ has been held constant to determine whether any functional dependence remains. None is evident.

Figure 14: v_{max} versus the magnitude of ζ_2. v_{max} = maximum tangential (rotational) wind velocity in dust devil, and ζ_2 = maximum slope in vorticity meter record in four minute interval about dust devil time, regardless of whether or not in same direction as dust devil rotation. The quantity $w_{max} d^{1/2}$ has been held constant to determine whether any functional dependence remains. The x's are averages of v_{max} in the intervals 0-0.2, 0.2-0.4, 0.4-0.6, and > 0.6. A correlation appears to be present.
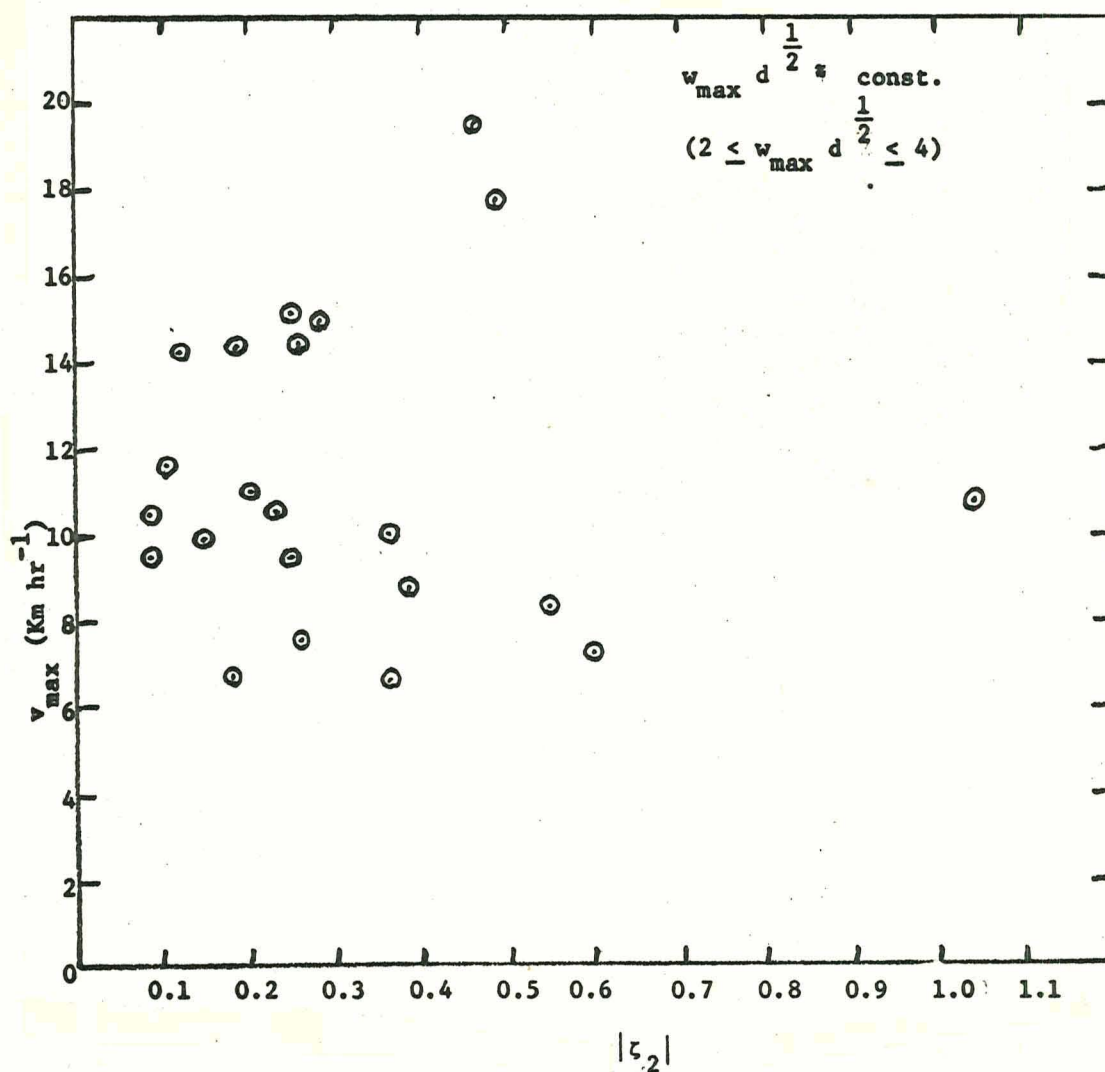
$$w_{max} d^{\frac{1}{2}} \approx const.$$

$$(1 \leq w_{max} d^{\frac{1}{2}} \leq 2)$$

v_{max} (Km hr^{-1})

$|\zeta_2|$

Figure 15: v_{max} versus the magnitude of ζ_2. The quantity $w_{max}\, d^{1/2}$ has been held constant to determine whether any functional dependence remains. None is evident. Comparison with Figure 14 shows that increasing $w_{max}\, d^{1/2}$ causes the apparent correlation in Figure 14 to disappear.

combination of non-constant w, and particularly from frictional effects which are contained implicitly in the data. It thus appears that h_L is some effective height of the inflow layer which itself is a function of ground friction and air viscosity.

A possible, and perhaps likely, source of dust devil angular momentum, in lieu of atmospheric vorticity, is the twisting term in the vorticity equation (Equation 4). This twisting term expresses conversion of the horizontal vorticity component due to the vertical shear in the horizontal flow, to a vertical component of vorticity by the radial gradient of the vertical velocity in the vicinity of the dust devil base. That this may indeed be responsible for maintaining dust devil rotation can be seen from the following arguments.

Equation 4 can be written in a more concise form, applicable to the present discussion, as

$$\frac{\partial \zeta}{\partial t} = -w\left(\frac{1}{r}\frac{\partial v}{\partial Z} + \frac{\partial}{\partial Z}\frac{\partial v}{\partial r}\right) - u\left(\frac{1}{r}\frac{\partial v}{\partial r} + \frac{\partial^2 v}{\partial r^2} - \frac{v}{r^2}\right)$$

$$\tag{8}$$

$$+ \zeta\frac{\partial w}{\partial Z} - \frac{\partial w}{\partial r}\frac{\partial v}{\partial Z} + \frac{\partial}{\partial Z}\left(\overline{k} \cdot \overline{\delta \times \tau}\right)$$

where $\zeta = \frac{v}{r} + \frac{\partial v}{\partial r}$ and τ is the vector wind stress. By definition, the first and second terms on the right hand side of the equation can only redistribute existing vorticity with the sign of the terms being determined by the gradients of v since the sign of u and w is fixed for our case. The third term depends upon the radial convergence of mass and the local existing vorticity which in general could have either sign, but since the sense of v determines that of ζ, only a variation in the sign of the convergence can change its sign. The

fourth (twisting) and fifth (rotational-frictional) terms are the only ones which can create and/or destroy vorticity.

In order to determine the relative contributions, to dust devil angular momentum, of the terms in Equation 8, data obtained by Sinclair (1966) on a mature dust devil (Sinclair's D.D. #1) were utilized. Sinclair's data are particularly applicable since they were taken at two levels above the surface. The values of u, v, w, $\frac{\partial v}{\partial r}$, and $\frac{\partial w}{\partial r}$, at both levels were obtained from the smoothed data at discrete values of $r > r_o$ with the finite differenced derivatives centered on the values of r. The two sets were averaged to the middle height, Z = 3.6m. The vertical derivatives were taken by finite differencing at each r. The higher order derivatives contained in the last term in Equation 8 unfortunately could not be evaluated since only two levels are available.

The results of these calculations are presented in Table 7. The last column $(\frac{\partial \zeta}{\partial t} -F)$ is the residual where F denotes the frictional term. While these magnitudes are approximate at best, the qualitative sense is probably quite good. Note that the twisting and covergence terms act positively everywhere and that the advective terms are negative. Also at $r = 3r_o$, all terms are nearly zero. The magnitude of the residual term reflects the cumulative error in the other four, so that its magnitude is the most suspect, but if the sign is correct, it implies that the local diffusion of vorticity is larger than the local increase, indicating that this DD is decaying at the observation time.

Table 7

MAGNITUDES OF TERMS IN VORTICITY EQN. FOR A

3 METER RADIUS DUST DEVIL AS MEASURED BY SINCLAIR

r	$-w\dfrac{\partial \zeta}{\partial Z}$	$-u\dfrac{\partial \zeta}{\partial r}$	$\zeta\dfrac{\partial w}{\partial Z}$	$-\dfrac{\partial w}{\partial r}\dfrac{\partial v}{\partial Z}$	$\dfrac{\partial \zeta}{\partial t}$ -F
3	−0.2	0	0	0.2	0
4	−2.5	−1.6	1.0	0	−3.1
5	−1.9	−2.2	1.2	0.1	−2.8
6	−0.6	−1.5	0.2	0.8	−1.1
7	−0.2	−0.5	0	0.7	0
8	−0.1	−0.4	0	0.4	−0.1
9	(−)0.0	−0.2	0	0.3	−0.1
10	(−)0.0	−0.1		0	−0.1

The most significant inference drawn from Table 7 is that the twisting term is of the same magnitude as the others. Furthermore, since in any convective vortex the flow outside of the core region will be characterized by $\frac{\partial w}{\partial r} < $ o and $\frac{\partial v}{\partial Z} > $ o near the lower boundary, the twisting term is always positive. Therefore it is concluded that the contribution of the twisting term is at least as significant as background vorticity to the growth and maintenance of a dust devil, once the spin up process begins.

4.2.6 Energy Measure

In Section 2.2.4, discussion was given to the energy approach for understanding dust devil generation. This approach assumes that an overturning of an unstable atmospheric layer occurs, with the resultant decrease of potential

and internal energy appearing as rotational energy. The present investigators derived an expression for v_{max}, Equation (3), relating it to the height of the dust devil, height of the superadiabatic layer, and temperature lapse rates (Ryan and Fish, 1965). The limitations of this approach were outlined in Section 2.2.4, along with the reasons why a kinematic or other approach was more desirable. Nevertheless, one of the original objectives of the present program was to check the validity of Equation 3. The purpose of this section is to do so.

The height h_d in Equation 3 represents the height to which rotary motion extends. Field observations of billow height indicate that the vortex begins to dissipate at height h, the point where the temperature lapse rate ceases to be superadiabatic. Hence it appears reasonable to let $h_D = h$. It has also been found, Section 4.2.1, that dust devil generation occurs in the highly superadiabatic layer adjacent to the ground. This implies that the h in Equation 3 should be replaced by h_s. However, the total energy in the $(h-h_s)$ column far exceeds, in most instances, that in h_s. Accordingly, both h and h_s are utilized, and the alternative forms of Equation 3, with $h_D = h$, become

$$v_{max(1)}^2 \approx hg \left[(\tfrac{dT}{dZ}/\nu_a) -1 \right] / (0.5 + 2 \ln n) \qquad (3a)$$

$$v_{max(2)}^2 \approx h_s^2 \, g \left[(\tfrac{\Delta T_s}{h_s}/\nu_a) -1 \right] / h \,(0.5 + 2 \ln n) \qquad (3b)$$

Taking n = 4, a typical value; $h_s \approx 10$ meters, typical from the field observations, and $g = 9.8m\ sec^{-2}$, these equations become

$$v^2_{max(1)} \tilde{=} 3h \; [(\frac{dT}{dZ}/\nu_a)-1] \; (m^2 sec^{-2}) \tag{3a$'$}$$

$$v^2_{max(2)} \tilde{=} 3 \times 10^2 \frac{\Delta T_s}{h_s} /\nu_a \; h \; (m^2 sec^{-2}) \tag{3b$'$}$$

Values for v_{max} appearing in these equations were computed for all dust devils in Table 1, utilizing the data in Volume II. The results are shown in Figures 16 and 17. Figure 16 shows v_{max} (measured) versus $v_{max(1)}$ while Figure 17 shows v_{max} (measured) versus $v_{max(2)}$, for all dust devils $\geq$1m in diameter. No correlation between measured and calculated v_{max} is evident (there is also no correlation for constant diameter). It is therefore concluded that, though the dust devil probably derives most if not all of its energy from atmospheric internal and potential energy, the manner in which it does so is not described by the above equations (nor, incidentally, by any of the energy equations obtained by other investigators).

4.3 Dust Devil Model; Summary of Results

4.3.1 Generation Phase

A basic purpose of this study has been to obtain quantitative expressions for the wind velocities developed in dust devils during their mature, or steady state, phase. However, the observations have also given some indications regarding how they are formed. For dust devil generation it is necessary for a highly superadiabatic temperature lapse rate to exist, specifically in the shallow (<10 meter) layer adjacent to the surface. It also appears necessary that atmospheric vorticity of some scale be present. The scale undoubtly varies, but appears to be sufficiently large in general that correlations were found between direction of vorticity meter and dust devil rotation for dust devil distances exceeding 100 meters. The base atmospheric layer is where
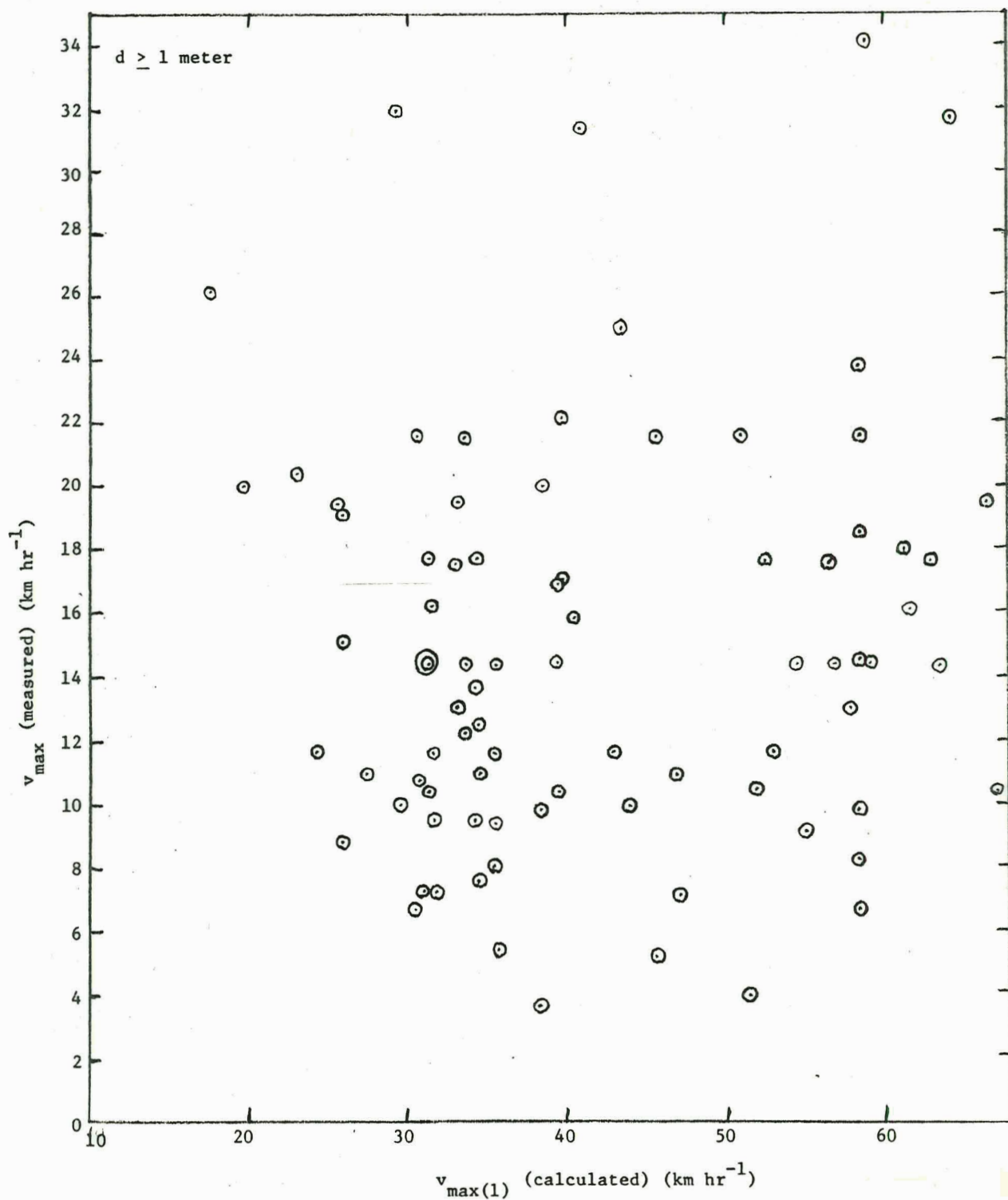
Figure 16: v_{max} (measured) versus $v_{max\,(1)}$ (calculated). No correlation is evident.
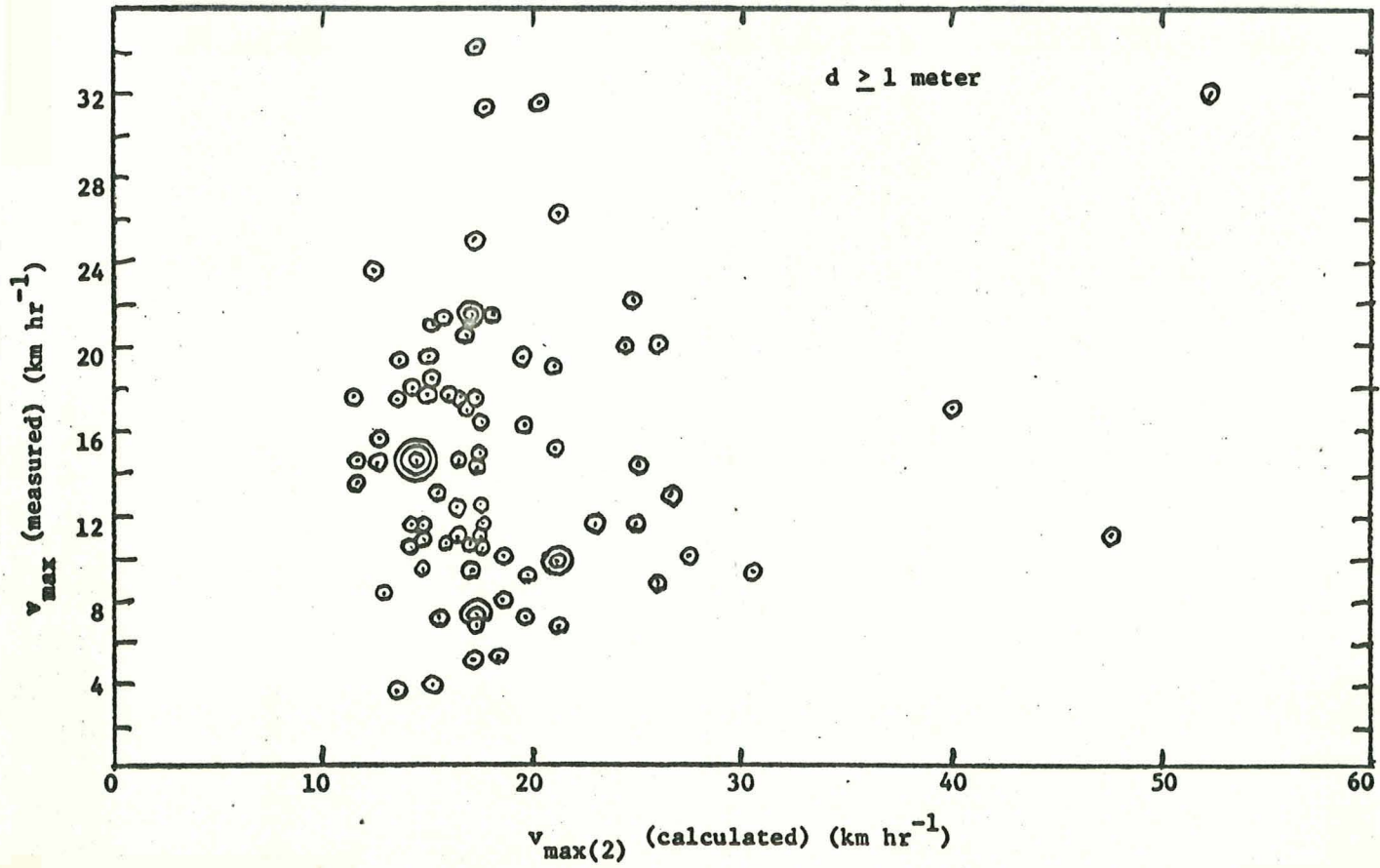
Figure 17: v_{max} (measured) versus v_{max} (2) (calculated). No correlation is evident.

triggering occurs, and the more superadiabatic this layer becomes the greater becomes the frequency of dust devil formation (dust devil frequency may also depend upon the amount of vorticity present, but further analysis of the data is required to prove this). The dust devil is probably initiated by some mechanism, such as wind action, which displaces an air parcel from its rest position. This causes acceleration of the parcel upwards as a result of bouyancy forces. These bouyancy forces increase in magnitude as the base layer becomes increasingly superadiabatic; at the same time the magnitude of the required disturbing force decreases. The maximum possible diameter of the resulting incipient dust devil increases as the lapse rate in the base layer increases, since the initial upward-moving parcel can cause triggering of parcels to a greater distance, as can the initial disturbance, due to increased instability. As the air parcels move upward they must be replaced by parcels from the side. Rotation has been established by atmospheric vorticity and a vortex begins to form. Once the velocity of the incoming air parcels reaches a critical value, granular material from the surface becomes entrained in the air stream, it is carried into the core region and then aloft.

4.3.2 Mature, or Steady State, Phase

In the mature phase, comprising most of the dust devil's life, a stable vortex is present. Air flow into the vortex occurs only in the friction layer adjacent to the surface. The vertical velocities in the dust devil are determined by the height and lapse rate in the slightly superadiabatic, thick, layer overlying the base layer. The vortex maintains its well defined structure at least to the top of this overlying layer, above which breakdown begins. Upward motion of the air parcels, however, continues, and appreciable

vertical wind velocities are still present several kilometers above the surface. In the inflow region (friction layer), air parcels are accelerated into the core from the surrounding area. Concentration of atmospheric vorticity appears to play a role in maintaining dust devil rotation in the smallest (< 1 meter diameter) dust devils. However, it appears that for all other dust devils, the initial rotation is maintained (possibly increased from the initial magnitude) by the conversion of horizontal inflow shear to vertical (twisting term). The rotational velocity (for $d \geq 1$ meter) is determined by the vertical velocity, the dust devil diameter, and the effective height of the inflow layer.

4.3.3 Decay Phase

Dissipation of the dust devil, specifically the dust devil vortex, can occur when one or more of the following events happen: (1) the dust devil enters an area in which insufficient atmospheric internal and potential energy is available; (2) the dust devil enters an area of downdrafts resulting from thermal convection; and (3) the dust devil enters an area where oppositely directed atmospheric vorticity is present of magnitude comparable to dust devil angular momentum. The first two possibilities have been noted by others. The third possibility suggested itself during the present study from close observations of dust devils for which it was often found that the rotation would cease almost instantaneously near the surface. This was particularly common for the smaller dust devils.

5.0 TRANSFORMATION TO MARS

5.1 Martian Temperature Regime

Determination of the temperature lapse rates that could occur in the lower Martian atmosphere is important to this program since these lapse rates play an important role in determining whether or not dust devils could occur on Mars. This section describes a model for computing the diurnal variation of temperature and presents the results obtained.

Atmospheric temperature changes are assumed to be due primarily to turbulent heat transfer processes in the vertical direction (radiative transfer and advection have been ignored for the present calculations). At the surface a balance of net solar radiation, turbulent heat transfer, and conductive heat exchange with the subsurface layer is assumed. Temperature changes in the subsurface layer are due to molecular conduction of heat, the thermal diffusivity of the Martian soil being assumed constant with depth and time.

The rate of temperature change at any subsurface level is

$$\frac{\partial T}{\partial t} = K \frac{\partial^2 T}{\partial Z^2} \tag{6}$$

where Z is the depth in the soil, t is time, T is the temperature of the soil, and K is the thermal conductivity of the soil (assumed constant).

The rate of temperature change in the atmosphere due to turbulent heat transfer is

$$\frac{\partial T'}{\partial t} = \frac{\partial}{\partial Z'} \left[K'(Z') \left(\frac{\partial T'}{\partial Z'} + \Gamma \right) \right] \tag{7}$$

where T' is the temperature of the atmosphere, Z' is height, $K'(Z')$ is the eddy diffusivity (varied with height), and Γ is the adiabatic lapse rate.

The boundary condition equation is

$$\sigma \varepsilon T_o^4 - K_s \frac{\partial T}{\partial Z}\bigg|_{Z=0} - \rho_a C_p K_s' \frac{\partial T'}{\partial Z'}\bigg|_{Z'=0} - (1-A)S_o = 0 \qquad (8)$$

where

σ = Stefan-Boltzman constant

ε = emissivity of the surface

K_s = thermal diffusivity (near surface)

K_s' = eddy diffusivity (near surface)

ρ_a = density of air

C_p = heat capacity of air

A = planetary albedo

S_o = solar radiation at surface.

Equations 6-8 are put in finite difference form for solution on the Univac 1108 digital computer. The Dufart-Frankel finite difference approximation is used for Eq. 6, and an extrapolation of this difference approximation is used for Eq. 7.

The finite difference equations are

$$\frac{T_j - T_j^{m-1}}{2\Delta t} = \frac{K}{(\Delta Z)^2}\left(T_{j+1}^m + T_{j-1}^m - T_j^{m+1} - T_j^{m-1}\right) \qquad (6')$$

and

$$\frac{T_j' - T_j'^{m-1}}{2\Delta t} = \frac{1}{4(\Delta Z')^2}\left(K_{j+1}' - K_{j-1}'\right)\left(T_{j+1}'^m - T_{j-1}'^m + 2\Gamma\Delta Z'\right) \qquad (7')$$

where the subscript refers to distance and the superscript to time. Equations $(6')$ and $(7')$ can be solved for T_j^{m+1} and $T_j'^{m+1}$ respectively to give

77

$$T_j^{m+1} = \frac{T_j^{m-1} + \frac{2K\Delta t}{(\Delta Z)^2}\left(T_{j+1}^m + T_{j-1}^m - T_m^{m-1}\right)}{1 + \frac{2K\Delta t}{(\Delta Z)^2}} \tag{6''}$$

$$T_j'^{m+1} = \left\{ T_j^{m-1} + \frac{2t}{(\Delta Z')^2} \frac{\left(K_{j+1}' - K_{j-1}'\right)\left(T_{j+1}'^m - T_{j-1}'^m + 2\Gamma\Delta Z'\right)}{4} \right. \tag{7''}$$

$$\left. + K_j\left(T_{j+1}'^m + T_{j-1}'^m - T_j'^{m-1}\right) \right\} \frac{1}{1 + \frac{2\Delta t K_i'}{(\Delta Z')^2}}$$

The finite difference analog of Eq. 8 is

$$\sigma\varepsilon T_o^4 + \frac{K_s}{\Delta Z}\left(T_o - T_1\right) + \frac{\rho_a C_p K_s'}{\Delta Z'}\left(T_o - T_1' - \Gamma\Delta Z'\right) - \left(1-A\right)S_o = 0 \tag{8'}$$

The root, T_o, satisfying (8') is found. This T_o is the surface temperature for the time iteration under consideration. Subsurface and air temperatures are obtained by solving (6") and (7") going up and down from the surface.

The numerical values used in the computations are:

K_s = 2.50x10^3 cm^2/sec

$K_s' = \begin{cases} T_o > T_{20 \text{ meters}} & 5.2\times10^4 \text{ cm}^2/\text{sec} \\ T_o \leq T_{20 \text{ meters}} & 1\times10^3 \text{ cm}^2/\text{sec} \end{cases}$

ρ_a = 2.975x10^{-3}/T gm cm^{-3}

ε = .85

A = .15

ΔZ = 0.2 cm

$\Delta Z'$ = 2,000 cm

Δt = 61.5574 sec = 1 Martian minute

$$C_p = (514 + 1.1T) \times 10^4$$

$$\sigma = 5.67 \times 10^{-5} \text{ cgs}$$

Solar Constant at Mars $= .626 \times 10^6$ erg/cm^2 sec

$$K = .474 \times 10^{-4} \text{ cm}^2/\text{sec}$$

$$K'(Z') = \begin{cases} Z' \leq 120 \text{ met.} \begin{cases} \text{unstable air} = 2.2 \times 10^3 \ z'^{4/3} \ \text{cm}^2/\text{sec} \\ \text{stable} \qquad = 1. \times 10^3 \qquad\quad \text{cm}^2/\text{sec} \end{cases} \\ Z' > 120 \text{ met.} \begin{cases} \text{unstable} \qquad = 1.303 \times 10^6 \qquad \text{cm}^2/\text{sec} \\ \text{stable} \qquad = 1. \times 10^3 \qquad\quad \text{cm}^2/\text{sec} \end{cases} \end{cases}$$

The space grid utilized is as follows: for the ground, 20 layers of equal thickness (Z), underlain by 8 layers of thickness 100x Z; for the air, starting from the surface, 6 layers of equal thickness (Z') overlain by 5 layers of thickness 10x Z', in turn overlain by 9 layers of thickness 100x Z'. The top 20 layers in the ground were iterated every Martian minute, and the bottom 17 every 120 Martian minutes.

The bottom 6 layers of the atmosphere were 20 meters thick, but because K' is large, they were iterated every 5 Martian seconds. The next 4 layers were iterated every 1 minute (K' is somewhat larger for them) and the top 8 layers every 120 minutes.

Some results of the computer computations of the model are illustrated in Figures 18 through 21. In these initial computations the temperature at time t = 0 is 237°K at 6 A.M. on Mars at all levels. The computer program is then allowed to run for ten days and the data for the tenth day is used. Figures 18a and b depict the change in the 6 a.m. temperature through the ten-day cycle. From the graphs it can be seen that by the ninth day the temperatures are approaching steady state values at all the selected levels.

Figures 18a and b illustrate the diurnal change in temperature at selected levels for the Martian equator at equinox. Inspection of the curves indicates that the temperature changes throughout the day are similar in manner to the changes observed in the earth's atmosphere and ground. In particular, it should be noted that the daytime surface temperature curve agrees fairly well with the Martian temperatures determined by remote sensing techniques (Sinton and Strong, 1960; Gifford, 1952). In addition, the maximum surface temperature agrees with the maximum temperature obtained by Ohring, et al. (1968) with their constant K model. However, their minimum temperature is approximately thirty-five degrees colder. On the other hand, the preliminary results of their K model give a similar minimum temperature as shown in Figure 19, but a much colder maximum temperature (i.e., 240°K). As can be seen from Figure 19 the dirunal range computed for the Martian surface is 96°K. The observed range on desert surfaces on Earth is approximately 40-50°K. At 20 meters the computed range is 53°K while the observed range on Earth at 20 meters is approximately 5-10°K.

The vertical temperature profiles computed for different times of the day at the equator at equinox are presented in Figures 20a & b. Although the temperature change with height between the surface and 20 meters at the time of the surface maximum (1 p.m.) temperature is -29.8°C, the greatest change with height is -30.2°C at noon. A similar temperature change over deserts on the earth would be approximately 15°K. Actually, in the earth's atmosphere most of this temperature change takes place in the first ten meters with over 70% of the change in the first meter above the surface. Ohring, et al. (1968) computed an approximate 80°K maximum change in the first km compared to 46°K from Figure 20a. Part of this difference is undoubtedly due to the fact that the Ohring, et al. model has

a constant eddy diffusivity while our model has a variable eddy diffusivity with the largest values near the ground, and a function of the stability. These curves illustrate quite well the response of the atmosphere to the eddy flux of heat from the surface.

The variation of the ground and 20 meter temperature with latitude is shown in Figures 21a & b. Figure 21a is for the equinox ($\delta = 0$) while b is for the summer and winter solstice ($\delta \pm 25$). These curves are based on calculations made for latitudes 0°, 30°, 45° and 90°. Although the temperatures at the equator and low latitudes agree fairly well with previous estimates, the polar regions do not (Michaux, 1967). The summer temperatures are higher and the winter temperatures are lower.

Finally, Figures 22-36 show atmospheric temperatures at various levels as a function of time during the day, with each figure representing a given latitude and time of year. These form the basis for the discussion, in the following section, concerning whether or not dust devils may occur on Mars.
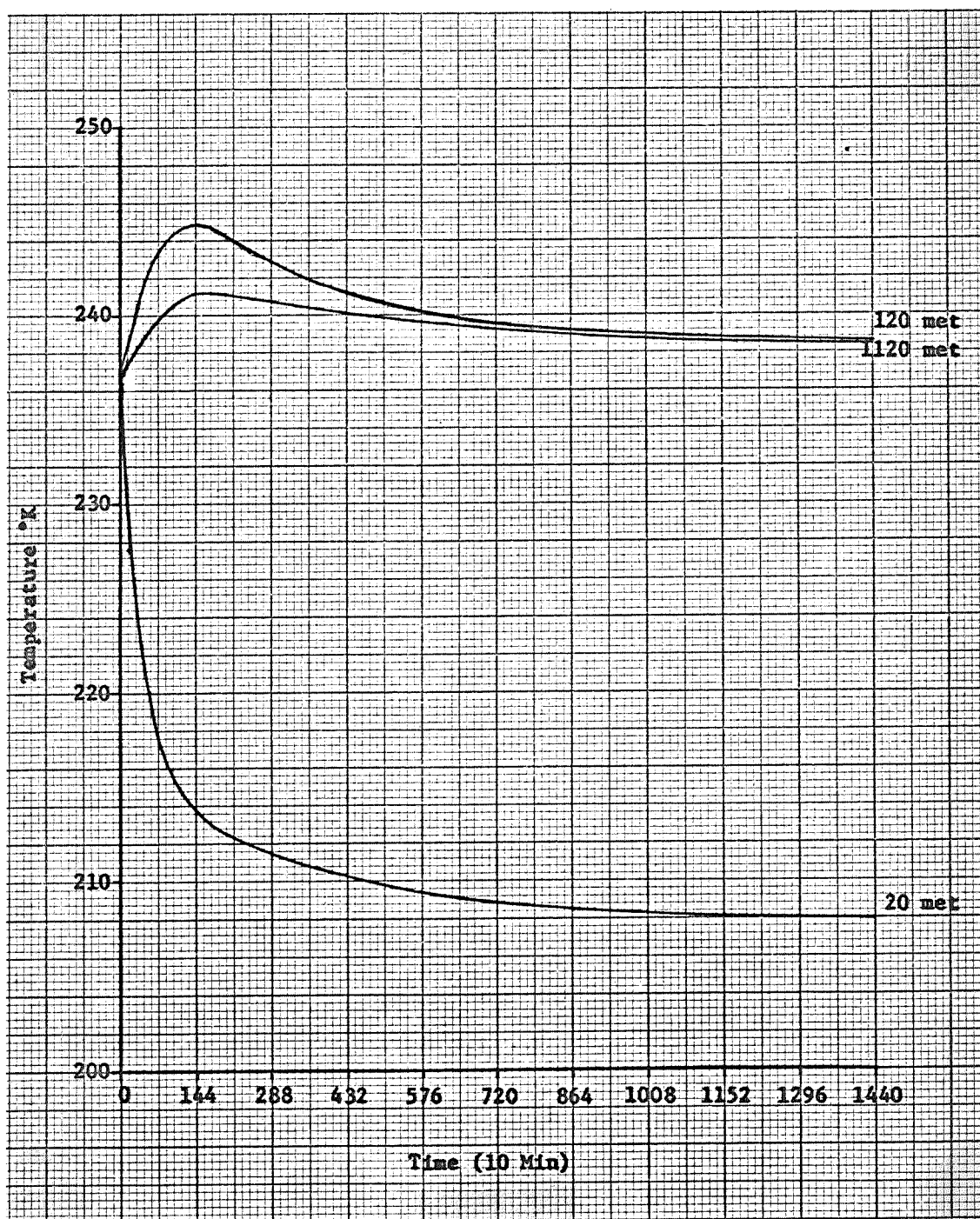
Figure 18a: Atmospheric temperature at Martian equator is 6 AM
over a ten-day period.

RM 30-692-6 (8-68)
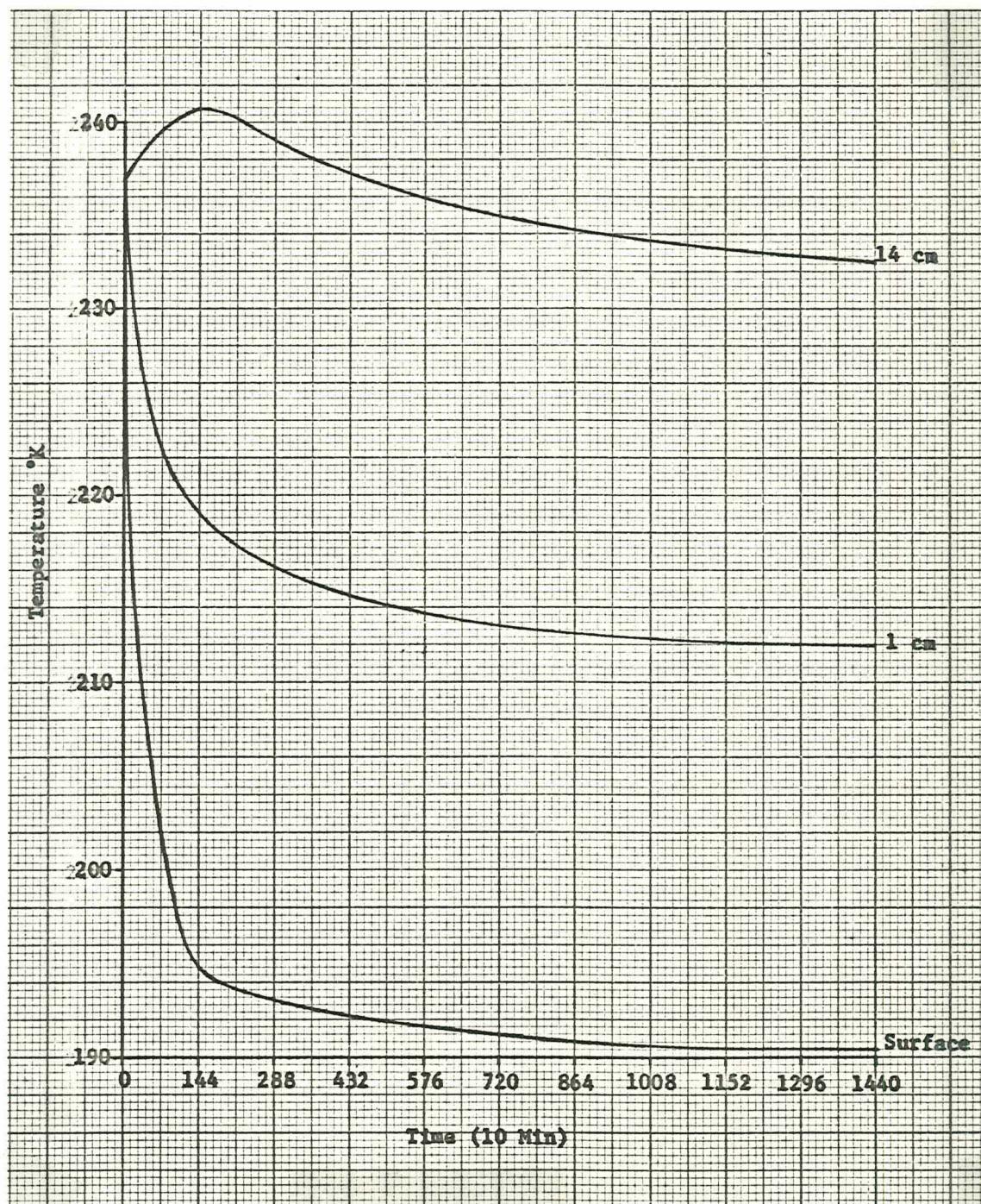
Figure 18b: Surface and interior temperatures at Martian
equator at 6 AM over a ten-day period.
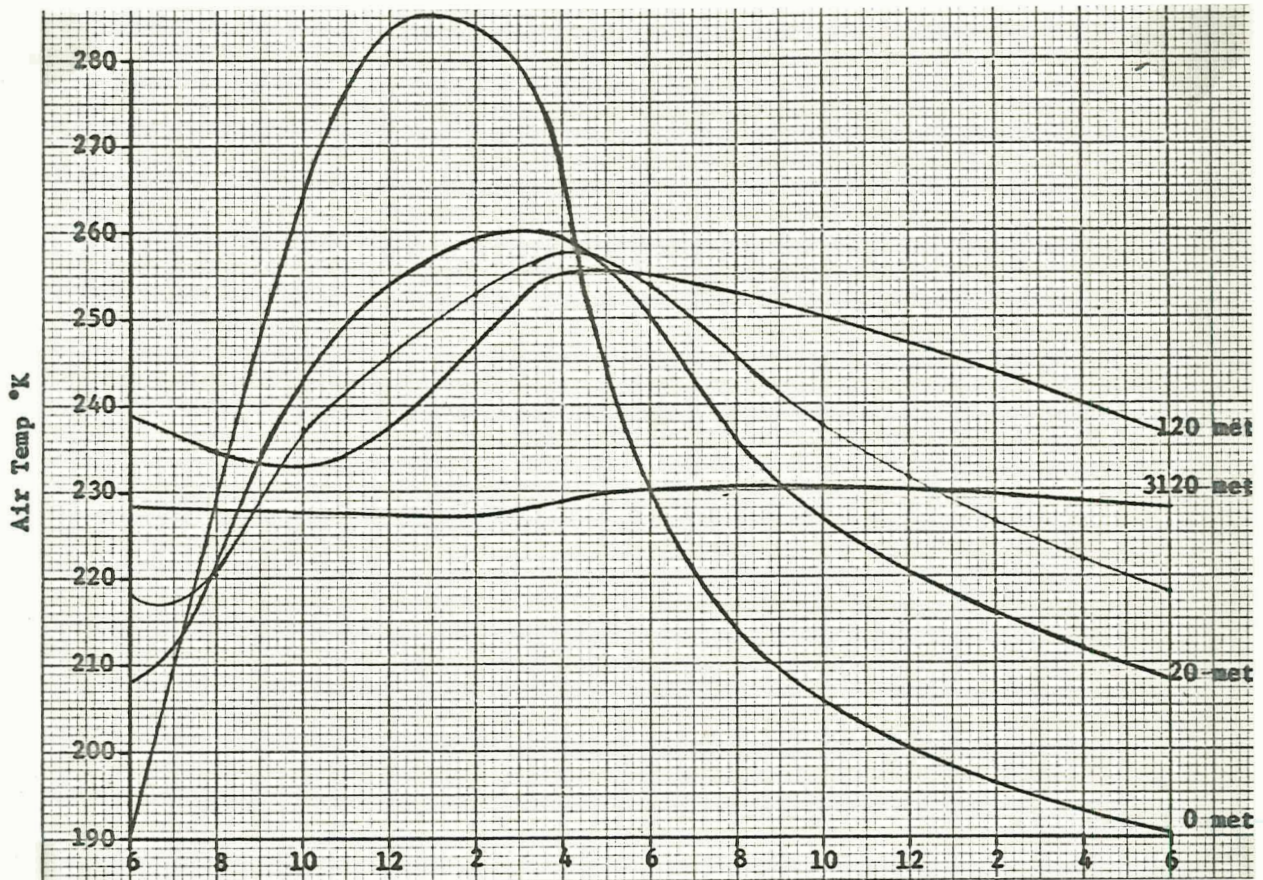
Figure 19a: Computed diurnal variation of the Martian Atmospheric
temperature at the equator at equinox.
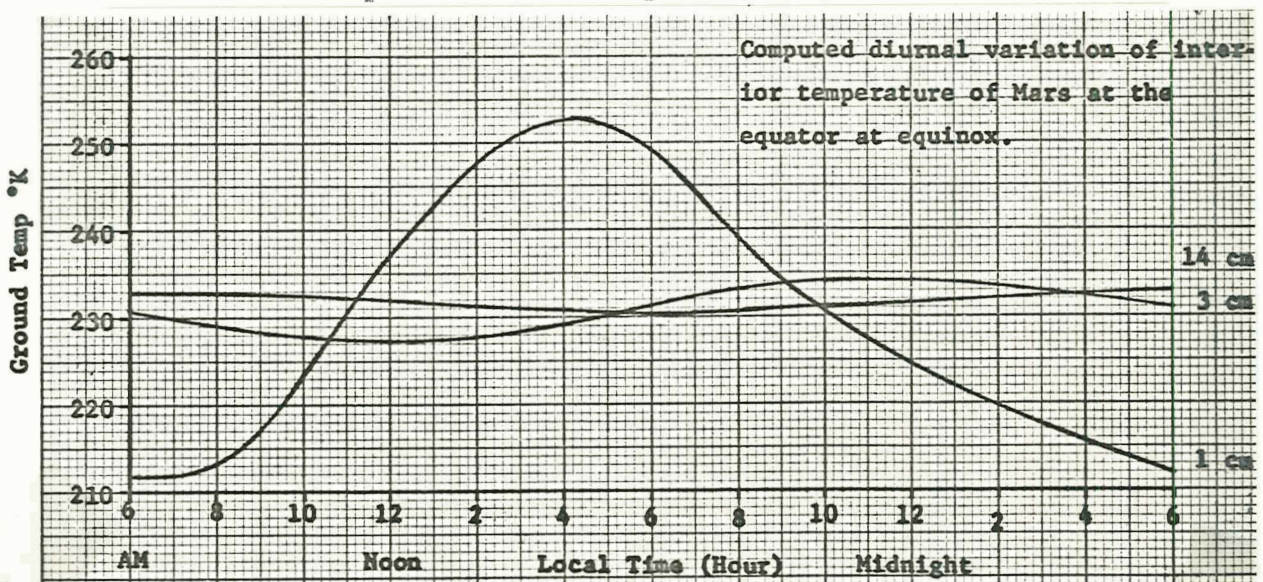
Figure 19b: Computed diurnal variation of interior temperature
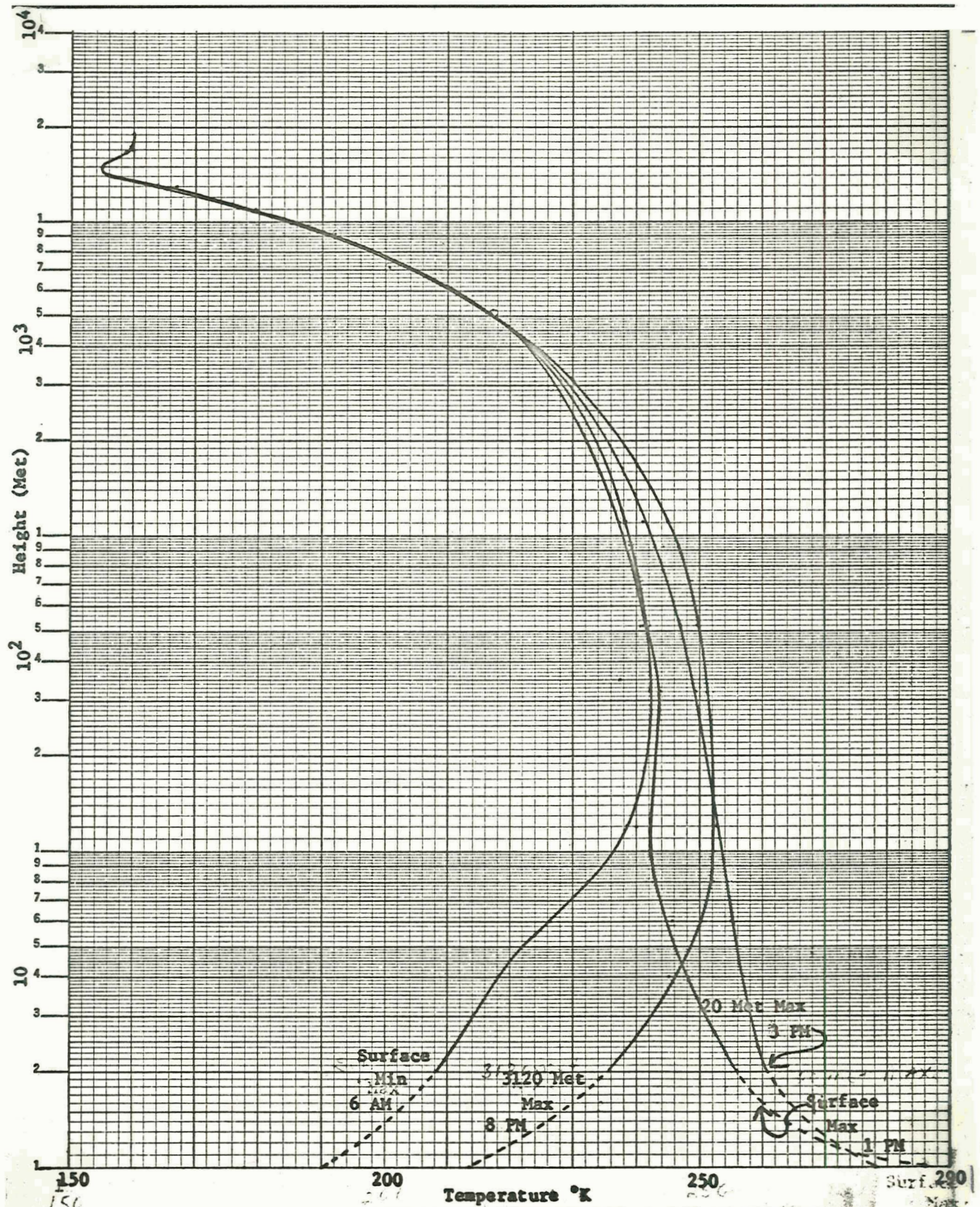of Mars at the equator at equinox.

Figure 20a: Computed atmospheric temperature profiles for various
times of day at Martian equator at equinox.
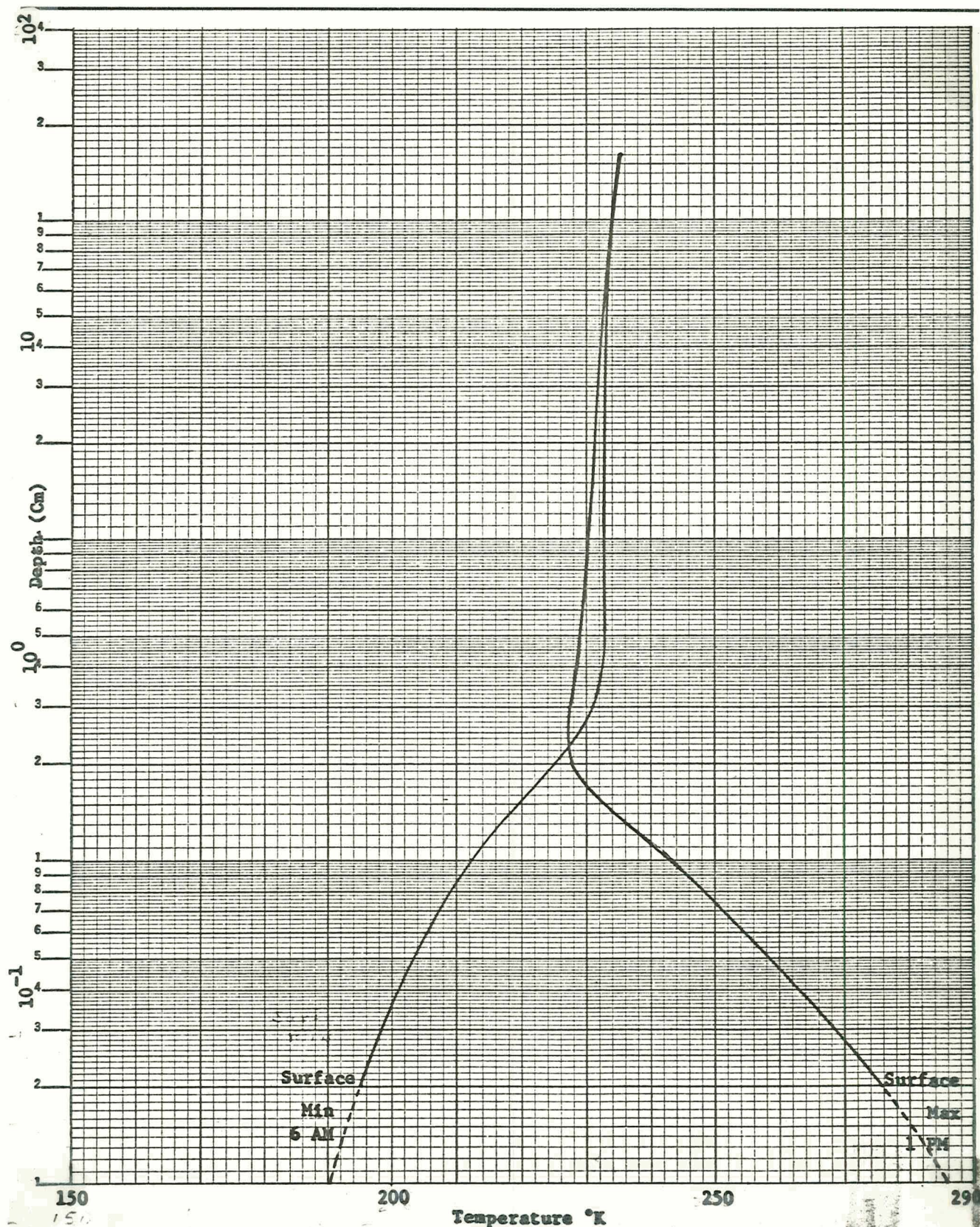
Figure 20b: Computed ground temperature profile for various
times of day at Martian equator at equinox.
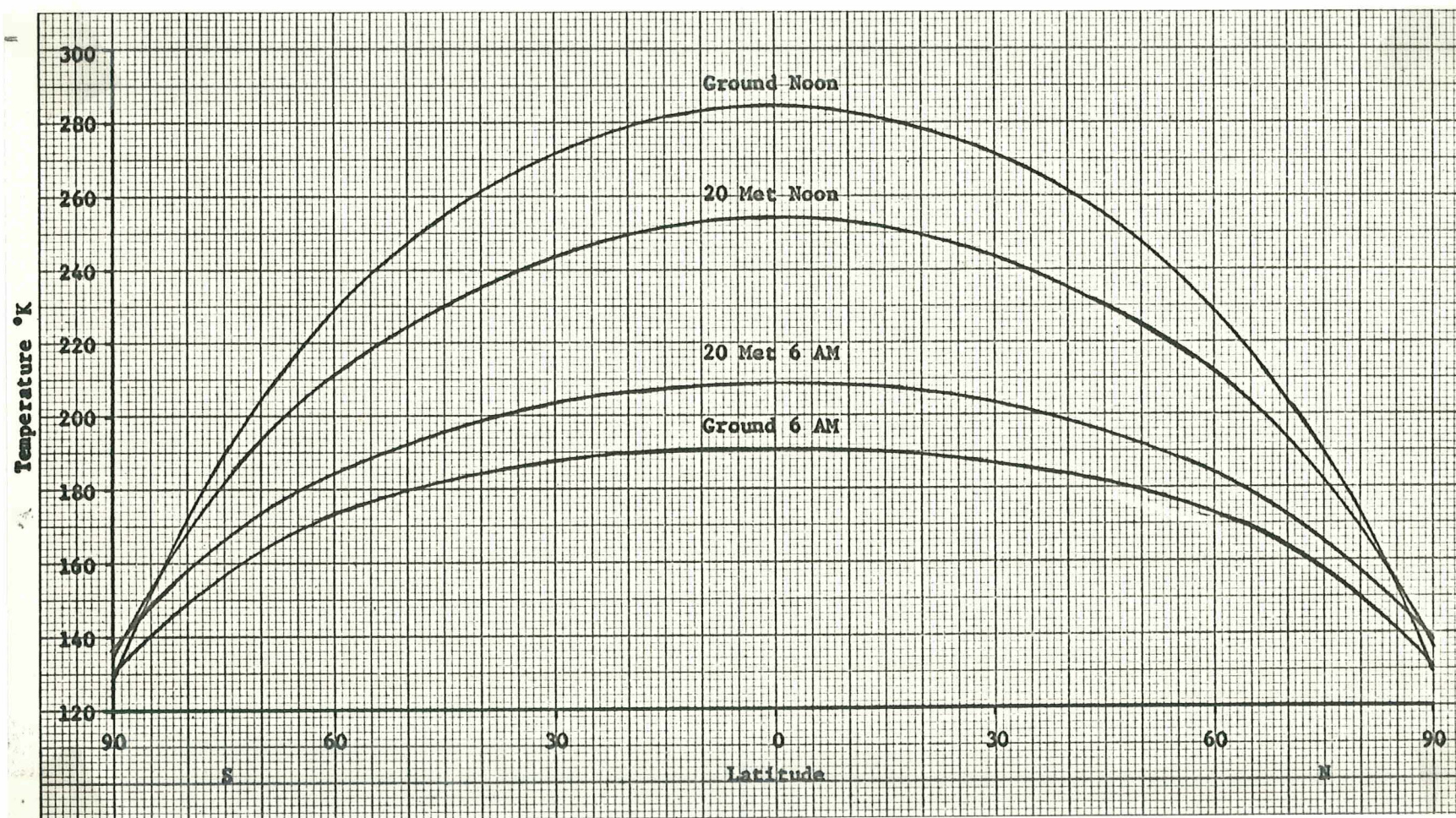
Figure 21a: Computed latitudinal variations of the 20 meter and surface temperatures of Mars (solar declination is 0°).
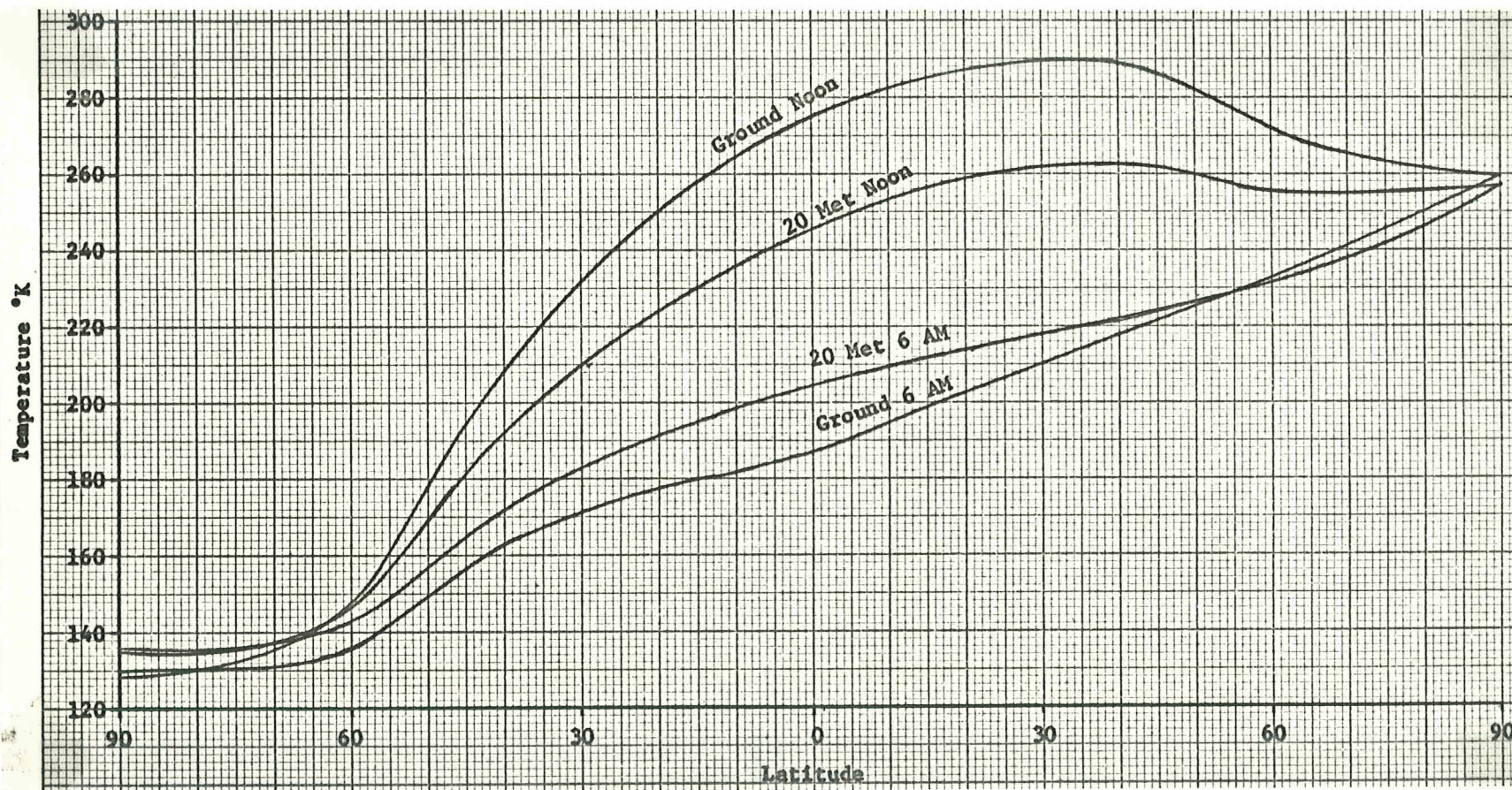
Figure 21b: Computed latitudinal variations of the 20 meter and surface temperatures of Mars (solar declination is ± 25°).
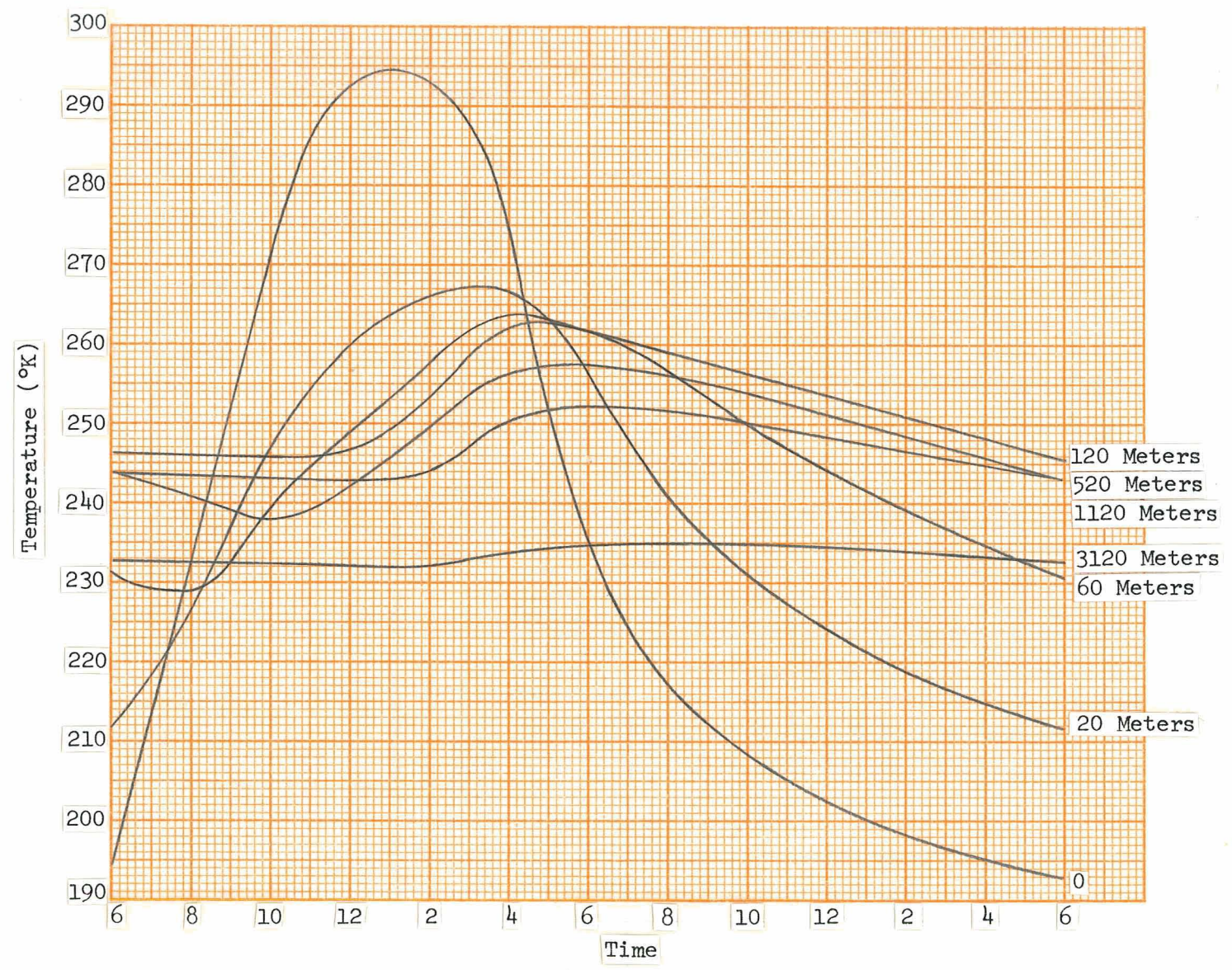
Figure 22: Temperature Profile, Equator, Summer Solstice (Perihelion)
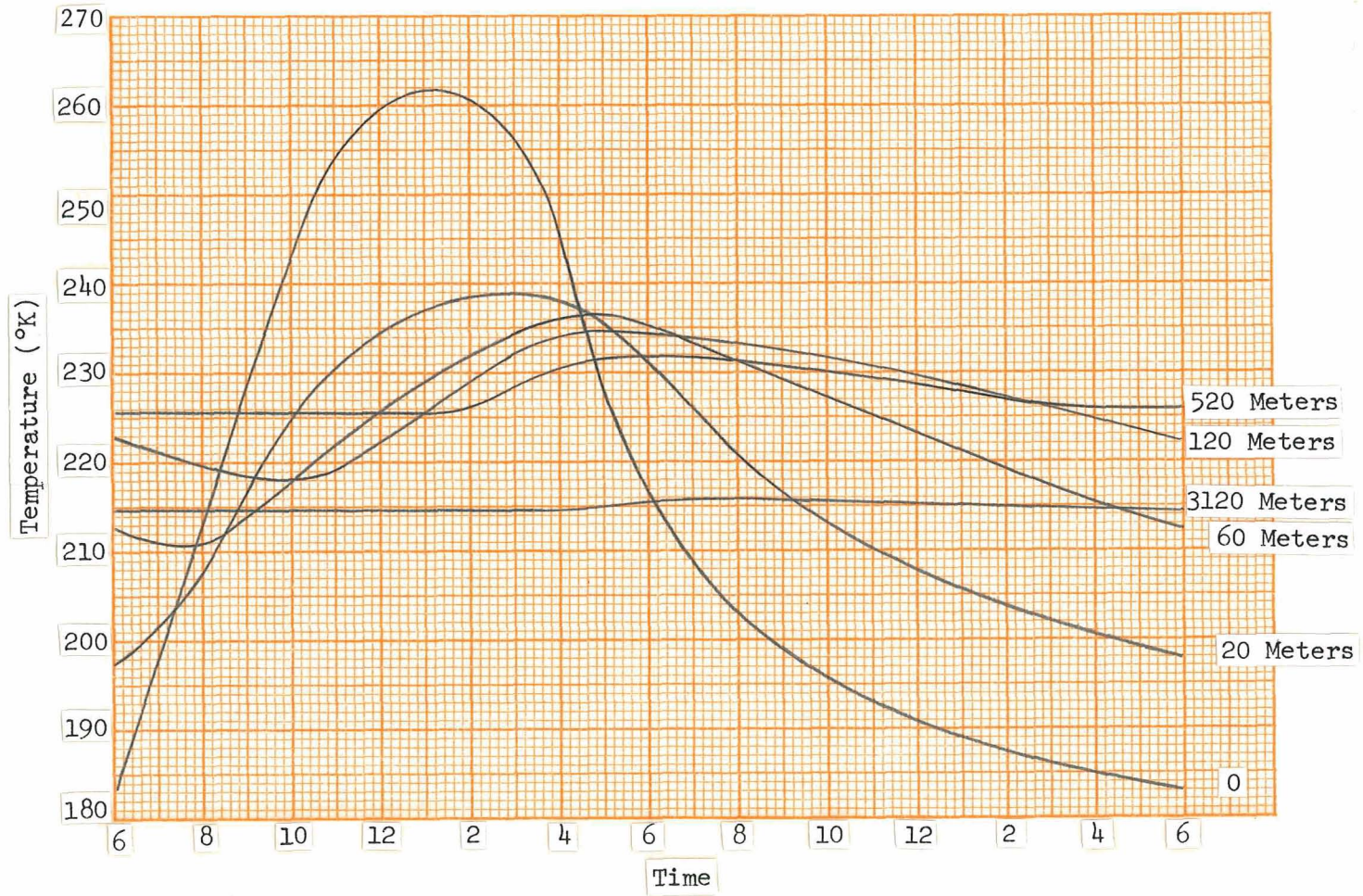
Figure 23:   Temperature Profile, Equator, Winter Solstice (Aphelion)

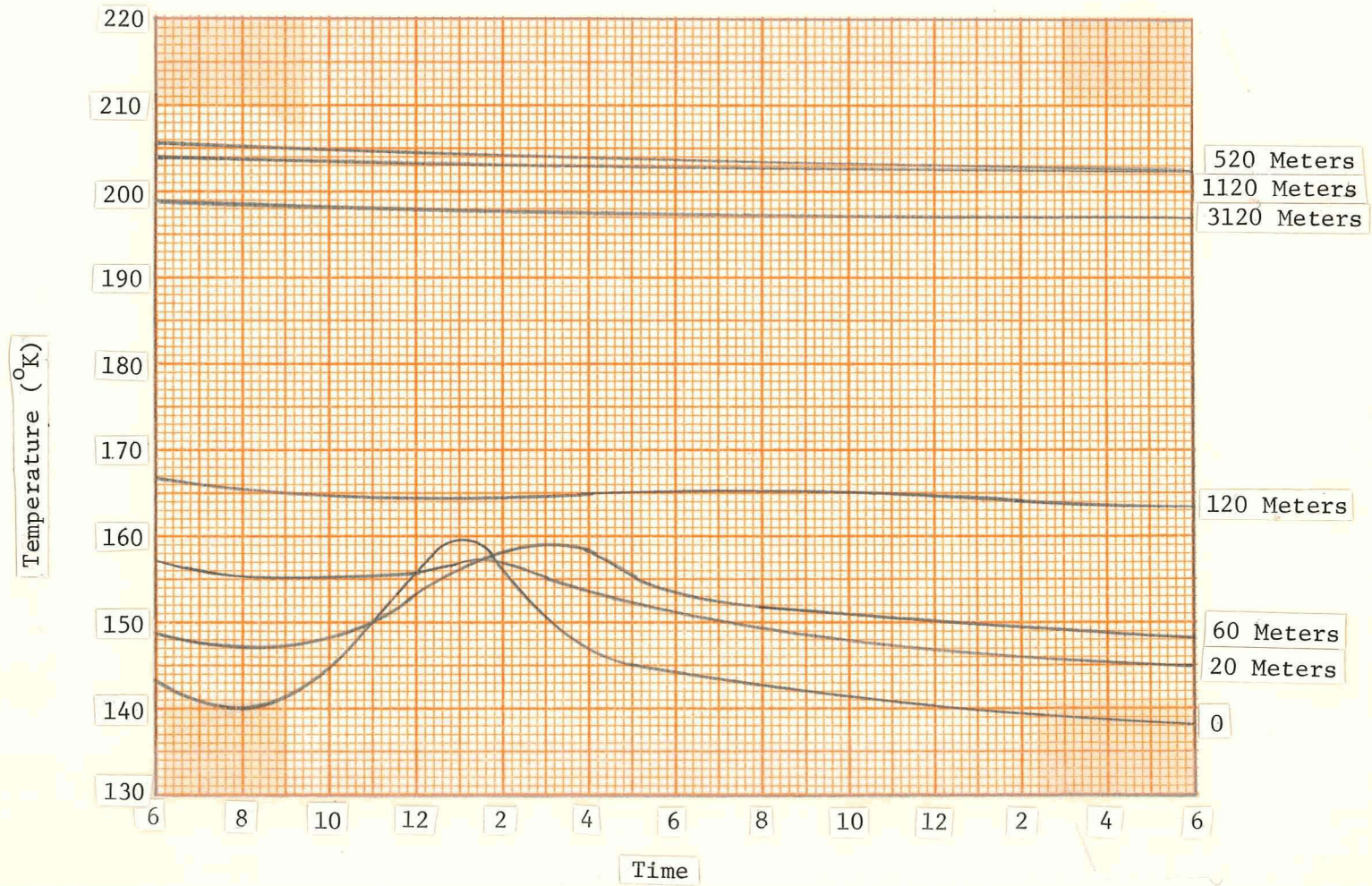Figure 24: Temperature Profile, 30°N Latitude, Winter Solstice

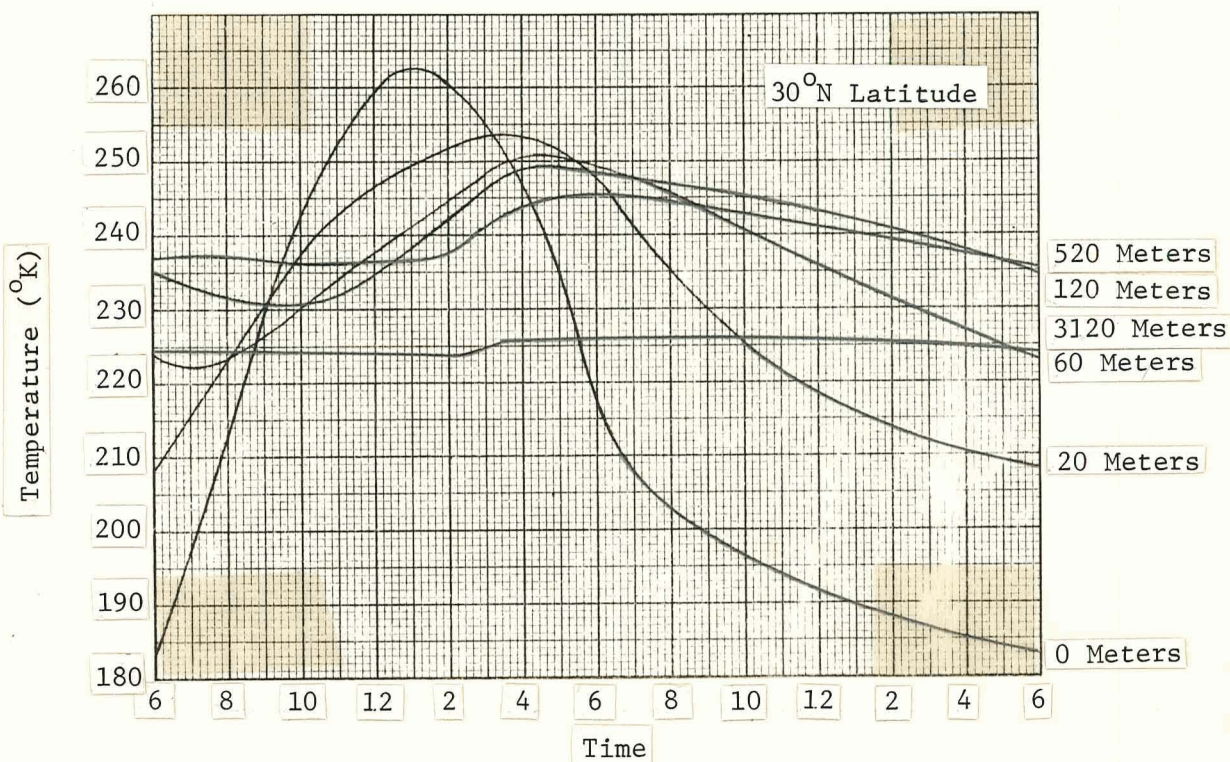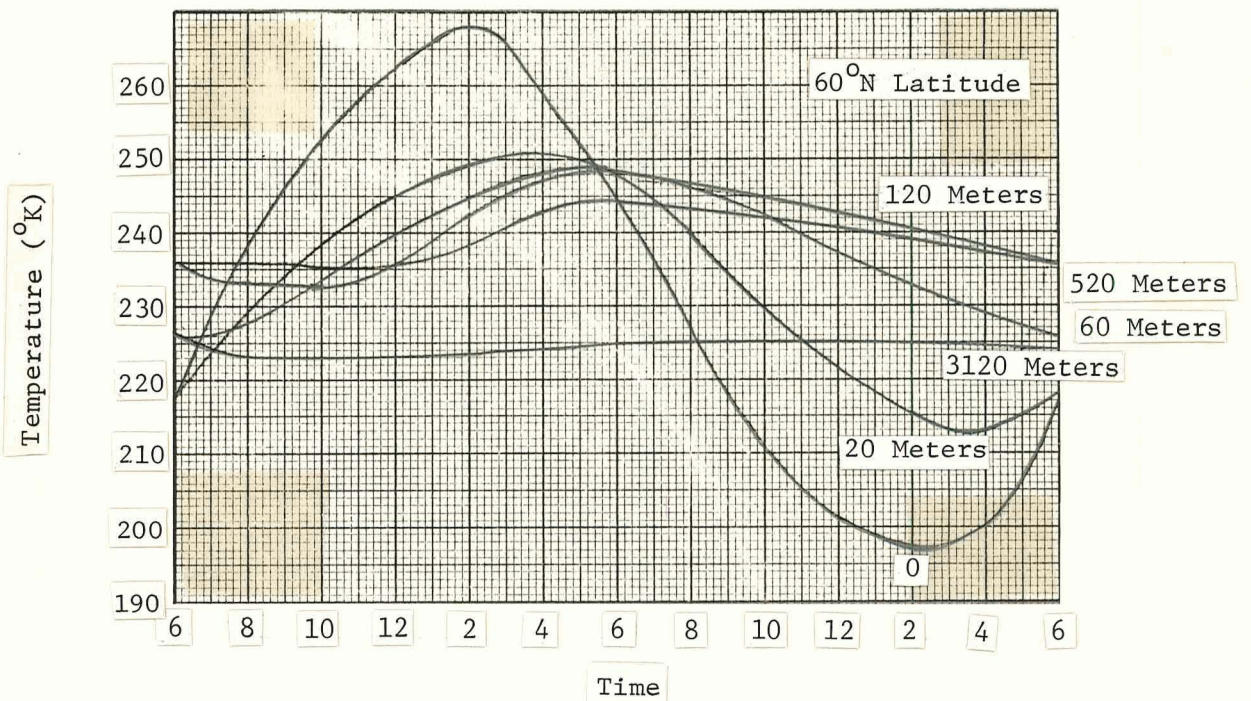Figure 25: Temperature Profile, 60°N Latitude, Winter Solstice

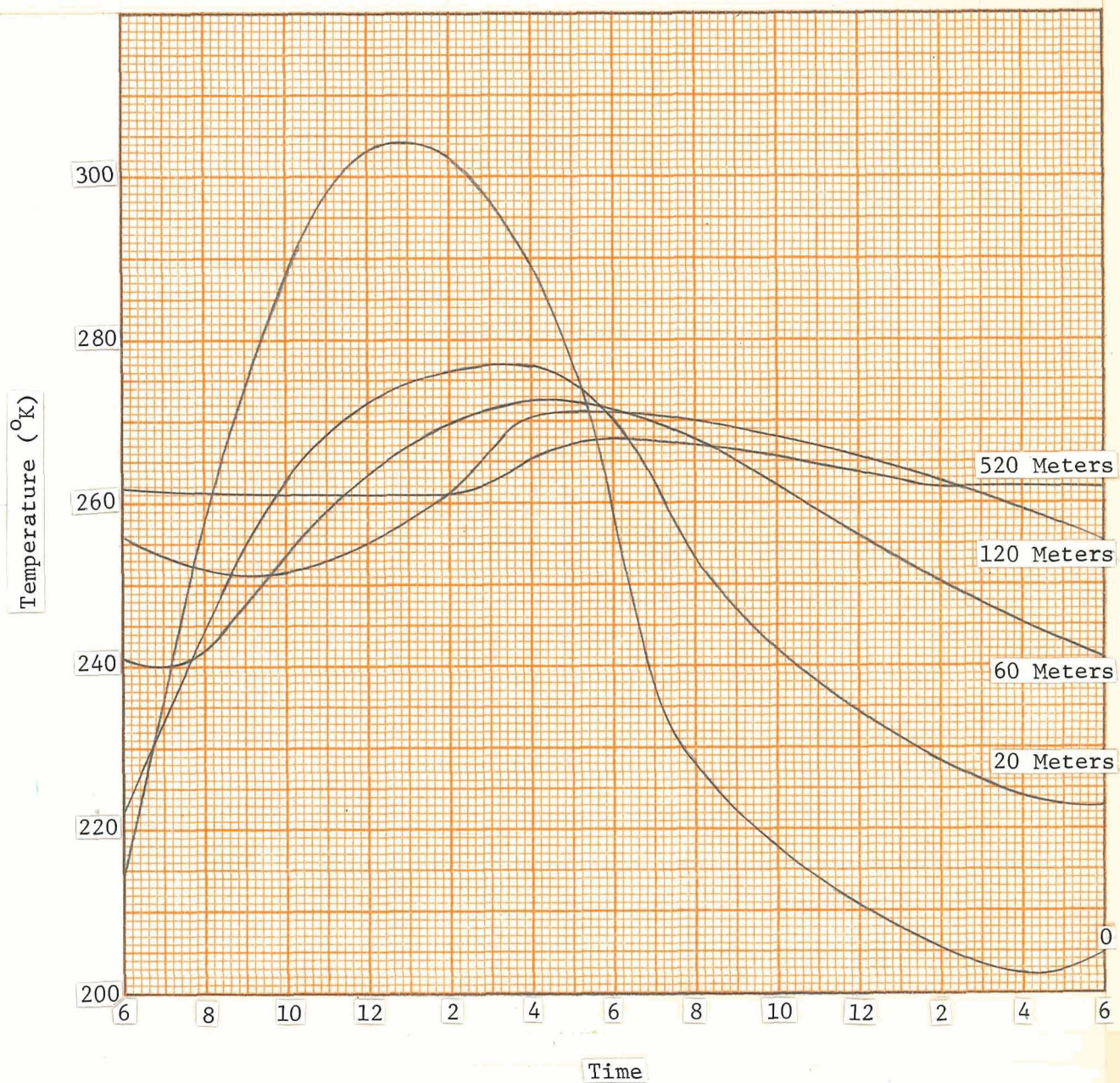Figure 26: Temperature Profile, Summer Solstice

Figure 27: Temperature Profile, 30°S Latitude, Summer Solstice
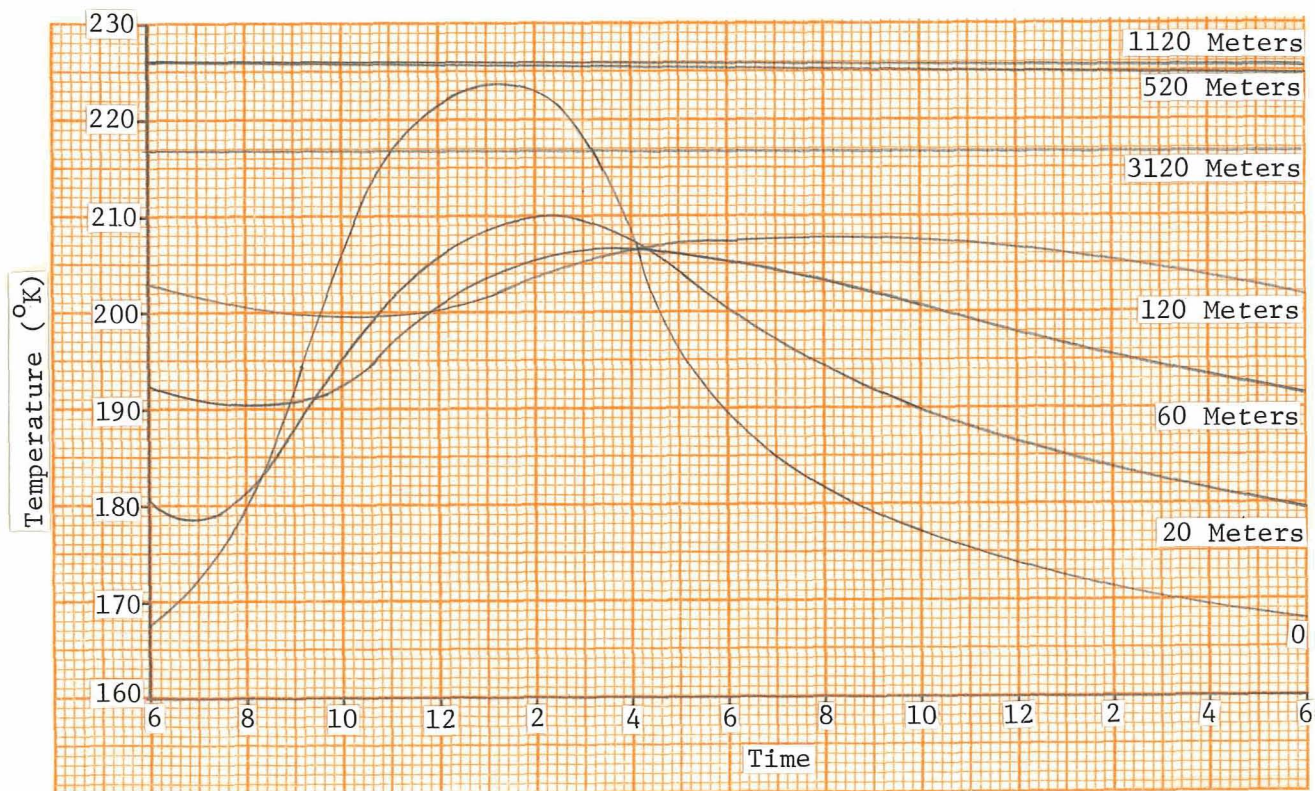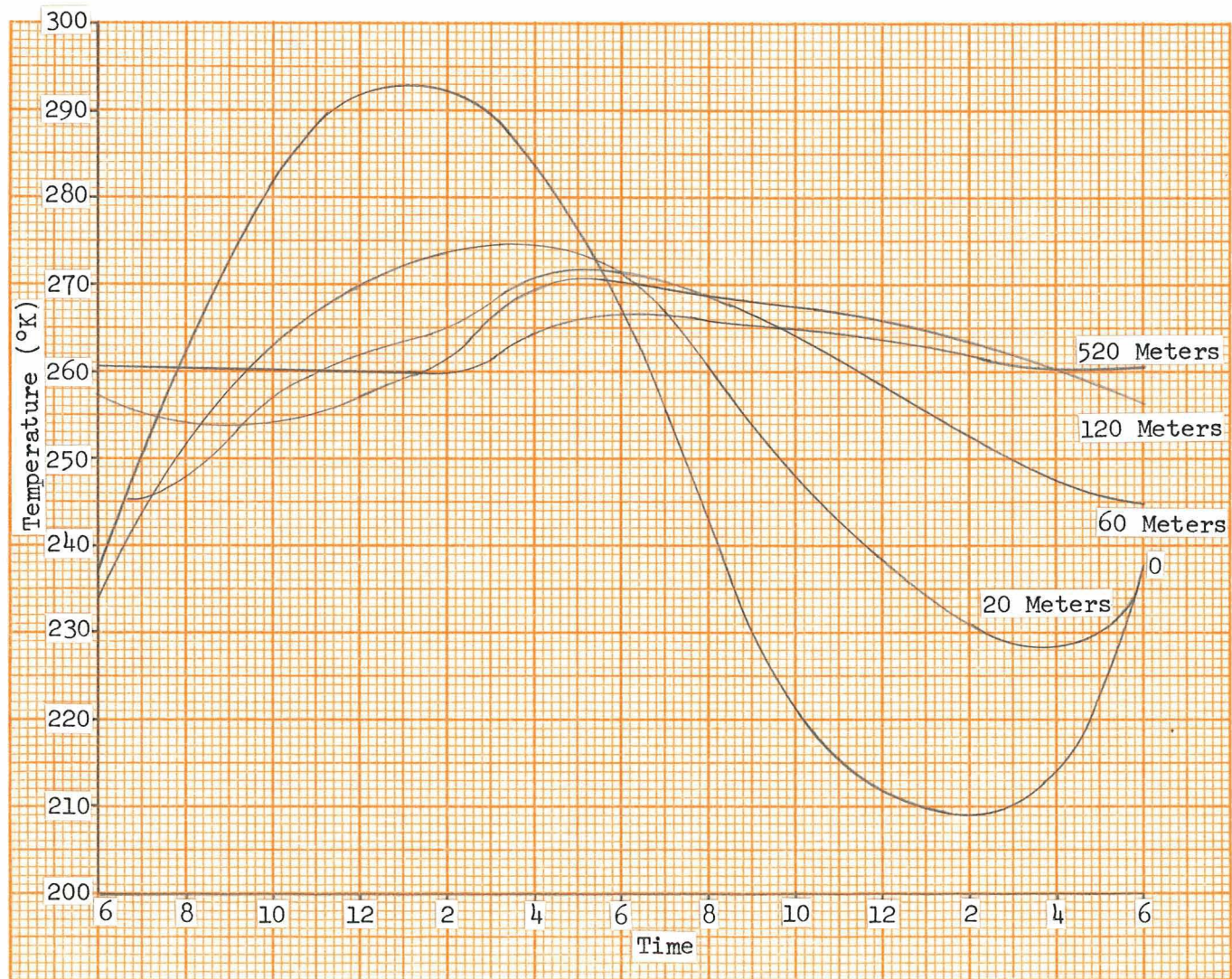
Figure 28: Temperature Profile, 30°S Latitude, Winter Solstice

Figure 29: Temperature Profile, 60°S Latitude, Summer Solstice
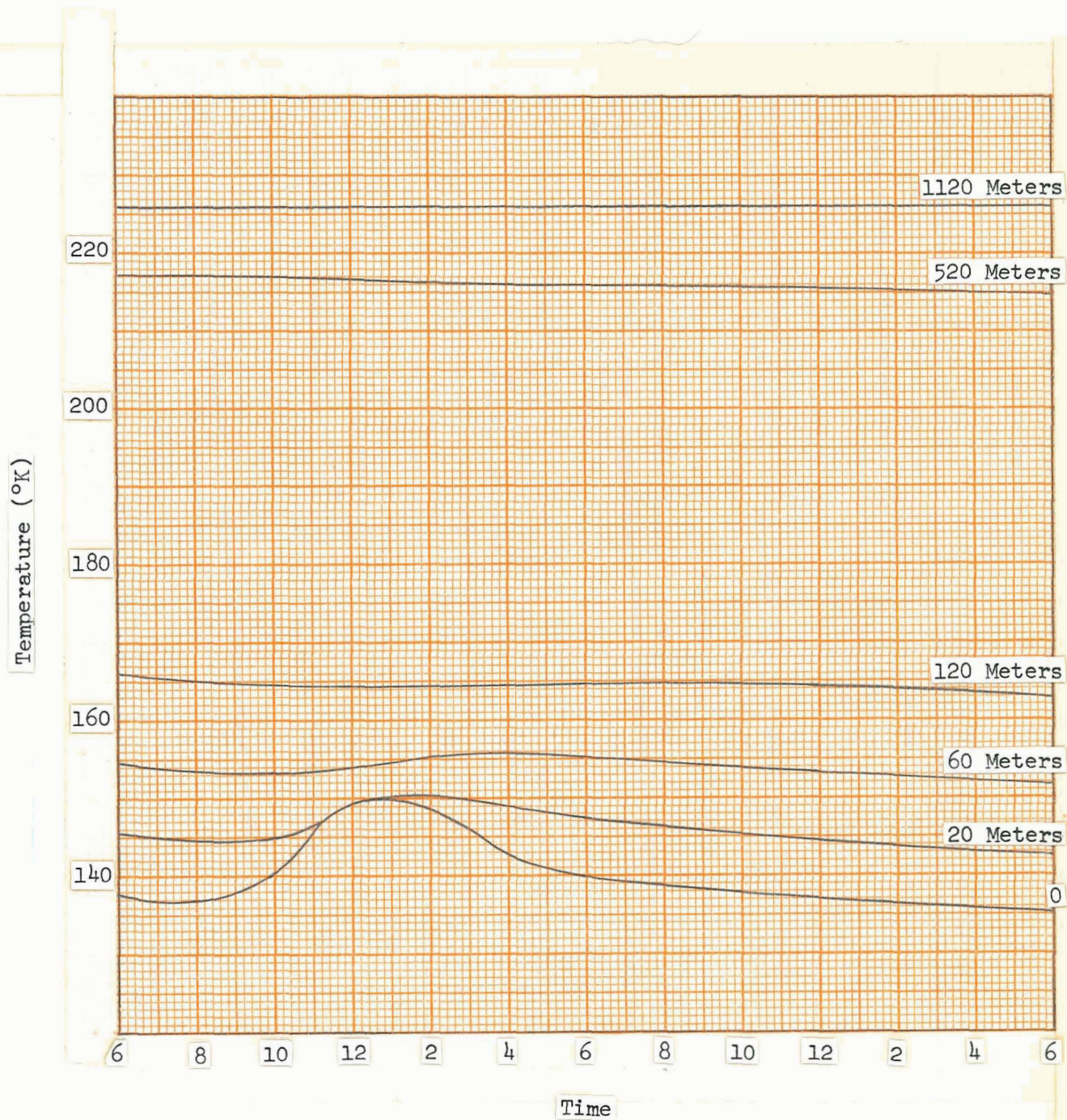
Figure 30: Temperature Profile, 60°S Latitude, Winter Solstice

Figure 31: Temperature Profile, Equator, North Autumnal Equinox

Figure 32: Temperature Profile, Equator, North Vernal Equinox

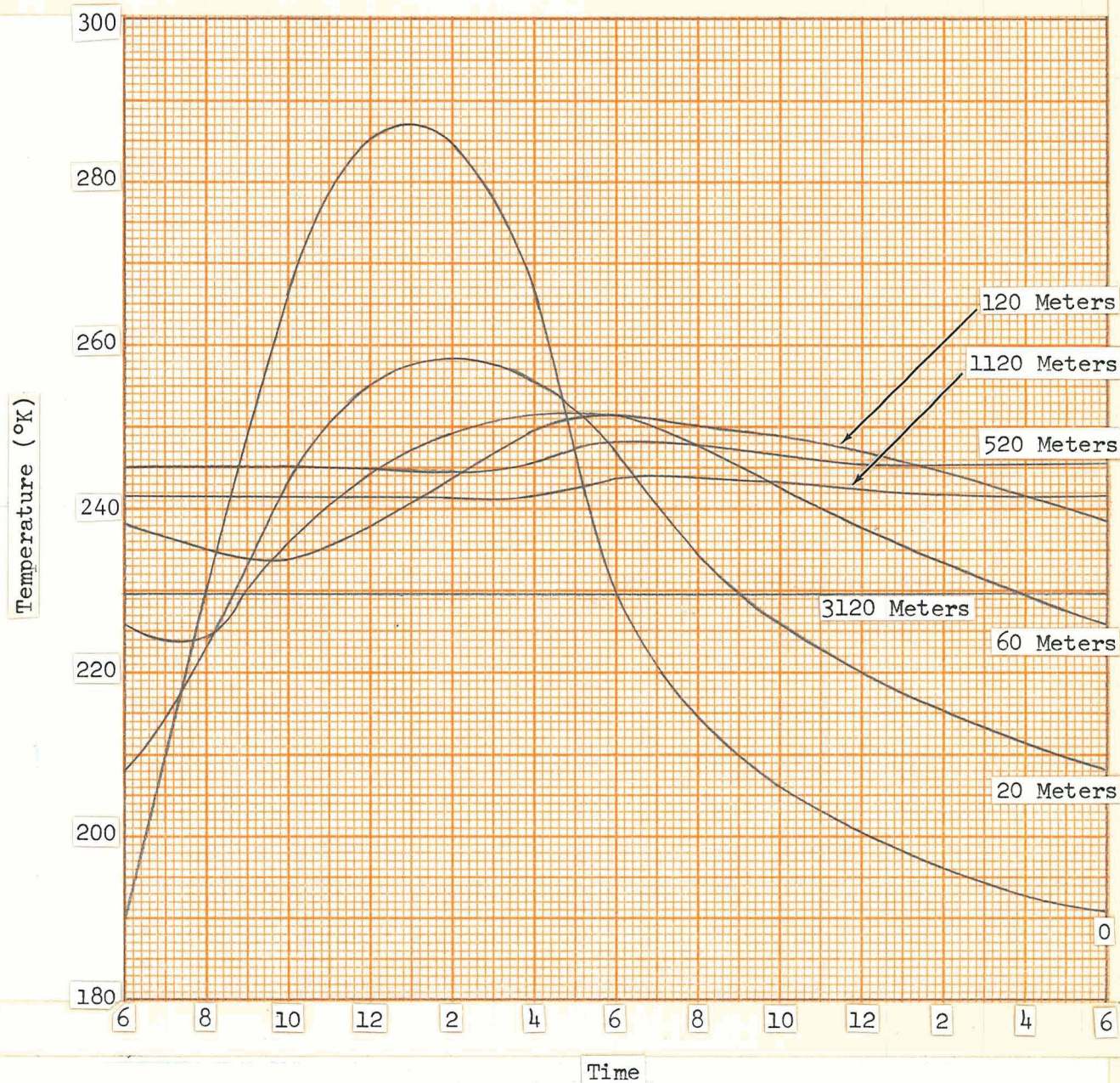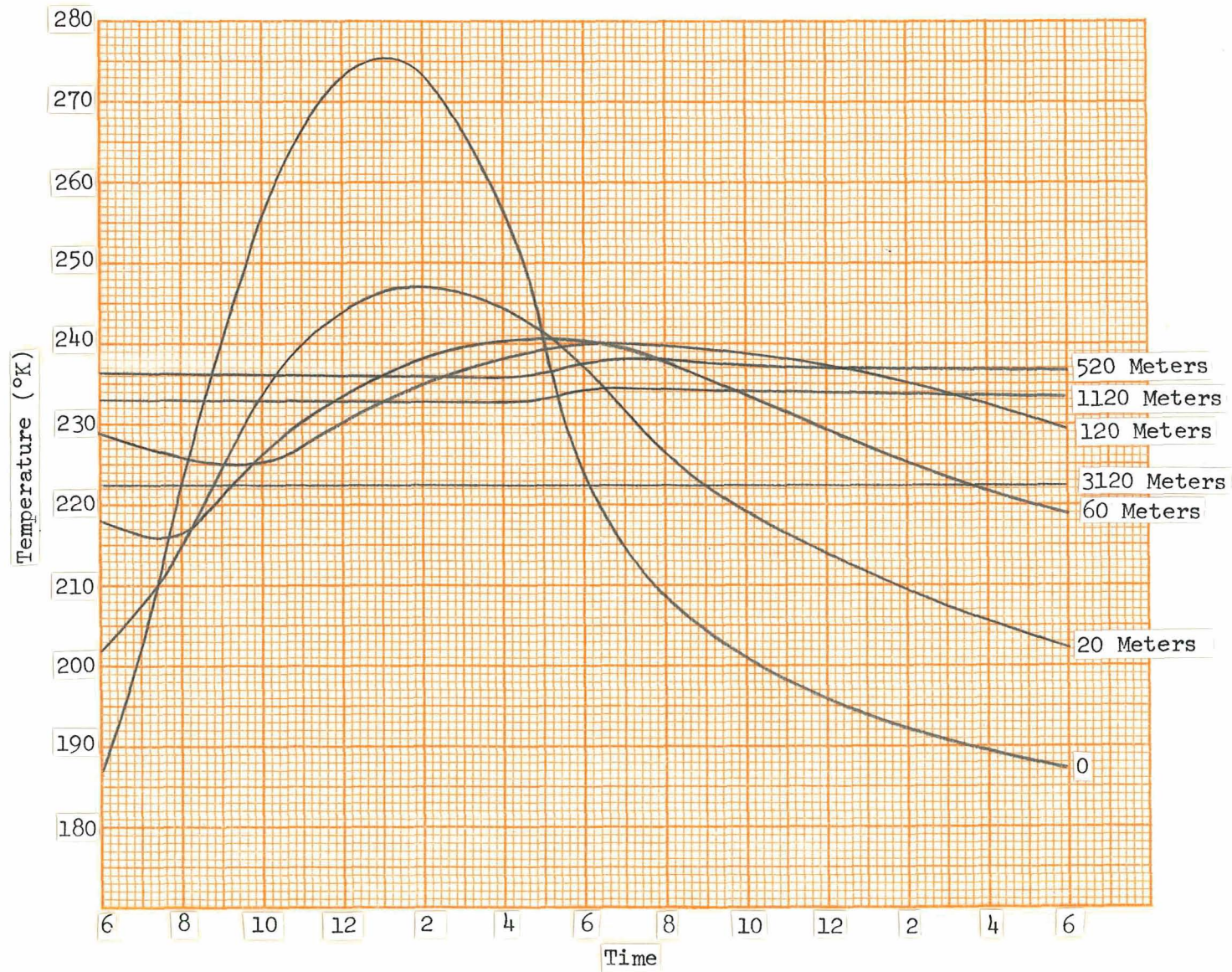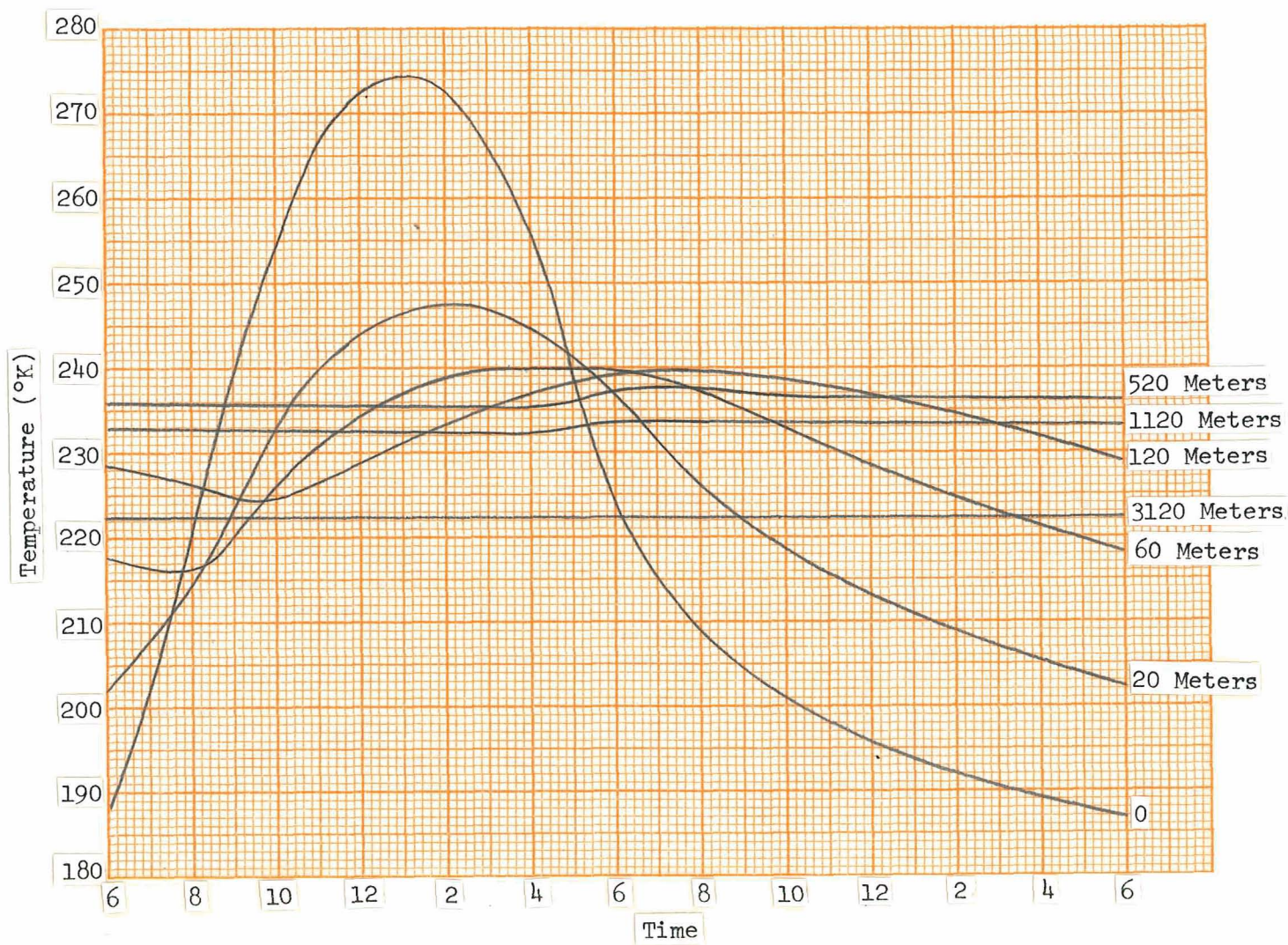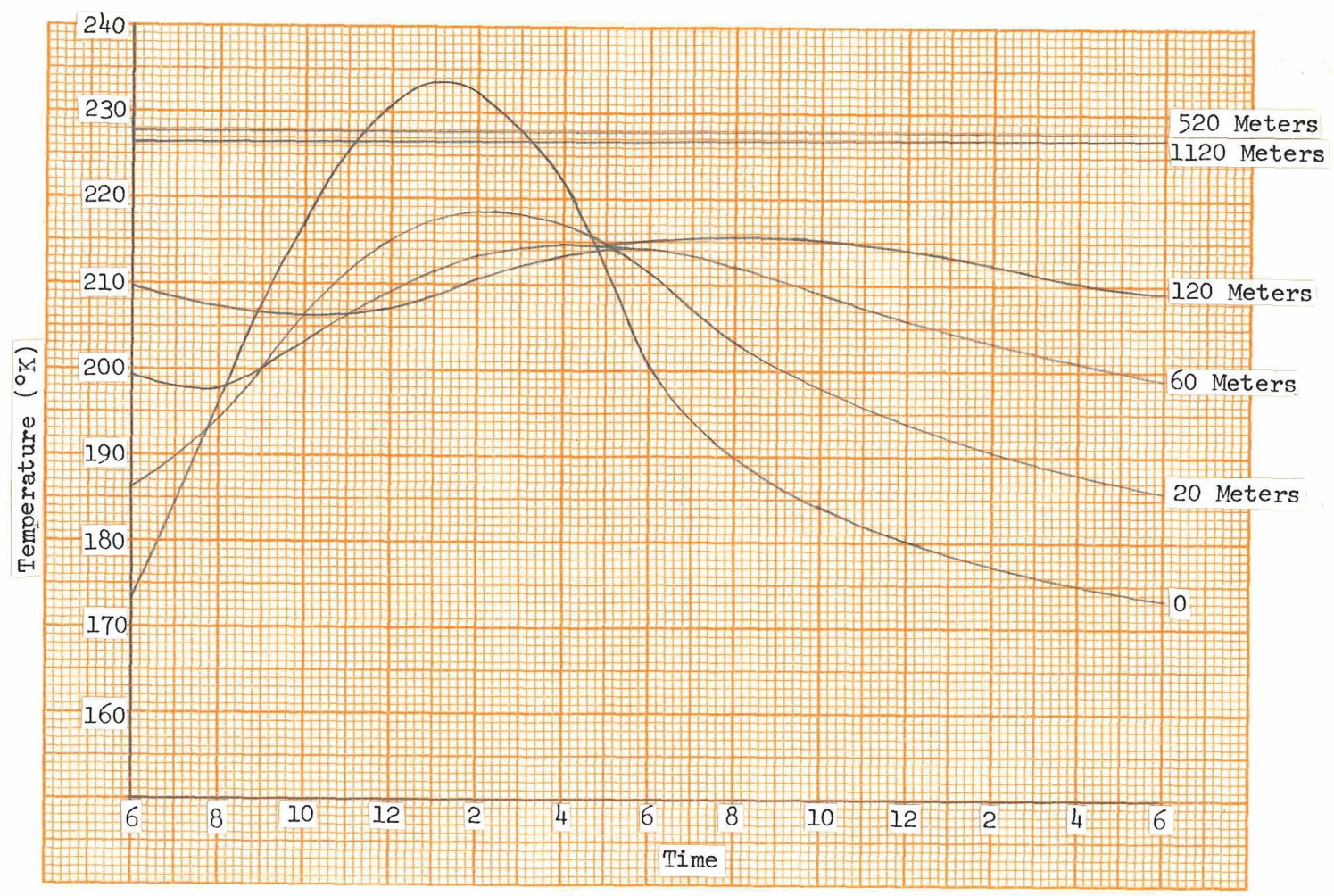Figure 33: Temperature Profile, 30°N Latitude, Autumnal Equinox

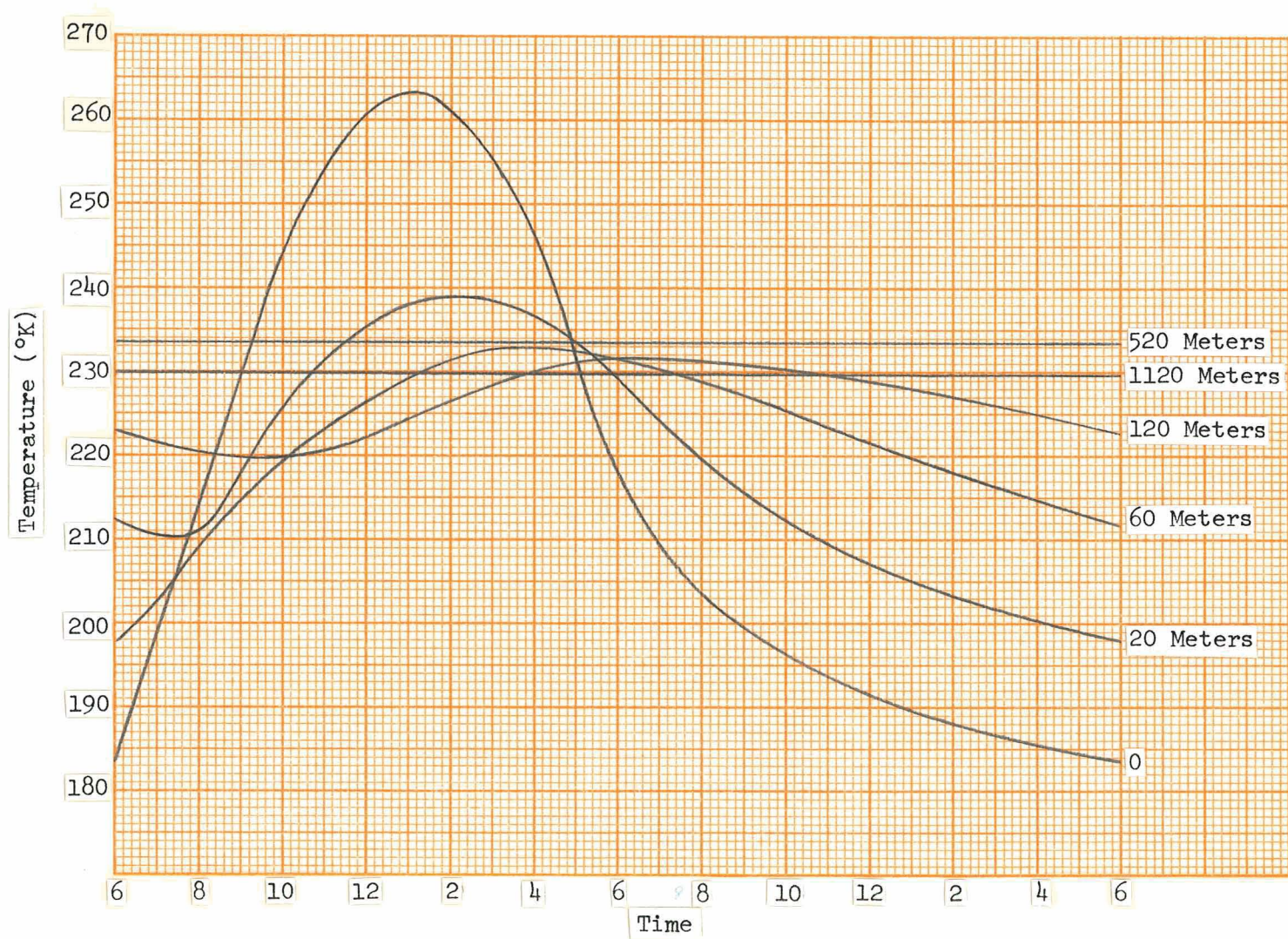Figure 34: Temperature Profile, 60°N Latitude, Autumnal Equinox

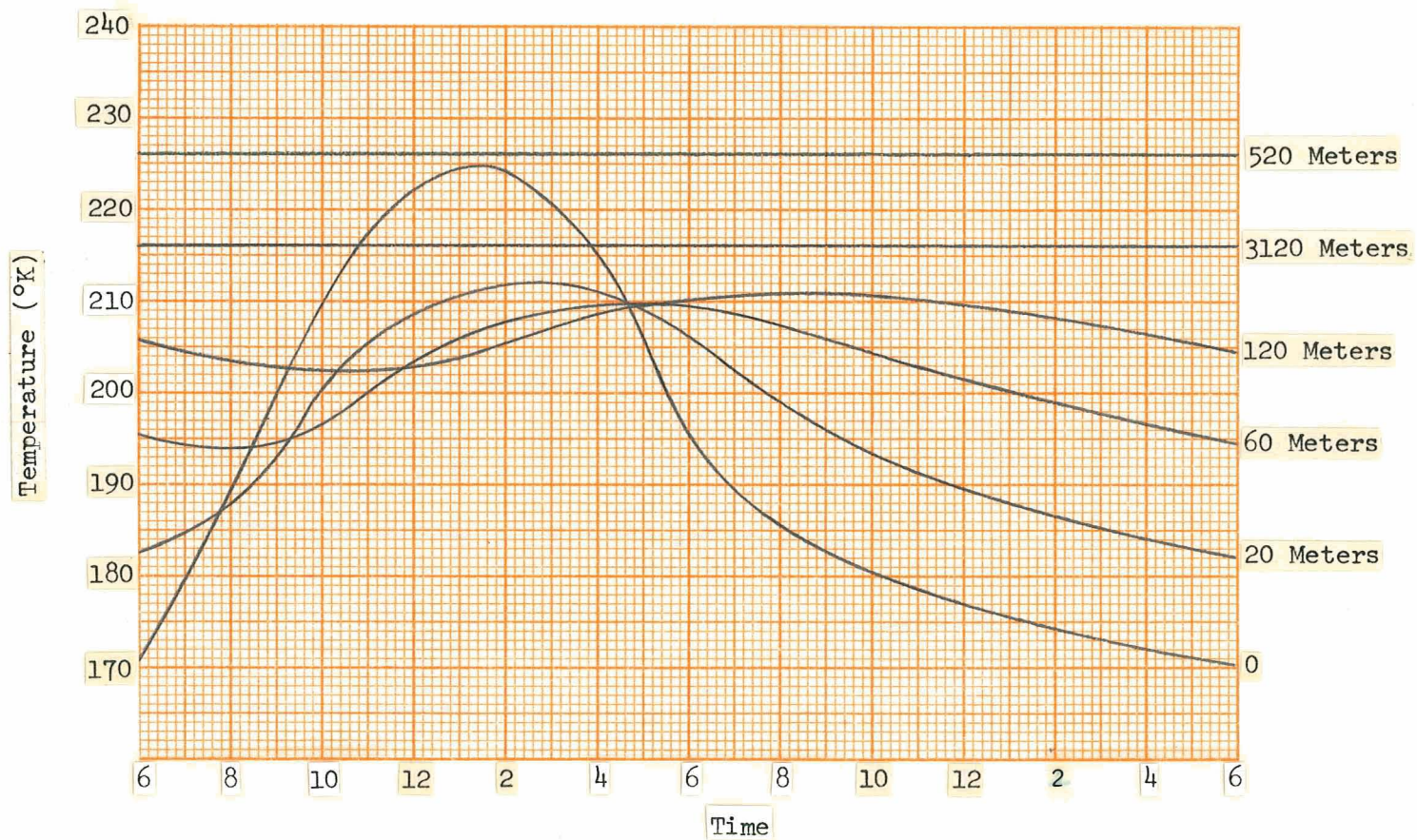Figure 35: Temperature Profile, 30°S Latitude, Autumnal Equinox

Figure 36: Temperature Profile, 60°S Latitude, Autumnal Equinox

5.2 Dust Devils on Mars

It has been found that a superadiabatic temperature lapse rate, with the presence of some degree of mechanical turbulence, is necessary for the generation of dust devils. Also, it is seen, from Section 5.1, that the Martian atmosphere can become highly superadiabatic up to considerable height (though the lapse rates computed are somewhat of an upper bound due to the neglect of advection, they should not be greatly in error). Finally, it is known that winds are present on Mars, at least part of the time, so that mechanical turbulence can be expected. Hence, it is reasonable to conclude that vortex systems of the dust devil type will be generated.

The frequency of occurrence of dust devils on Earth depends importantly upon the temperature lapse rate in the shallow, highly superadiabatic, layer adjacent to the surface. The resultant dust devil diameters are also so determined. Though further, and more detailed, calculations with the computer program are required to determine the nature of such a base layer on Mars, the findings to date indicate that the Martian atmosphere can become significantly more superadiabatic than the Earth's. It is reasonable to expect the same to be true for the base layer. Hence, the tendency should be for dust-devil-like vorticies to form more frequently on Mars and to be of larger diameter.

The question remains, however, as to whether sufficiently high wind velocities can be generated in these dust-devil-like vorticies to cause movement of granular material, and to carry this material aloft. To answer this question, consider the basic equations relating vortex wind velocities to environmental parameters:

$$w_{max} \cong (const._1) g^{\frac{1}{2}} h_2^{\frac{1}{2}} \ dT/dZ \ /\gamma_a$$

$$v_{max} \cong (const._2) \ w_{max} \ d^{\frac{1}{2}} \ / \ h_L^{\frac{1}{2}}$$

The constants in these equations can be obtained from Figures 2b and 7b. The equations then become:

$$w_{max} \cong 10^{-2} \ g^{\frac{1}{2}} h_2^{\frac{1}{2}} \ \frac{dT}{dZ} \ / \ \gamma_a$$

$$v_{max} \cong (10^2 \ km^{-1/2}) \ w_{max} \ d^{\frac{1}{2}}$$

where the velocities are expressed in $km \ hr^{-1}$, g in $km \ hr^{-2}$, and h_2 and d in km. Note that the "constant" in the v_{max} equation contains h_L, the effective height of the inflow layer. This quantity was not measured during the field program, hence its magnitude must be estimated (since it is related to the friction – boundary layer its value is most probably less than 10^{-2} km; it is also undoubtedly not a constant, but its variability is probably reasonably small and in any case it appears to the one-half power in the equation). The boundary layer thickness on Mars, assuming an atmospheric surface density one-hundreth that on Earth, should be about ten times that on Earth (the functional dependence upon ρ is as $\rho^{-1/2}$). Neglecting the variability of h_L, for order of magnitude wind velocity calculations, the equations for Mars can be written as

$$w_{max \ M} \cong 2h_2^{\frac{1}{2}} \ dT/dZ \ / \ \gamma_a$$

$$v_{max \ M} \cong 40 \ w_{max \ M} \ d^{\frac{1}{2}}$$

$$\cong 80 \ h_2^{\frac{1}{2}} \ d^{\frac{1}{2}} \ dT/dZ \ / \ \gamma_a$$

where the Martian gravitational acceleration has been taken as 4.8×10^4 km hr^{-2} (3.7 m sec^{-2}). The wind velocity, at 2m height, required to initiate movement of granular material on Mars, for a reasonable surface model (Ryan, 1964) can be estimated to be about 400 km hr^{-1} (surface pressure of ~10 mb). This can be reduced, possibly by a factor of two (Neubauer, 1966) in the presence of turbulence. This 400 km hr^{-1} requirement places requirements on the temperature lapse rates and thickness of the superadiabatic layer. These, for various dust devil diameters, are as follows:

d (meters)	1	10	100
$h_2^{\frac{1}{2}} \frac{dT}{dZ}$ (°C km$^{-1/2}$)	750	250	75

where the dry adiabatic lapse rate has been taken as 5°C/km. The rather extreme values of $h_2^{\frac{1}{2}} \frac{dT}{dZ}$ required for the smaller dust devils indicates it is quite unlikely that these smaller vortices could pick up surface material. This can be seen clearly by determining $h_2^{\frac{1}{2}} \frac{dT}{dZ}$ from the temperature profiles given in Figures 22-36. Sample results are shown in Table 8.

It is seen that the smallest dust devil that can pick up granular material, for a required wind velocity of 400 km hr^{-1}, is about 25 meters in diameter. This minimum occurs during midday at the equator, around perihelion. At the equinoxes the minimum rises to about 40 meters, and at around aphelion to 80 meters. For 30°N latitude the minimum diameter is about 45 meters, occurring at the equinoxes, increasing to about 70 meters at the northern winter solstice and 200 meters at the northern summer solstice. The behavior is similar at 60°N latitude, the minimum diameter, about 120 meters, occurring at the equinoxes. At 30°S latitude, the minimum diameter, about 45 meters, occurs at southern summer solstice, increases slightly to about 50 meters at the equinoxes and to about 95 meters at the winter solstice. At 60°S latitude the minimum diameter, about

Table 8

DUST DEVILS ON MARS

Location on Planet	Time of Year	Time of Day	h_2 (km.)	$\dfrac{dT}{dZ}$ ($°C/km$)	Minimum vortex diameter for granular material to be moved (meters)	
					400 km hr^{-1} required	200 km hr^{-1} required
Equator	S. Summer Solstice ($\approx$Perihelion)	8 A.M.	0.03	267	280	70
		9 A.M.	0.06	317	110	27
		10 A.M.	0.06	550	34	9
		11 A.M.	0.07	600	25	6
		12 A.M.	0.25	170	85	21
		1 P.M.	0.30	160	84	21
		2 P.M.	1.0	49	260	65
Equator	S. Winter Solstice ($\approx$Aphelion)	8 A.M.	0.04	125	1000	250
		9 A.M.	0.08	189	220	55
		10 A.M.	0.12	208	120	30
		11 A.M.	0.20	180	96	24
		12 A.M.	0.20	195	82	20
		1 P.M.	0.25	148	114	28
		2 P.M.	0.5	68	270	67

Table 8 (Cont'd)

30°N Latitude	N. Summer Solstice	10 A.M.	.08	150	355	89
		11 A.M.	.15	140	215	54
		12 A.M.	.20	125	200	50
		1 P.M.	.20	125	200	50
		2 P.M.	1.5	20	1000	250
30°N Latitude	N. Winter Solstice	9 A.M.	.025	200	620	155
		10 A.M.	.09	255	105	26
		11 A.M.	.13	254	75	19
		12 A.M.	.15	246	68	17
		1 P.M.	.19	195	86	21
		2 P.M.	.21	157	120	30
60°N Latitude	N. Summer Solstice	9 A.M.	.06	250	170	43
		10 A.M.	.10	200	157	39
		11 A.M.	.16	150	172	43
		12 A.M.	.24	112	207	52
		1 P.M.	.30	93	240	
60°N Latitude	N. Winter Solstice	11 A.M.			Sub Adiabatic	
		12 A.M.	.06	50	4200	1050
		1 P.M.	.05	50	2200	550
		2 P.M.			Sub Adiabatic	

Table 8 (Cont'd)

30°S	S. Summer Solstice	8 A.M.	.06	233	192	48
		9 A.M.	.06	433	55	14
		10 A.M.	.12	308	55	14
		11 A.M.	.16	280	49	12
		12 A.M.	.18	278	45	11
		1 P.M.	.20	240	55	14
		2 P.M.	.25	180	77	19
30°S	S. Winter Solstice	9 A.M.	.025	120	1700	425
		10 A.M.	.05	240	220	35
		11 A.M.	.06	330	94	23
		12 A.M.	.085	260	110	27
		1 P.M.	.10	220	130	32
60°S	S. Summer Solstice	9 A.M.	.07	285	110	27
		10 A.M.	.12	230	95	24
		11 A.M.	.15	225	80	20
		12 A.M.	.18	195	90	22
		1 P.M.	.20	175	100	25
		2 P.M.	.30	110	170	42

Table 8 (Cont'd)

60°S	S. Winter Solstice	–	–	–	Large	Large
Equator	N. Antumnal Equinox	9 A.M.	0.07	240	150	38
		10 A.M.	0.10	320	61	15
		11 A.M.	0.12	350	43	11
		12 A.M.	0.13	360	37	9
		1 P.M.	0.14	330	41	10
		2 P.M.	0.17	275	52	13
		3 P.M.	0.30	125	140	35
Equator	N. Vernal Equinox	9 A.M.	0.06	320	104	26
		10 A.M.	0.10	300	70	17
		11 A.M.	0.11	360	43	11
		12 A.M.	0.14	370	46	12
		1 P.M.	0.15	285	51	13
		2 P.M.	0.20	200	78	19
30°N Latitude	Autumnal Equinox	9 A.M.	0.06	300	116	29
		10 A.M.	0.10	300	70	17
		11 A.M.	0.13	310	51	13
		12 A.M.	0.14	315	45	11
		1 P.M.	0.16	275	52	13
		2 P.M.	0.17	240	63	16

110

Table 8 (Cont'd)

60°N Latitude	Autumnal Equinox	9 A.M.	0.04	200	390	98
		10 A.M.	0.06	240	180	45
		11 A.M.	0.09	220	140	35
		12 A.M.	0.11	220	120	30
		1 P.M.	0.13	185	140	35
30°S Latitude	Autumnal Equinox	9 A.M.	0.06	250	165	41
		10 A.M.	0.09	290	83	21
		11 A.M.	0.10	330	57	14
		12 A.M.	0.12	325	50	12
		1 P.M.	0.14	270	60	15
60°S Latitude	Autumnal Equinox	9 A.M.	0.03	230	380	95
		10 A.M.	0.06	220	220	55
		11 A.M.	0.07	240	150	38
		12 A.M.	0.08	250	125	31
		1 P.M.	0.11	200	140	35
		2 P.M.	0.12	160	210	52

80 meters, also occurs at the summer solstice, increasing to about 125 meters at the equinoxes and becoming quite large as the winter solstice approaches.

It was argued previously that vortices should occur more frequently, and with larger diameter on Mars than on Earth (disregarding whether or not they can pick up granular material). Nevertheless, dust devils on Earth with diameters greater than 100 meters are quite rare. It is reasonable to expect that somewhat of the same situation should apply on Mars. Accordingly, it is seen that dust-raising vorticies should occur most frequently on Mars in the vicinity of the equator, and around perihelion. It is also seen that these could occur thoughout the year, at the equator, but with somewhat lesser frequency. This is in accord with the summaries of yellow cloud frequency (in the equatorial region) given by Gifford (1964) and Wells (1966) which show activity to be at a minimum about aphelion, and reaching a broad maximum around perihelion with appreciable activity through the equinoxes.

In the northern hemisphere, dust-raising vorticies should occur much less frequently than at the equator (also than in the southern hemisphere). Greatest frequency should be at the equinoxes, and at high latitudes dust devils should occur only on rare occassions. These findings are also in accord with the yellow cloud tabulations of Gifford and Wells (though it must be noted that apparent agreement with an equinox maximum is based on only eight samples).

In the southern hemisphere, dust-raising vorticies should be somewhat less frequent than at the equator (for latitudes of about 30° and less), but much more frequent than in the northern hemisphere. The occurrence characteristics should be quite similar to those at the equator, minimum frequency occurring around aphelion with a broad maximum extending between the equinoxes and peaking around perihelion. These findings are again in general agreement with Gifford's

and Well's yellow cloud tabulations.

Finally, it should be noted that the vertical winds in Martian dust devils should be quite large. This can be seen by utilizing the data given in Table 8 and the expression for w_{max}. These values are well in excess of those required to maintain granular material aloft (Ryan, 1964). Hence, once motion of granular material begins, this material should be rapidly and easily carried aloft. From comparison with the data for dust devil heights and vertical wind velocities on Earth, it appears evident that the granular material in Martian dust devils should reach great height.

In summary, it is concluded that dust-devil-like vortices are quite likely to occur on Mars. Due to the more highly superadiabatic lapse rates that may occur, compared to what is found on Earth, the frequency of occurrence, and diameter, of these vortices (disregarding whether or not they contain granular material) should tend to be greater than on Earth. However, large wind velocities are required to initiate motion of granular material on Mars, hence only the larger of these vortices can entrain such material. Dust devil activity should reach a maximum around perihelion in the equatorial region and in the southern hemisphere, with greatest frequency at the equator. In the northern hemisphere activity should peak about at the equinoxes. The frequency in the northern hemisphere should be significantly less than at the equator or comparable southern latitudes. These findings are in general accord with observed yellow cloud frequencies and locations. It hence appears quite possible that dust devil activity is responsible for yellow cloud generation.

6.0 RECOMMENDED FUTURE WORK

The present study has resulted in the accumulation of a considerable amount of field experimental data. These data have been used to derive a physical dust devil model. However, this utilization has by no means involved extraction of all possible useful information from the data. Accordingly, it is felt that further data analysis is desirable, particularly as regards the role(s) of wind velocity and vorticity in dust devil generation and decay. This information would aid in prediction of dust devil frequency and sizes on Mars, compared to what is found on earth.

Further work is also desirable in the prediction of temperature lapse rates in the lowermost Martian atmosphere, particularly to determine under what conditions the three layer temperature profiles, as found during the field studies, could exist on Mars. This has important implications for predicting dust devil frequency.

Finally, more detailed studies are desirable to more precisely delineate how the processes responsible for dust devil generation on Mars may scale in magnitude and effectiveness to their terrestrial counterparts.

ACKNOWLEDGEMENTS

REFERENCES

Anders, E. and J. R. Arnold, Age of craters on Mars, Science 149, 1494, 1965.

Baldwin, R. B., Mars: An estimate of the age of its surface, Science 149, 1498, 1965.

Battan, L. J., Energy of a dust devil, J. Meteor, 15, 235-237, 1958.

Dergarabedian, P. and F. Fendell, On the generation and structure of tornadoes, presented at Conference on Weather Forecasting, AMS, Fort Worth, Texas, Nov. 1967.

Flowers, W. D., Sand devils, Gr. Brit., Meteor. Off., Prof. Notes, No. 71, 1936.

Gifford, F. A., A study of Martian yellow clouds that display movement, Mon. Weather Rev., 92, 435-440, 1964.

Gifford, F., Jr., Surface temperatures of the planet Mars, in The Study of Planetary Atmospheres, Final Report, Lowell Obs., Flagstaff, Ariz., 208-249, 1952.

Gutman, L. N., Theoretical model of a waterspout, Akademia Nauk SSSR, Geophysics Series, pp. 87-103, Jan. - June 1957.

Ives, R. L., Behavior of dust devils, Bull. Amer. Meteor. Soc., 28, 168, 1947.

Kuiper, G. P., in Proc. Lunar and Plan. Explor. Coll., 2, 32, 1961.

Kuo, H. L., On the dynamics of convective atmospheric vortices, J. Atmos. Sci., 23, 25-42, 1966.

Kuo, H. L., Note on the similarity solutions of the vortex equations in an unstably stratified atmosphere, J. Atmos. Sci., 24, 95-97, 1967.

Leighton, R. B., Results from the Mariner, presented at Caltech-JPL Lunar and Planetary Conference, Pasadena, California, Sept. 13-18, 1965.

Leighton, R. B., B. C. Murray, and R. P. Sharp, Mariner IV photography of Mars: Initial results, Science, 149, 627, 1965.

Michaux, C. M., Handbook of the Planet Mars, NASA SP3030, 1967.

Neubauer, F. M., Thermal convection in the Martian atmosphere, J. Geophys. Res., 71, 2419, 1966.

Ohring, G., W. Tang, J. Mariano, and G. Desanto, Planetary Meteorology, Final Report, Contract NASw-1574, GCA-TR-68-4-N, May 1968.

Opik, E. J., The Martian surface, Science, 153, 255-265, 1966.

Ryan, J. A., Notes on the Martian yellow clouds, J. Geophys. Res., 69, 3759, 1964a.

Ryan, J. A., Eolian transport of granular material on Mars, presented at 12th International Meeting of Internat. Astron. Union, Hamburg, Germany, August-September, 1964b.

Ryan, J. A. and F. F. Fish, The Martian yellow clouds, presented at annual meeting, AAAS, Univ. Cal., Berkeley, December 1965.

Sagan, C., P. L. Hanst, and A. T. Young, Nitrogen oxides on Mars, Planet. Space Sci., 13, 73, 1965.

Scorer, R. S., Natural Aerodynamics, Pergamon Press, 1958.

Sinclair, P. C., Some preliminary dust devil measurements, Mon. Weather Rev., 92, 363, 1964.

Sinclair, P. C., A microbarophone for dust devil pressure measurements, J. App. Meteor., 4, 116, 1965a.

Sinclair, P. C., On the rotation of dust devils, Bull. Amer. Meteor. Soc., 1965b.

Sinclair, P. C., A quantitative analysis of the dust devil, Ph.D Dissertation, The University of Arizona, 1966.

Sinton, W. M., Publ. Astr. Soc. Pac., 73, 125, 1961.

Sinton, W. M. and J. Strong, Radiometric observations of Mars, A. J., 131, 459-464, 1960.

Sutton, O. G., Micrometeorology, McGraw Hill Book Company, New York, 1953.

Taylor, G. I., Motion of solids in fluids when the flow is not irrotational, Proc. Roy. Soc., A, 93, 99, 1917.

Taylor, G. I., Experiments in rotating fluids, Proc. Roy. Soc., A, 100, 114, 1921.

Wells, R. A., An analysis of Martian clouds and their topographical relationships, Scientific Note, ESRO SN-54, 1966.

Williams, N. R., Development of dust whirls and similar small-scale vortices, Bull. Amer. Meteor. Soc., 29, 106, 1948.

Witting, J., F. Narin, and C. A. Stone, Mars: Age of its craters, Science, 149, 1496, 1965.